

# Homogeneous shear turbulence as a second-order cone program

Luoyi Tao\*

*Department of Aerospace Engineering  
Indian Institute of Technology Madras  
Chennai 600 036, India*

(Dated: September 1, 2020)

To help resolve issues of non-realizability and restriction to homogeneity faced by analytical theories of turbulence, we explore three-dimensional homogeneous shear turbulence of an incompressible Newtonian fluid within the context of optimal control and convex optimization. The framework is composed of multi-point spatial correlations of velocity and pressure fluctuations up to the degenerate fourth order, their evolution equations and constraints. It is argued that the integral of the trace of the second order correlations is the objective functional to be maximized. The sources of the constraints are discussed, such as the Cauchy-Schwarz inequality and the non-negativity of variance of products. Two models are introduced: the second-order model uses the contracted and degenerate third order correlations as the control variables; the third-order model takes the degenerate fourth order correlations as the control variables. Both model are second-order cone programs when discretized. The nature of large-scale and huge-scale computations and the link to big data are commented on. It is shown that the exponential growth rates of the asymptotic states are bounded from above by zero. The asymptotic steady state of the second-order model is solved numerically. Three bounded characteristic macro length scales are predicted, streamwise, vertical, and spanwise, beyond which the two-point correlations are negligible. The predicted values of the anisotropy tensor are consistent with experimental data qualitatively (in regard to the relative numerical order pattern of the diagonal components), albeit with significant quantitative differences. Such differences are attributed to the non-enforceability of the non-negativity of variance of products within the second-order model. Compared with DNS data, the predicted second order correlation functions contain flawed features of local minima either too large in magnitude or present spuriously. The third-order model is expected to improve predictions, because of its ability to include constraints generated by the non-negativity of variance of products and its mathematical structure formulated in an enlarged space of control variables. The issue of how to solve this huge-scale problem is yet open.

## I. INTRODUCTION

As regards the analytical theories of turbulence for an incompressible Newtonian fluid [1–5], especially the quasi-normal model (QN) and a few of its variants concerned, there are known issues of non-realizability (a large part of the turbulent energy spectrum becoming negative in isotropic turbulence [1, 6, 7]) and restriction to homogeneity (“Two-point models are restricted, more or less, to homogeneous turbulence (unlike one-point models), but nevertheless they have proved very popular.” [1]). In this study, we explore a framework of optimal control and convex optimization to help resolve these issues. We choose three-dimensional homogeneous shear turbulence as a test problem, considering the relative simplicity of the motion and the availability of experimental and direct numerical simulation (DNS) data [8–10].

To determine the statistically averaged structure of three-dimensional homogeneous shear turbulence, we start with the relations resulting from the Navier-Stokes equations, the Reynolds decomposition, and the ensemble average operation, following conventional practice. Our attention is restricted to a framework accounting for the multi-point spatial correlations of velocity and pressure fluctuations up to the degenerate fourth order. It is guided by the general structure of analytical theories, the consideration of mathematical and computational demands, and the availability of experimental data [11]. One part of the relations concerns the dynamical equations of evolution for the correlations and is derived in conventional fashion. The other part involves the constraints of equality and inequality for the correlations that are the essence of realizability and whose comprehensive enforcement in the proposed framework is a departure from the practice of analytical theories. Satisfaction of these constraints provides a solution to the issue of non-realizability. Alternatively, one may pursue a comprehensive statistical formulation of turbulence with a probability density functional which produces functional equations governing the evolution of the characteristic

---

\* luoyitao@iitm.ac.in

functional [12, 13]. Such a formalism, however, faces the challenge of solving the functional equations and in going beyond homogeneous turbulence.

There are several sources, physically and mathematically, that give rise to constraints in ensemble averaged turbulence modeling. The constraints of equality come from the self-consistency of the definitions of correlations, the divergence-free fluctuating velocity field from the supposed incompressibility, and certain symmetries that arise from the mean flow characteristics. The constraints of inequality are constructed mathematically from the applications of the Cauchy-Schwarz inequality and the non-negativity of variance of products. These inequalities include, as special cases, physically motivated and known constraints, such as the positive semi-definiteness of the Reynolds stress tensor and the non-negativity of the viscous dissipation, that are the realizability conditions usually addressed in engineering turbulence modeling methodology [14]. However, the vast majority of these inequalities are ignored or even nonenforceable within conventional schemes of turbulence modeling.

Here, a conventional scheme means a closure approach which approximates the highest order correlations in terms of lower ones, in the form of equalities, within a turbulence model. In QN, for example, the fourth order correlations are represented by certain combinations of the products of the second order correlations in the Fourier wave-number space; the specific numerical simulation of isotropic turbulence has demonstrated the emergence of nonphysical negative energy spectrum in this specific model [6, 7]. It is thus inferred that in general such a scheme cannot satisfy all the constraints aforementioned. This observation motivates us to pursue an optimal control approach: the realization of the constraints is taken as essential; an objective is optimized, subject to the dynamical equations and the constraints. One possible choice for the objective is Shannon entropy and its maximization [15–19], which poses difficulties of formidable computational size and numerical integration in very high dimensions. Shannon entropy, however, provides guidance on selection of the integral associated with the second order correlations,  $\int_{\mathbb{R}^3} d\mathbf{r} U_{kk}(\mathbf{r})$ , as the objective functional to be maximized. This form is also substantiated from the strong mixing perspective of physical turbulence.

Two models are introduced, motivated by the structure of the dynamical equations of evolution. The second-order model takes the contracted and degenerate third order correlations as the control variables. The third-order model takes the degenerate fourth order correlations as the control variables. In their discretized forms, both models are second-order cone programs (SOCP) according to the criteria defined in [20–22]. There is a constitutive difference between them: The second-order model cannot include any constraints from the non-negativity of variance of products, while the third-order model includes those constraints from the non-negativity requirement involving only the second, third, and fourth order correlations. The significance of this difference lies in that such constraints provide a mechanism to bound the correlations and their exponential growth rate in the asymptotic states. It is noted that these constraints demand that the maximum growth rate of the correlations be zero ( $\max \sigma = 0$ ), contradicting experimental and DNS data [8, 10, 23].

Restricted by computational feasibility at present, we focus on the numerical solution of the second-order model in the asymptotic steady state in this paper. As part of the basis to evaluate the framework, we compute the non-trivial components of the anisotropy tensor  $b_{ij}^{(\infty)}$ , against experimental data summarized in [8]. Both our prediction and the experimental data are given here: (a)  $b_{11}^{(\infty)} = 0.5031 > b_{33}^{(\infty)} = -0.2080 > b_{22}^{(\infty)} = -0.2951$  (Prediction) versus  $b_{11}^{(\infty)} = 0.203 > b_{33}^{(\infty)} = -0.06 > b_{22}^{(\infty)} = -0.143$  (Experiment); (b)  $b_{12}^{(\infty)} = -0.1161$  (Prediction) versus  $b_{12}^{(\infty)} = -0.156$  (Experiment). The comparison shows that the model produces values matching qualitatively with the order pattern of the experimental data, albeit with significant quantitative differences. Such differences are attributed to the non-enforceability of the non-negativity requirement within the second-order model. With regard to the prediction of the second order correlation functions, three bounded characteristic length scales are obtained, streamwise, spanwise, and vertical, beyond which the two-point correlations are effectively negligible; the relative numerical order of the length scales is compatible with the physical flow. Compared with the DNS data of [10], however, the predicted spatial distributions of the correlation functions are flawed in that the local negative minima are either too large in magnitude or present spuriously.

The third-order model is expected to improve predictions, because it is formulated in an enlarged control variable space and it contains a bounding mechanism produced by the non-negativity requirement. However, the computational scale of the model is huge according to the criteria listed in [24], a great effort is required with regard to the mathematical formulation, algorithms, codes, etc. The third-order model has a close link to big data [25] and research in the field of big data may help explore and implement the model.

The present paper is organized as follows. In Sec. II, we develop the dynamical equations of evolution for the correlations, define the two models, and discuss the constraints. The issue of closure and choice of objective functional is addressed, and the basic features are summarized. In Sec. III, we consider the asymptotic states of two models at large time and present one consequence of the non-negativity of variance of products — the maximum exponential growth rate of the correlations is zero. Also, we comment on the issues of huge-scale computation and DNS. In Sec. IV, we study numerically the asymptotic steady state of the second-order model. The predicted values of the anisotropy tensor and other quantities are compared against experimental data, the role of the non-negativity of

variance constraints is examined, and the predictions of the second order correlation functions are evaluated against DNS data. The main results of the present work are summarized in Sec. V. Appendices provide details of certain analytical, numerical, and computational aspects.

## II. BASIC FRAMEWORK

Consider homogeneous shear turbulence of an incompressible Newtonian fluid of mass density  $\rho$  and kinematic viscosity  $\nu$  in  $\mathbb{R}^3$  and in the Cartesian coordinate system  $x_i$  with the mean velocity field,

$$V_i = \delta_{i1} S x_2, \quad (1)$$

where  $\delta_{ij}$  is the Kronecker delta and  $S$  is the spatially uniform mean shear rate, positive and constant. The equations of motion governing the fluctuation fields of velocity  $w_i(\mathbf{x}, t)$  and scaled pressure  $q(\mathbf{x}, t) = p(\mathbf{x}, t)/\rho$  can be derived from the Navier-Stokes equations, using Eqs. (1) and the Reynolds decomposition. Next, dimensionless quantities (accented) are defined via

$$t = t'/S, \quad x_i = (\nu/S)^{1/2} x'_i, \quad w_i = (\nu S)^{1/2} w'_i, \quad q = \nu S q'. \quad (2)$$

The aforementioned equations of fluctuation fields are non-dimensionalized to give

$$\frac{\partial w_k}{\partial x_k} = 0, \quad \frac{\partial w_i}{\partial t} + x_2 \frac{\partial w_i}{\partial x_1} + \delta_{i1} w_2 + \frac{\partial(w_i w_k)}{\partial x_k} = -\frac{\partial q}{\partial x_i} + \frac{\partial^2 w_i}{\partial x_k \partial x_k}, \quad (3)$$

where the accent ' is removed for brevity.

Some clarification is required regarding the above treatment. Within the present formulation, the infinite domain  $\mathbb{R}^3$  is necessary to realize homogeneity throughout the whole domain. It is conventionally known that this homogeneous shear flow has the macro timescale  $S^{-1}$ , but it has no characteristic outer length scale, except for the Kolmogorov micro length scale whose value is yet to be determined. In Eqs. (2), both  $S$  and  $\nu$  are combined to produce a length scale  $(\nu/S)^{1/2}$  [9], and consequently, Eqs. (3) are free of controlling parameters. Our numerical simulation suggests that in homogeneous shear turbulence there are statistically averaged characteristic macro length scales, streamwise, vertical, and spanwise, as presented in Subsec. IV B.

As done in [26], Eqs. (3) are used to construct the dynamical equations governing the evolution of the second order correlations  $\overline{w_i(\mathbf{x})w_j(\mathbf{y})}$  and the third order correlations  $\overline{w_i(\mathbf{x})w_j(\mathbf{y})w_k(\mathbf{z})}$ , along with those governing the spatial correlations  $\overline{q(\mathbf{x})w_j(\mathbf{y})}$ ,  $\overline{q(\mathbf{x})w_j(\mathbf{y})w_k(\mathbf{z})}$ , and  $\overline{q(\mathbf{x})q(\mathbf{y})}$ , where the dependence of the correlations on  $t$  is suppressed. Further, homogeneity is adopted to simplify the mathematical treatment. The structure of the dynamical equations and homogeneity lends grounds to define

$$\begin{aligned} U_{ij}(\mathbf{r}) &= \overline{w_i(\mathbf{x})w_j(\mathbf{y})}, \quad U_{(ij)k}(\mathbf{r}) = \overline{w_i(\mathbf{x})w_j(\mathbf{x})w_k(\mathbf{y})}, \quad U_{ijk}(\mathbf{r}, \mathbf{s}) = \overline{w_i(\mathbf{x})w_j(\mathbf{y})w_k(\mathbf{z})}, \\ U_{(ij)kl}(\mathbf{r}, \mathbf{s}) &= \overline{w_i(\mathbf{x})w_j(\mathbf{x})w_k(\mathbf{y})w_l(\mathbf{z})}, \quad U_{ijkl}(\mathbf{s}', \mathbf{r}, \mathbf{s}) = \overline{w_i(\mathbf{x})w_j(\mathbf{z}')w_k(\mathbf{y})w_l(\mathbf{z})}, \\ Q(\mathbf{r}) &= \overline{q(\mathbf{x})q(\mathbf{y})}, \quad Q_j(\mathbf{r}) = \overline{q(\mathbf{x})w_j(\mathbf{y})}, \quad Q_{jk}(\mathbf{r}, \mathbf{s}) = \overline{q(\mathbf{x})w_j(\mathbf{y})w_k(\mathbf{z})}, \end{aligned} \quad (4)$$

where  $\mathbf{r} = \mathbf{y} - \mathbf{x}$ ,  $\mathbf{s} = \mathbf{z} - \mathbf{x}$ ,  $\mathbf{s}' = \mathbf{z}' - \mathbf{x}$ . The dynamical equations are

$$\begin{aligned} \frac{\partial U_{kj}(\mathbf{r})}{\partial r_k} &= 0, \quad \left\{ \frac{\partial}{\partial s_l}, \quad \frac{\partial}{\partial r_k} + \frac{\partial}{\partial s_k} \right\} U_{kjl}(\mathbf{r}, \mathbf{s}) = 0, \quad \frac{\partial U_{(ij)kl}(\mathbf{r}, \mathbf{s})}{\partial r_k} = 0, \quad \frac{\partial Q_k(\mathbf{r})}{\partial r_k} = 0, \quad \frac{\partial Q_{kl}(\mathbf{r}, \mathbf{s})}{\partial r_k} = 0, \\ \left( \frac{\partial}{\partial s'_i} + \frac{\partial}{\partial r_i} + \frac{\partial}{\partial s_i} \right) &U_{ijkl}(\mathbf{s}', \mathbf{r}, \mathbf{s}) = 0, \\ \left( \frac{\partial}{\partial t} + r_2 \frac{\partial}{\partial r_1} \right) &U_{ij}(\mathbf{r}) + \delta_{i1} U_{2j}(\mathbf{r}) + \delta_{j1} U_{i2}(\mathbf{r}) - \frac{\partial U_{ikj}(\mathbf{0}, \mathbf{r})}{\partial r_k} + \frac{\partial U_{jki}(\mathbf{0}, -\mathbf{r})}{\partial r_k} = \frac{\partial Q_j(\mathbf{r})}{\partial r_i} - \frac{\partial Q_i(-\mathbf{r})}{\partial r_j} + 2 \frac{\partial^2 U_{ij}(\mathbf{r})}{\partial r_k \partial r_k}, \\ \left( \frac{\partial}{\partial t} + r_2 \frac{\partial}{\partial r_1} + s_2 \frac{\partial}{\partial s_1} \right) &U_{ijk}(\mathbf{r}, \mathbf{s}) + \delta_{i1} U_{2jk}(\mathbf{r}, \mathbf{s}) + \delta_{j1} U_{i2k}(\mathbf{r}, \mathbf{s}) + \delta_{k1} U_{ij2}(\mathbf{r}, \mathbf{s}) - \left( \frac{\partial}{\partial r_l} + \frac{\partial}{\partial s_l} \right) U_{(il)jk}(\mathbf{r}, \mathbf{s}) \\ &+ \frac{\partial U_{(jl)ik}(-\mathbf{r}, \mathbf{s} - \mathbf{r})}{\partial r_l} + \frac{\partial U_{(kl)ij}(-\mathbf{s}, \mathbf{r} - \mathbf{s})}{\partial s_l} = \left( \frac{\partial}{\partial r_i} + \frac{\partial}{\partial s_i} \right) Q_{jk}(\mathbf{r}, \mathbf{s}) - \frac{\partial Q_{ik}(-\mathbf{r}, \mathbf{s} - \mathbf{r})}{\partial r_j} - \frac{\partial Q_{ij}(-\mathbf{s}, \mathbf{r} - \mathbf{s})}{\partial s_k} \\ &+ 2 \left( \frac{\partial^2}{\partial r_l \partial r_l} + \frac{\partial^2}{\partial s_l \partial s_l} + \frac{\partial^2}{\partial r_l \partial s_l} \right) U_{ijk}(\mathbf{r}, \mathbf{s}), \end{aligned} \quad (5)$$

$$\begin{aligned} \frac{\partial^2 Q(\mathbf{r})}{\partial r_k \partial r_k} &= -2 \frac{\partial Q_2(\mathbf{r})}{\partial r_1} - \frac{\partial^2 Q_{kl}(\mathbf{r}, \mathbf{r})}{\partial r_k \partial r_l}, & \frac{\partial^2 Q_j(\mathbf{r})}{\partial r_k \partial r_k} &= 2 \frac{\partial U_{2j}(\mathbf{r})}{\partial r_1} - \frac{\partial^2 U_{lkj}(\mathbf{0}, \mathbf{r})}{\partial r_k \partial r_l}, \\ \left( \frac{\partial}{\partial r_l} + \frac{\partial}{\partial s_l} \right) \left( \frac{\partial}{\partial r_l} + \frac{\partial}{\partial s_l} \right) Q_{jk}(\mathbf{r}, \mathbf{s}) &= 2 \left( \frac{\partial}{\partial r_1} + \frac{\partial}{\partial s_1} \right) U_{2jk}(\mathbf{r}, \mathbf{s}) - \left( \frac{\partial}{\partial r_m} + \frac{\partial}{\partial s_m} \right) \left( \frac{\partial}{\partial r_l} + \frac{\partial}{\partial s_l} \right) U_{(lm)jk}(\mathbf{r}, \mathbf{s}). \end{aligned}$$

These dynamical equations of evolution act as constraints of equality and can be viewed as such. They represent mathematically the core physics of homogeneous shear turbulence.

To ensure self-consistency, definitions (4) themselves impose the equality constraints of symmetry,

$$\begin{aligned} U_{ij}(\mathbf{r}) &= U_{ji}(-\mathbf{r}), & U_{(ij)k}(\mathbf{r}) &= U_{(ji)k}(\mathbf{r}), & U_{(ij)k}(\mathbf{0}) &= U_{(ik)j}(\mathbf{0}), \\ U_{ijk}(\mathbf{r}, \mathbf{s}) &= U_{ikj}(\mathbf{s}, \mathbf{r}) = U_{jik}(-\mathbf{r}, \mathbf{s} - \mathbf{r}) = U_{kij}(-\mathbf{s}, \mathbf{r} - \mathbf{s}), & U_{(ij)kl}(\mathbf{r}, \mathbf{s}) &= U_{(ji)kl}(\mathbf{r}, \mathbf{s}) = U_{(ij)lk}(\mathbf{s}, \mathbf{r}), \\ U_{(ij)kl}(\mathbf{r}, \mathbf{r}) &= U_{(kl)ij}(-\mathbf{r}, -\mathbf{r}), & U_{(ij)kl}(\mathbf{0}, \mathbf{r}) &= U_{(ik)jl}(\mathbf{0}, \mathbf{r}), & Q(\mathbf{r}) &= Q(-\mathbf{r}), & Q_{ij}(\mathbf{r}, \mathbf{s}) &= Q_{ji}(\mathbf{s}, \mathbf{r}). \end{aligned} \quad (6)$$

Further, motivated by experimental data [5, 8] that give  $U_{13}(\mathbf{0}) = U_{23}(\mathbf{0}) = 0$  and the need to reduce computational size of the problem, we consider the geometric and kinematic symmetries underlying the mean velocity field (1). They suggest inversion and mirror symmetries described by

$$\begin{aligned} U_{ij}(\mathbf{r}) &= U_{ij}(-\mathbf{r}) = (-1)^{\delta_{i3} + \delta_{j3}} U_{\underline{ij}}(\mathbf{r}'), & U_{(ij)k}(\mathbf{r}) &= -U_{(ij)k}(-\mathbf{r}) = (-1)^{\delta_{i3} + \delta_{j3} + \delta_{k3}} U_{(\underline{ij})\underline{k}}(\mathbf{r}'), \\ U_{ijk}(\mathbf{r}, \mathbf{s}) &= -U_{ijk}(-\mathbf{r}, -\mathbf{s}) = (-1)^{\delta_{i3} + \delta_{j3} + \delta_{k3}} U_{\underline{ijk}}(\mathbf{r}', \mathbf{s}'), \\ U_{(ij)kl}(\mathbf{r}, \mathbf{s}) &= U_{(ij)kl}(-\mathbf{r}, -\mathbf{s}) = (-1)^{\delta_{i3} + \delta_{j3} + \delta_{k3} + \delta_{l3}} U_{(\underline{ij})\underline{kl}}(\mathbf{r}', \mathbf{s}'), & Q(\mathbf{r}) &= Q(-\mathbf{r}) = Q(\mathbf{r}'), \\ Q_i(\mathbf{r}) &= -Q_i(-\mathbf{r}) = (-1)^{\delta_{i3}} Q_{\underline{i}}(\mathbf{r}'), & Q_{ij}(\mathbf{r}, \mathbf{s}) &= Q_{ij}(-\mathbf{r}, -\mathbf{s}) = (-1)^{\delta_{i3} + \delta_{j3}} Q_{\underline{ij}}(\mathbf{r}', \mathbf{s}'). \end{aligned} \quad (7)$$

Here,  $\mathbf{r}' = (r_1, r_2, -r_3)$  and  $\mathbf{s}' = (s_1, s_2, -s_3)$ . The summation rule is suspended for the subscripts underlined. The derivation of the equalities is outlined in Appendix A.

Owing to the convenience of explicit representation of the constraints and objective in terms of the control variables and the need to generate standard conic forms for numerical simulation, the problem is formulated in the Fourier wave-number space with the help of Fourier transforms,

$$\begin{aligned} \phi(\mathbf{r}) &= \int_{\mathbb{R}^3} d\mathbf{k} \tilde{\phi}(\mathbf{k}) \exp(i\mathbf{k} \cdot \mathbf{r}), & \phi(\mathbf{r}, \mathbf{s}) &= \int_{\mathbb{R}^3 \times \mathbb{R}^3} d\mathbf{k} d\mathbf{l} \tilde{\phi}(\mathbf{k}, \mathbf{l}) \exp[i(\mathbf{k} \cdot \mathbf{r} + \mathbf{l} \cdot \mathbf{s})], \\ \phi(\mathbf{s}', \mathbf{r}, \mathbf{s}) &= \int_{\mathbb{R}^3 \times \mathbb{R}^3 \times \mathbb{R}^3} d\mathbf{m} d\mathbf{k} d\mathbf{l} \tilde{\phi}(\mathbf{m}, \mathbf{k}, \mathbf{l}) \exp[i(\mathbf{m} \cdot \mathbf{s}' + \mathbf{k} \cdot \mathbf{r} + \mathbf{l} \cdot \mathbf{s})]. \end{aligned}$$

In the wave-number space,  $\tilde{U}_{ij}$ ,  $\tilde{U}_{(ij)kl}$ ,  $\tilde{U}_{ijkl}$ ,  $\tilde{Q}$ , and  $\tilde{Q}_{ij}$  are real,  $\tilde{U}_{(ij)k}$ ,  $\tilde{U}_{ijk}$ , and  $\tilde{Q}_j$  are purely imaginary and are transformed according to

$$\tilde{U}_{(ij)k}(\mathbf{k}) = i \tilde{U}_{(ij)k}^{(I)}(\mathbf{k}), \quad \tilde{U}_{ijk}(\mathbf{k}, \mathbf{l}) = i \tilde{U}_{ijk}^{(I)}(\mathbf{k}, \mathbf{l}), \quad \tilde{Q}_i(\mathbf{k}) = i \tilde{Q}_i^{(I)}(\mathbf{k}). \quad (8)$$

Equations (5) through (7) are transformed as

$$\begin{aligned} k_k \tilde{U}_{kj}(\mathbf{k}) &= 0, & k_k \tilde{U}_{(ij)k}^{(I)}(\mathbf{k}) &= 0, & k_j \tilde{U}_{kjl}^{(I)}(\mathbf{k}, \mathbf{l}) &= 0, & (k_k + l_k) \tilde{U}_{kij}^{(I)}(\mathbf{k}, \mathbf{l}) &= 0, & k_k \tilde{U}_{(ij)kl}(\mathbf{k}, \mathbf{l}) &= 0, \\ (m_i + k_i + l_i) \tilde{U}_{ijkl}(\mathbf{m}, \mathbf{k}, \mathbf{l}) &= 0, \end{aligned} \quad (9a)$$

$$\tilde{Q}(\mathbf{k}) = -\frac{2k_1 \tilde{Q}_2^{(I)}(\mathbf{k})}{|\mathbf{k}|^2} - \frac{k_k k_l}{|\mathbf{k}|^2} \int_{\mathbb{R}^3} d\mathbf{l} \tilde{Q}_{kl}(\mathbf{k} - \mathbf{l}, \mathbf{l}), \quad (9b)$$

$$\tilde{Q}_j^{(I)}(\mathbf{k}) = -\frac{2k_1 \tilde{U}_{2j}(\mathbf{k})}{|\mathbf{k}|^2} - \frac{k_k k_l}{|\mathbf{k}|^2} \int_{\mathbb{R}^3} d\mathbf{l} \tilde{U}_{lkj}^{(I)}(\mathbf{l}, \mathbf{k}), \quad (9c)$$

$$\tilde{Q}_{jk}(\mathbf{k}, \mathbf{l}) = \frac{2(k_1 + l_1) \tilde{U}_{2jk}^{(I)}(\mathbf{k}, \mathbf{l})}{|\mathbf{k} + \mathbf{l}|^2} - \frac{(k_m + l_m)(k_l + l_l) \tilde{U}_{(lm)jk}(\mathbf{k}, \mathbf{l})}{|\mathbf{k} + \mathbf{l}|^2}, \quad (9d)$$

$$\begin{aligned} & \left( \frac{\partial}{\partial t} - k_1 \frac{\partial}{\partial k_2} + 2|\mathbf{k}|^2 \right) \tilde{U}_{ij}(\mathbf{k}) + \delta_{i1} \tilde{U}_{2j}(\mathbf{k}) + \delta_{j1} \tilde{U}_{i2}(\mathbf{k}) \\ & = -k_i \tilde{Q}_j^{(I)}(\mathbf{k}) + k_j \tilde{Q}_i^{(I)}(-\mathbf{k}) - k_k \int_{\mathbb{R}^3} \left( \tilde{U}_{ijk}^{(I)}(\mathbf{k}, \mathbf{l}) - \tilde{U}_{jik}^{(I)}(-\mathbf{k}, \mathbf{l}) \right) d\mathbf{l}, \end{aligned} \quad (9e)$$

$$\begin{aligned} & \left( \frac{\partial}{\partial t} - k_1 \frac{\partial}{\partial k_2} - l_1 \frac{\partial}{\partial l_2} + 2(|\mathbf{k}|^2 + |\mathbf{l}|^2 + \mathbf{k} \cdot \mathbf{l}) \right) \tilde{U}_{ijk}^{(I)}(\mathbf{k}, \mathbf{l}) + \delta_{i1} \tilde{U}_{2jk}^{(I)}(\mathbf{k}, \mathbf{l}) + \delta_{j1} \tilde{U}_{i2k}^{(I)}(\mathbf{k}, \mathbf{l}) + \delta_{k1} \tilde{U}_{ij2}^{(I)}(\mathbf{k}, \mathbf{l}) \\ & = k_i \tilde{Q}_{jk}(\mathbf{k}, \mathbf{l}) + l_i \tilde{Q}_{jk}(\mathbf{k}, \mathbf{l}) - k_j \tilde{Q}_{ik}(-\mathbf{k} - \mathbf{l}, \mathbf{l}) - l_k \tilde{Q}_{ij}(-\mathbf{k} - \mathbf{l}, \mathbf{k}) + (k_l + l_l) \tilde{U}_{(il)jk}(\mathbf{k}, \mathbf{l}) \\ & \quad - k_l \tilde{U}_{(jl)ik}(-\mathbf{k} - \mathbf{l}, \mathbf{l}) - l_l \tilde{U}_{(kl)ij}(-\mathbf{k} - \mathbf{l}, \mathbf{k}), \end{aligned} \quad (9f)$$

and

$$\begin{aligned} \tilde{U}_{ij}(\mathbf{k}) &= \tilde{U}_{ji}(\mathbf{k}) = \tilde{U}_{ij}(-\mathbf{k}) = (-1)^{\delta_{i3} + \delta_{j3}} \tilde{U}_{\underline{j}\underline{i}}(\mathbf{k}'), \quad \tilde{U}_{(ij)k}^{(I)}(\mathbf{k}) = \tilde{U}_{(ji)k}^{(I)}(\mathbf{k}) = -\tilde{U}_{(ij)k}^{(I)}(-\mathbf{k}) = (-1)^{\delta_{i3} + \delta_{j3} + \delta_{k3}} \tilde{U}_{(\underline{j}\underline{i})\underline{k}}^{(I)}(\mathbf{k}'), \\ \tilde{U}_{ijk}^{(I)}(\mathbf{k}, \mathbf{l}) &= \tilde{U}_{ikj}^{(I)}(\mathbf{l}, \mathbf{k}) = \tilde{U}_{jik}^{(I)}(-\mathbf{k} - \mathbf{l}, \mathbf{l}) = \tilde{U}_{kij}^{(I)}(-\mathbf{k} - \mathbf{l}, \mathbf{k}) = -\tilde{U}_{ijk}^{(I)}(-\mathbf{k}, -\mathbf{l}) = (-1)^{\delta_{i3} + \delta_{j3} + \delta_{k3}} \tilde{U}_{\underline{j}\underline{i}\underline{k}}^{(I)}(\mathbf{k}', \mathbf{l}'), \\ \tilde{U}_{(ij)kl}(\mathbf{k}, \mathbf{l}) &= \tilde{U}_{(ji)kl}(\mathbf{k}, \mathbf{l}) = \tilde{U}_{(ij)lk}(\mathbf{l}, \mathbf{k}) = \tilde{U}_{(ij)kl}(-\mathbf{k}, -\mathbf{l}) = (-1)^{\delta_{i3} + \delta_{j3} + \delta_{k3} + \delta_{l3}} \tilde{U}_{(\underline{j}\underline{i})\underline{k}\underline{l}}(\mathbf{k}', \mathbf{l}'), \\ \int_{\mathbb{R}^3} d\mathbf{k} \left[ \tilde{U}_{(ij)kl}(\mathbf{k}, \mathbf{l}) - \tilde{U}_{(ik)jl}(\mathbf{k}, \mathbf{l}) \right] &= 0, \quad \int_{\mathbb{R}^3} d\mathbf{l} \left[ \tilde{U}_{(ij)kl}(\mathbf{k} + \mathbf{l}, -\mathbf{l}) - \tilde{U}_{(kl)ij}(\mathbf{k} + \mathbf{l}, -\mathbf{l}) \right] = 0, \\ \tilde{Q}(\mathbf{k}) &= \tilde{Q}(-\mathbf{k}) = \tilde{Q}(\mathbf{k}'), \quad \tilde{Q}_i^{(I)}(\mathbf{k}) = -\tilde{Q}_i^{(I)}(-\mathbf{k}) = (-1)^{\delta_{i3}} \tilde{Q}_{\underline{i}}^{(I)}(\mathbf{k}'), \\ \tilde{Q}_{ij}(\mathbf{k}, \mathbf{l}) &= \tilde{Q}_{ij}(-\mathbf{k}, -\mathbf{l}) = \tilde{Q}_{ji}(\mathbf{l}, \mathbf{k}) = (-1)^{\delta_{i3} + \delta_{j3}} \tilde{Q}_{\underline{j}\underline{i}}(\mathbf{k}', \mathbf{l}'), \end{aligned} \quad (10)$$

where  $\mathbf{k}' = (k_1, k_2, -k_3)$ ,  $\mathbf{l}' = (l_1, l_2, -l_3)$ .

The structure of Eqs. (9) provides the ground to introduce the second-order model and the third-order model.

### A. The second-order model

Equations (9c) and (9e) indicate that  $\tilde{U}_{ijk}^{(I)}$  affect  $\tilde{U}_{ij}$  only through the degenerate and contracted  $k_k \tilde{U}_{(ki)j}^{(I)}(\mathbf{k})$ . Therefore, the second-order model is formulated with

$$\tilde{\Gamma}_{ij}(\mathbf{k}) = k_k \tilde{U}_{(ki)j}^{(I)}(\mathbf{k}) \quad (11)$$

as the control variables. The constraint of  $k_j \tilde{\Gamma}_{ij}(\mathbf{k}) = 0$  from Eqs. (9a) yields

$$\tilde{\Gamma}_{j3}(\mathbf{k}) = -\frac{(k_1 \tilde{\Gamma}_{j1} + k_2 \tilde{\Gamma}_{j2})(\mathbf{k})}{k_3}, \quad (12)$$

which implies that  $\tilde{\Gamma}_{ij}$ ,  $i = 1, 2, 3$ ,  $j = 1, 2$ , act as the primary control variables.

Correlations  $\tilde{U}_{ij}$  are state variables. Equations (9a) are solved to obtain

$$\tilde{U}_{j3}(\mathbf{k}) = -\frac{(k_1 \tilde{U}_{j1} + k_2 \tilde{U}_{j2})(\mathbf{k})}{k_3}, \quad j = 1, 2, \quad \tilde{U}_{33}(\mathbf{k}) = \frac{((k_1)^2 \tilde{U}_{11} + (k_2)^2 \tilde{U}_{22} + 2k_1 k_2 \tilde{U}_{12})(\mathbf{k})}{(k_3)^2}. \quad (13)$$

That is,  $\tilde{U}_{11}$ ,  $\tilde{U}_{12}$ , and  $\tilde{U}_{22}$  are treated as the primary components of  $\tilde{U}_{ij}$ . Their equations of evolution are derived from Eqs. (9e),

$$\begin{aligned} & \frac{\exp[-2H(\mathbf{k})]}{2|\mathbf{k}|^4} \left( \frac{\partial}{\partial t} - k_1 \frac{\partial}{\partial k_2} \right) \left( |\mathbf{k}|^4 \exp[2H(\mathbf{k})] \tilde{U}_{22}(\mathbf{k}) \right) = \frac{k_2 k_l \tilde{\Gamma}_{l2}(\mathbf{k})}{|\mathbf{k}|^2} - \tilde{\Gamma}_{22}(\mathbf{k}), \\ & \frac{\exp[-2H(\mathbf{k})]}{|\mathbf{k}|^2} \left( \frac{\partial}{\partial t} - k_1 \frac{\partial}{\partial k_2} \right) \left( |\mathbf{k}|^2 \exp[2H(\mathbf{k})] \tilde{U}_{12}(\mathbf{k}) \right) + \left( 1 - \frac{2(k_1)^2}{|\mathbf{k}|^2} \right) \tilde{U}_{22}(\mathbf{k}) \\ & = \frac{k_l [k_1 \tilde{\Gamma}_{l2}(\mathbf{k}) + k_2 \tilde{\Gamma}_{l1}(\mathbf{k})]}{|\mathbf{k}|^2} - \tilde{\Gamma}_{12}(\mathbf{k}) - \tilde{\Gamma}_{21}(\mathbf{k}), \\ & \frac{\exp[-2H(\mathbf{k})]}{2} \left( \frac{\partial}{\partial t} - k_1 \frac{\partial}{\partial k_2} \right) \left( \exp[2H(\mathbf{k})] \tilde{U}_{11}(\mathbf{k}) \right) + \left( 1 - \frac{2(k_1)^2}{|\mathbf{k}|^2} \right) \tilde{U}_{12}(\mathbf{k}) = \frac{k_1 k_l \tilde{\Gamma}_{l1}(\mathbf{k})}{|\mathbf{k}|^2} - \tilde{\Gamma}_{11}(\mathbf{k}), \end{aligned} \quad (14)$$

where

$$H(\mathbf{k}) = -\frac{k_2}{k_1} \left( (k_1)^2 + \frac{1}{3}(k_2)^2 + (k_3)^2 \right).$$

The remaining component equations of Eqs. (9e) are redundant. These differential equations may be solved under initial conditions and the boundary conditions of

$$\lim_{k_2 \rightarrow \pm\infty} \tilde{U}_{ij}(\mathbf{k}) = 0, \quad (15)$$

owing to the physical boundedness of  $U_{ij}(\mathbf{r})$ .

Four sets of constraints are present for  $\{\tilde{\Gamma}_{ij} : i = 1, 2, 3, j = 1, 2\}$ . (a) The symmetries of  $\tilde{U}_{ij}$  in Eqs. (10), linked by Eqs. (13) and (14). (b) The symmetries of  $\tilde{U}_{(ij)k}$  in Eqs. (10) require that

$$\tilde{\Gamma}_{ij}(\mathbf{k}) = \tilde{\Gamma}_{ij}(-\mathbf{k}) = (-1)^{\delta_{i3} + \delta_{j3}} \tilde{\Gamma}_{\underline{ij}}(\mathbf{k}'), \quad \mathbf{k}' = (k_1, k_2, -k_3). \quad (16)$$

(c) The conditions  $(k_k + l_k)\tilde{U}_{kij}^{(I)}(\mathbf{k}, \mathbf{l}) = 0$  from Eqs. (9a) result in (details in Appendix B)

$$\int_{-\infty}^0 dk_1 \int_{\mathbb{R}^2} dk_2 dk_3 \left( \tilde{\Gamma}_{ij}(\mathbf{k}) + \tilde{\Gamma}_{ji}(\mathbf{k}) \right) = 0, \quad i \leq j. \quad (17)$$

(d) Constraints of inequality (25) formulated in Subsec. II C.

Correlations  $\tilde{Q}_j^{(I)}$  are state variables. Equations (9c), (12), and (13) yield

$$k_j \tilde{Q}_j^{(I)}(\mathbf{k}) = 0. \quad (18)$$

Combining the contracted Eqs. (9e) ( $i = j$ ) and Eq. (18) produces

$$\left( \frac{\partial}{\partial t} - k_1 \frac{\partial}{\partial k_2} + 2|\mathbf{k}|^2 \right) \tilde{U}_{jj}(\mathbf{k}) + 2\tilde{U}_{12}(\mathbf{k}) = -2\tilde{\Gamma}_{jj}(\mathbf{k}). \quad (19)$$

Next, combination of Eqs. (17) and (19) leads to the known relationship,

$$\frac{\partial U_{jj}(\mathbf{0})}{\partial t} + 2U_{12}(\mathbf{0}) - 2 \frac{\partial^2 U_{jj}(\mathbf{r})}{\partial r_k \partial r_k} \Big|_{\mathbf{r}=\mathbf{0}} = 0, \quad (20)$$

which is satisfied automatically. The structures of Eqs. (19) and (20) indicate that Eqs. (17) and (18) play the known role of distributing  $\tilde{U}_{kk}$  among its components  $\tilde{U}_{\underline{ii}}$  and distributing  $U_{kk}(\mathbf{0})$  among its components  $U_{\underline{ii}}(\mathbf{0})$ .

It is noticed that the second-order model has  $\{\tilde{U}_{ij}, U_{ij}, \tilde{Q}_j^{(I)}, Q_j\}$  as its state variables and  $\tilde{\Gamma}_{ji}$  as the control variables.

## B. The third-order model

The third-order model contains correlations up to the degenerate fourth order  $\tilde{U}_{(ij)kl}$ .  $\tilde{U}_{ij}$ ,  $\tilde{U}_{ijk}^{(I)}$ ,  $\tilde{Q}$ ,  $\tilde{Q}_i^{(I)}$ ,  $\tilde{Q}_{ij}$ , and their correspondences in the physical space are the state variables,  $\tilde{U}_{(ij)kl}$  and  $U_{(ij)kl}$  act as the control variables.

The evolution of  $\tilde{U}_{ij}$  is governed by Eqs. (13) and (14).  $\tilde{Q}$ ,  $\tilde{Q}_i^{(I)}$ , and  $\tilde{Q}_{ij}$  are given by Eqs. (9b) through (9d). It follows from Eqs. (9a) and (10) that  $\tilde{U}_{ijk}^{(I)}$  may be represented linearly in terms of  $\tilde{U}_{111}^{(I)}$ ,  $\tilde{U}_{112}^{(I)}$ ,  $\tilde{U}_{122}^{(I)}$ , and  $\tilde{U}_{222}^{(I)}$  as the primary components (details in Appendix C). The equations of evolution for these primary components are derived

from Eqs. (9f),

$$\begin{aligned}
& \frac{\exp[-H(\mathbf{k}, \mathbf{l})]}{|\mathbf{k}|^2 |\mathbf{l}|^2 |\mathbf{k} + \mathbf{l}|^2} \left( \frac{\partial}{\partial t} - k_1 \frac{\partial}{\partial k_2} - l_1 \frac{\partial}{\partial l_2} \right) \left( |\mathbf{k}|^2 |\mathbf{l}|^2 |\mathbf{k} + \mathbf{l}|^2 \exp[H(\mathbf{k}, \mathbf{l})] \tilde{U}_{222}^{(I)}(\mathbf{k}, \mathbf{l}) \right) \\
&= (k_l + l_l) \tilde{U}_{(2l)22}(\mathbf{k}, \mathbf{l}) - (k_2 + l_2) \frac{(k_m + l_m)(k_l + l_l)}{|\mathbf{k} + \mathbf{l}|^2} \tilde{U}_{(lm)22}(\mathbf{k}, \mathbf{l}) - \left( k_l \tilde{U}_{(2l)22} - k_2 \frac{k_m k_l}{|\mathbf{k}|^2} \tilde{U}_{(lm)22} \right) (-\mathbf{k} - \mathbf{l}, \mathbf{l}) \\
&\quad - \left( l_l \tilde{U}_{(2l)22} - l_2 \frac{l_m l_l}{|\mathbf{l}|^2} \tilde{U}_{(lm)22} \right) (-\mathbf{k} - \mathbf{l}, \mathbf{k}), \\
& \frac{\exp[-H(\mathbf{k}, \mathbf{l})]}{|\mathbf{k}|^2 |\mathbf{l}|^2} \left( \frac{\partial}{\partial t} - k_1 \frac{\partial}{\partial k_2} - l_1 \frac{\partial}{\partial l_2} \right) \left( |\mathbf{k}|^2 |\mathbf{l}|^2 \exp[H(\mathbf{k}, \mathbf{l})] \tilde{U}_{122}^{(I)}(\mathbf{k}, \mathbf{l}) \right) + \left( 1 - \frac{2(k_1 + l_1)^2}{|\mathbf{k} + \mathbf{l}|^2} \right) \tilde{U}_{222}^{(I)}(\mathbf{k}, \mathbf{l}) \\
&= (k_l + l_l) \tilde{U}_{(1l)22}(\mathbf{k}, \mathbf{l}) - (k_1 + l_1) \frac{(k_m + l_m)(k_l + l_l)}{|\mathbf{k} + \mathbf{l}|^2} \tilde{U}_{(lm)22}(\mathbf{k}, \mathbf{l}) - \left( k_l \tilde{U}_{(2l)12} - k_2 \frac{k_m k_l}{|\mathbf{k}|^2} \tilde{U}_{(lm)12} \right) (-\mathbf{k} - \mathbf{l}, \mathbf{l}) \\
&\quad - \left( l_l \tilde{U}_{(2l)12} - l_2 \frac{l_m l_l}{|\mathbf{l}|^2} \tilde{U}_{(lm)12} \right) (-\mathbf{k} - \mathbf{l}, \mathbf{k}), \\
& \frac{\exp[-H(\mathbf{k}, \mathbf{l})]}{|\mathbf{l}|^2} \left( \frac{\partial}{\partial t} - k_1 \frac{\partial}{\partial k_2} - l_1 \frac{\partial}{\partial l_2} \right) \left( |\mathbf{l}|^2 \exp[H(\mathbf{k}, \mathbf{l})] \tilde{U}_{112}^{(I)}(\mathbf{k}, \mathbf{l}) \right) + \left( 1 - \frac{2(k_1 + l_1)^2}{|\mathbf{k} + \mathbf{l}|^2} \right) \tilde{U}_{122}^{(I)}(-\mathbf{k} - \mathbf{l}, \mathbf{l}) \\
&+ \left( 1 - \frac{2(k_1)^2}{|\mathbf{k}|^2} \right) \tilde{U}_{122}^{(I)}(\mathbf{k}, \mathbf{l}) = (k_l + l_l) \tilde{U}_{(1l)12}(\mathbf{k}, \mathbf{l}) - (k_1 + l_1) \frac{(k_m + l_m)(k_l + l_l)}{|\mathbf{k} + \mathbf{l}|^2} \tilde{U}_{(lm)12}(\mathbf{k}, \mathbf{l}) \\
&\quad - \left( k_l \tilde{U}_{(1l)12} - k_1 \frac{k_m k_l}{|\mathbf{k}|^2} \tilde{U}_{(lm)12} \right) (-\mathbf{k} - \mathbf{l}, \mathbf{l}) - \left( l_l \tilde{U}_{(2l)11} - l_2 \frac{l_m l_l}{|\mathbf{l}|^2} \tilde{U}_{(lm)11} \right) (-\mathbf{k} - \mathbf{l}, \mathbf{k}), \\
& \exp[-H(\mathbf{k}, \mathbf{l})] \left( \frac{\partial}{\partial t} - k_1 \frac{\partial}{\partial k_2} - l_1 \frac{\partial}{\partial l_2} \right) \left( \exp[H(\mathbf{k}, \mathbf{l})] \tilde{U}_{111}^{(I)}(\mathbf{k}, \mathbf{l}) \right) + \left( 1 - \frac{2(k_1 + l_1)^2}{|\mathbf{k} + \mathbf{l}|^2} \right) \tilde{U}_{112}^{(I)}(\mathbf{l}, -\mathbf{k} - \mathbf{l}) \\
&+ \left( 1 - \frac{2(k_1)^2}{|\mathbf{k}|^2} \right) \tilde{U}_{112}^{(I)}(\mathbf{l}, \mathbf{k}) + \left( 1 - \frac{2(l_1)^2}{|\mathbf{l}|^2} \right) \tilde{U}_{112}^{(I)}(\mathbf{k}, \mathbf{l}) = (k_l + l_l) \tilde{U}_{(1l)11}(\mathbf{k}, \mathbf{l}) - (k_1 + l_1) \frac{(k_m + l_m)(k_l + l_l)}{|\mathbf{k} + \mathbf{l}|^2} \tilde{U}_{(lm)11}(\mathbf{k}, \mathbf{l}) \\
&\quad - \left( k_l \tilde{U}_{(1l)11} - k_1 \frac{k_m k_l}{|\mathbf{k}|^2} \tilde{U}_{(lm)11} \right) (-\mathbf{k} - \mathbf{l}, \mathbf{l}) - \left( l_l \tilde{U}_{(1l)11} - l_1 \frac{l_m l_l}{|\mathbf{l}|^2} \tilde{U}_{(lm)11} \right) (-\mathbf{k} - \mathbf{l}, \mathbf{k}),
\end{aligned} \tag{21}$$

where

$$H(\mathbf{k}, \mathbf{l}) = H(\mathbf{k}) + H(\mathbf{l}) + H(\mathbf{k} + \mathbf{l}).$$

The remaining component equations of Eqs. (9f) are redundant. Equations (21) may be solved with initial conditions and the boundary conditions of

$$\lim_{k_2 \rightarrow \pm\infty} \tilde{U}_{ijk}^{(I)}(\mathbf{k}, \mathbf{l}) = \lim_{l_2 \rightarrow \pm\infty} \tilde{U}_{ijk}^{(I)}(\mathbf{k}, \mathbf{l}) = 0, \tag{22}$$

owing to the physical boundedness of  $U_{ijk}(\mathbf{r}, \mathbf{s})$ . All the state variables may be represented in terms of  $\tilde{U}_{(ij)kl}$  linearly via the equations presented.

As control variables,  $\tilde{U}_{(ij)kl}$  are simplified further with the solution of Eqs. (9a),

$$\tilde{U}_{(ij)3l}(\mathbf{k}, \mathbf{l}) = -\frac{k_1}{k_3} \tilde{U}_{(ij)1l}(\mathbf{k}, \mathbf{l}) - \frac{k_2}{k_3} \tilde{U}_{(ij)2l}(\mathbf{k}, \mathbf{l}), \quad ij = 11, 12, 13, 22, 23, 33, \quad l = 1, 2, 3. \tag{23}$$

The specifically listed  $\tilde{U}_{(ij)kl}$  are the primary components of  $\tilde{U}_{(ij)kl}$  and the primary control variables. The components not present are found via Eqs. (10).

The last of Eqs. (9a) are integrated to produce

$$\int_{\mathbb{R}^3 \times \mathbb{R}^3} d\mathbf{k} d\mathbf{l} [k_i (\tilde{U}_{(ik)jl}(\mathbf{k}, \mathbf{l}) + \tilde{U}_{(ij)kl}(\mathbf{k}, \mathbf{l})) + l_i \tilde{U}_{(ij)kl}(\mathbf{k}, \mathbf{l})] = 0. \tag{24}$$

Further,  $\tilde{U}_{(ij)kl}$  are constrained by Eqs. (10) and (25) and those outlined in Subsec. II D.

The third-order model faces the issue of whether the multi-point correlations are experimentally measurable and how its predictions are evaluated, this is briefly commented on here: (a) Two-point correlations involving  $w_i(\mathbf{x})$  and

$w_j(\mathbf{y})$ , such as  $U_{ij}(\mathbf{r})$ ,  $U_{ijk}(\mathbf{0}, \mathbf{r})$ , and  $U_{(ij)kl}(\mathbf{0}, \mathbf{r})$ , may be measured experimentally for  $\mathbf{x}$  and  $\mathbf{y}$  in certain subregions by two hot-wire probes (restricted by interferences with the flow and between the probes) [27]. (b) These two-point correlations may be computed from  $\tilde{U}_{ij}$ ,  $\tilde{U}_{ijk}$ , and  $\tilde{U}_{(ij)kl}$  within the model, the predicted values may be compared with the measured ones.

We use the Cauchy-Schwarz inequality and the non-negativity of variance of products to construct constraints for the state and control variables. These constraints are classified into two groups, based on whether they involve only  $\tilde{U}_{ij}$  or involve  $\tilde{U}_{(ij)kl}$ , and are discussed in the two succeeding subsections.

### C. Constraints of inequality involving only $\tilde{U}_{ij}$

This subsection focuses on the constraints of inequality involving only  $\tilde{U}_{ij}$  that may be enforced within either of the two models. The constraints are constructed on the basis of the Cauchy-Schwarz inequality  $|\overline{ab}|^2 \leq \overline{aa} \overline{bb}$  applied to  $\overline{w_i(\mathbf{x})w_j(\mathbf{y})}$  and related structure functions.

It is straight-forward to apply  $|\overline{ab}|^2 \leq \overline{aa} \overline{bb}$  to

$$\overline{w_i(\mathbf{x})w_j(\mathbf{y})}, \overline{w_i(\mathbf{x})w_{j,k}(\mathbf{y})}, \overline{w_{i,k}(\mathbf{x})w_{j,l}(\mathbf{y})}, \dots$$

to generate constraints for  $\tilde{U}_{ij}$ . The structure of these integral inequalities in the wave-number space motivate us to adopt

$$0 \leq \tilde{U}_{ii}(\mathbf{k}), \quad |\tilde{U}_{ij}(\mathbf{k})|^2 \leq \tilde{U}_{ii}(\mathbf{k}) \tilde{U}_{jj}(\mathbf{k}), \quad i < j. \quad (25)$$

These six inequalities play a rather elementary or fundamental role, as demonstrated below by examples.

Firstly, as a special and physical case, Eqs. (25) guarantee the positive semi-definiteness of the Reynolds stress tensor  $\overline{w_i(\mathbf{x})w_j(\mathbf{x})}$  and the non-negativity of the viscous dissipation  $\overline{w_{j,k}(\mathbf{x})w_{j,k}(\mathbf{x})}$ ; These are the realizability conditions usually addressed in engineering turbulence modeling methodology [14].

Secondly, it is verified directly (see Appendix D) that Eqs. (25) result in

$$0 \leq \overline{\tilde{\omega}_i \tilde{\omega}_i}(\mathbf{k}), \quad |\overline{\tilde{\omega}_i \tilde{\omega}_j}(\mathbf{k})|^2 \leq \overline{\tilde{\omega}_i \tilde{\omega}_i}(\mathbf{k}) \overline{\tilde{\omega}_j \tilde{\omega}_j}(\mathbf{k}), \quad |\overline{\tilde{w}_i \tilde{\omega}_j}(\mathbf{k})|^2 \leq \tilde{U}_{ii}(\mathbf{k}) \overline{\tilde{\omega}_j \tilde{\omega}_j}(\mathbf{k}). \quad (26)$$

Here,  $\omega_i$  denotes the vorticity fluctuation field,

$$\omega_i(\mathbf{x}) = \epsilon_{imn} w_{m,n}(\mathbf{x}), \quad \overline{\tilde{\omega}_i \tilde{\omega}_j}(\mathbf{k}) = \epsilon_{imn} \epsilon_{jkl} k_n k_l \tilde{U}_{mk}(\mathbf{k}), \quad \overline{\tilde{w}_i \tilde{\omega}_j}(\mathbf{k}) = \nu \epsilon_{j pq} k_q \tilde{U}_{ip}(\mathbf{k}), \quad (27)$$

$\epsilon_{ijk}$  is the alternating tensor. Together with Eqs. (25), Eqs. (26) guarantee satisfaction of the integral constraints generated by the application of  $|\overline{ab}|^2 \leq \overline{aa} \overline{bb}$  to

$$\overline{w_i(\mathbf{x})\omega_j(\mathbf{y})}, \overline{\omega_i(\mathbf{x})\omega_j(\mathbf{y})}, \overline{\omega_i(\mathbf{x})\omega_{j,k}(\mathbf{y})}, \dots$$

Thirdly, the structure of the aforementioned integral inequalities, together with Eqs. (25) and (26), suggests that the following group be considered,

$$|\tilde{c}(\mathbf{k})|^2 \leq \tilde{a}(\mathbf{k}) \tilde{b}(\mathbf{k}), \quad 0 \leq \tilde{a}(\mathbf{k}), \quad 0 \leq \tilde{b}(\mathbf{k}); \quad |f_c|^2 \leq f_a f_b, \quad 0 \leq f_a, \quad 0 \leq f_b, \quad (28)$$

where  $f_a$ ,  $f_b$ , and  $f_c$  are non-stochastic functions of  $\mathbf{k}$ , spatial vectors, and time, associated with  $\tilde{a}$ ,  $\tilde{b}$ , and  $\tilde{c}$ , respectively. Inequalities (28) can be operated on to obtain (see Appendix D)

$$\left| \int_{\mathbb{R}^3} d\mathbf{k} \tilde{c}(\mathbf{k}) f_c \right|^2 \leq \int_{\mathbb{R}^3} d\mathbf{k} \tilde{a}(\mathbf{k}) f_a \int_{\mathbb{R}^3} d\mathbf{k} \tilde{b}(\mathbf{k}) f_b. \quad (29)$$

Inequalities (28) and (29) are applicable to the constraints generated by  $|\overline{ab}|^2 \leq \overline{aa} \overline{bb}$  like the combinatoric sets from

$$a, b \in \{w_i(\mathbf{y}) - w_i(\mathbf{x}) + \alpha[w_i(\mathbf{z}') - w_i(\mathbf{z})], \quad \omega_i(\mathbf{z}') - \omega_i(\mathbf{z}) - \beta[\omega_i(\mathbf{y}) - \omega_i(\mathbf{x})]\}, \quad (30)$$

where  $\alpha$  and  $\beta$  are non-stochastic functions of time and spatial vectors (details in Appendix D).

A general argument for the role of Eqs. (25) in cases other than Eqs. (28) is not yet obtained. The advantage of Eqs. (25) is that they are local (relative to Eq. (29)) and they eliminate the great computational size and complexity associated with the global integral and space-dependent constraint (29). The resulting simplification allows us to solve the second-order model numerically.

### D. Constraints of inequality involving $\tilde{U}_{(ij)kl}$

The third-order model includes constraints involving  $\tilde{U}_{(ij)kl}$ . One way to construct such constraints is to apply the Cauchy-Schwarz inequality  $|\overline{ab}|^2 \leq \overline{aa}\overline{bb}$  to a correlation among  $w_i(\mathbf{x})$ ,  $q(\mathbf{y})$ , and their spatial and temporal derivatives, such as

$$\overline{w_i(\mathbf{x})w_j(\mathbf{y})w_k(\mathbf{z})}, \quad \overline{q(\mathbf{x})w_i(\mathbf{y})}, \quad \overline{w_i(\mathbf{x})w_j(\mathbf{x})w_k(\mathbf{y})w_l(\mathbf{z})}, \quad \overline{q(\mathbf{x})q(\mathbf{y})}, \quad \overline{q(\mathbf{x})w_i(\mathbf{y})w_j(\mathbf{z})}, \quad \overline{w_i(\mathbf{x})\partial w_j(\mathbf{y})/\partial t}, \quad \dots$$

The condition is that the resulting inequality involves only the state and control variables within the model. Similarly, we may apply  $|\overline{ab}|^2 \leq \overline{aa}\overline{bb}$  to structure functions involving the above correlations. These constraints are not formulated here, since the present study focuses on the second-order model. To reduce computational size, two closely related issues pertinent to our investigation are yet to be studied: (a) how to generate selectively the structure function-based inequalities without much redundancy; (b) whether there are elementary inequalities analogous to Eqs. (25).

Within the third-order model, we may also construct constraints involving  $\tilde{U}_{(ij)kl}$  by applying the non-negativity of variance of products,

$$0 \leq \overline{(ab - \overline{ab})^2}, \quad (\overline{ab})^2 \leq \overline{aabb}. \quad (31)$$

For instance, in the simple cases of

$$\{a = w_i(\mathbf{x}), b = w_j(\mathbf{y})\} \text{ and } \{a = w_{\underline{i}}(\mathbf{x}) - w_{\underline{j}}(\mathbf{x}), b = w_{\underline{i}}(\mathbf{y}) + w_{\underline{j}}(\mathbf{y})\},$$

Eq. (31), along with Eqs. (10), produces

$$(U_{ij}(\mathbf{r}))^2 \leq U_{(\underline{ii})\underline{jj}}(\mathbf{r}, \mathbf{r}), \quad |U_{\underline{ii}}(\mathbf{r}) - U_{\underline{jj}}(\mathbf{r})|^2 \leq U_{(\underline{ii})\underline{ii}}(\mathbf{r}, \mathbf{r}) + U_{(\underline{jj})\underline{jj}}(\mathbf{r}, \mathbf{r}) + 2U_{(\underline{ii})\underline{jj}}(\mathbf{r}, \mathbf{r}) - 4U_{(\underline{ij})\underline{ij}}(\mathbf{r}, \mathbf{r}). \quad (32)$$

More such inequalities may be produced via

$$a, b \in \{w_{\underline{i}}(\mathbf{y}) + \alpha w_{\underline{j}}(\mathbf{x}), \omega_{\underline{i}}(\mathbf{y}) + \alpha \omega_{\underline{j}}(\mathbf{x}), w_j(\mathbf{y}) - w_j(\mathbf{x}) + \alpha[w_j(\mathbf{z}) - w_j(\mathbf{x})], \omega_j(\mathbf{y}) - \omega_j(\mathbf{x}) + \alpha[\omega_j(\mathbf{z}) - \omega_j(\mathbf{x})], \dots\}.$$

The condition on the choice of  $a$  and  $b$  is that  $\overline{ab}$  and  $\overline{aabb}$  are resolvable within the third-order model.

Since Eqs. (14) and (21) imply that  $\tilde{U}_{ij}$  depend linearly on  $\tilde{U}_{(ij)kl}$  (peculiar to homogeneous turbulence), the left-hand sides of Eqs. (32) and (31) depend on  $\tilde{U}_{(ij)kl}^{(\infty)}$  quadratically while the right-hand sides depend on  $\tilde{U}_{(ij)kl}^{(\infty)}$  linearly. It then follows that, along with constraints from the Cauchy-Schwarz inequality, Eqs. (32) and (31) impose an upper bound on  $|\tilde{U}_{(ij)kl}|$  and in turn an upper bound on  $|U_{ij}|$  and an upper bound on  $|U_{ijk}|$ .

### E. Closure and objective functional

To make the models closed, a conventional scheme, like QN [3], adds another set of equality constraints, such as approximating the fourth order correlations in terms of the lower ones within the third-order model. The added ones act effectively as exact equality constraints in simulation and tend to be incompatible with some of the constraints discussed above, as demonstrated specifically in the case of isotropic turbulence [6, 7]. This incompatibility is also hinted at by the inequalities (32). In the light of the large number and varied origins of constraints, it is expected that such an equality closure approach cannot satisfy all of them. These observations motivate us to pursue a framework where all the constraints and the dynamical equations are satisfied through the adoption of an objective to be optimized, inspired by theories of optimal control and optimization. This strategy transfers the task of closure to the construction of an adequate objective.

Since the present framework involves ensemble statistical average of the fluctuating velocity and pressure fields, a probability density functional is required, parallel to Eqs. (3). However, from the perspective of numerical simulation, the domain of motion is approximated by a computational box, the fluctuation velocity and pressure fields are approximated by the use of a truncated Fourier series, an effective probability density function  $f$  may then be used to describe the discretized fluctuations statistically. Next,  $f$  is used to construct a Shannon entropy. Motivated by the underlying idea of unbiased guess and many successful applications [15–18], the maximization of Shannon entropy is employed to determine the structure of  $f$ ; The optimal  $f$  has the broadest spread-out. The analysis is straight-forward but lengthy, and is presented in Appendix E.

It is impractical to implement the Shannon entropy maximization because of its formidable computational size and numerical integration of high dimensions. The analysis, however, reveals the necessity of  $U_{kk}(\mathbf{r})$  as an alternative objective to be maximized, on the following grounds. (a) The optimal  $f$  is characterized partially by large values of the second order moments, this results in overall large  $U_{ii}(\mathbf{r})$ . (b) Since  $U_{ii}(\mathbf{r})$  are the lowest order correlations in the framework, they satisfy the need that an objective characterize directly and collectively the effects of all the dynamical equations and all the constraints. (c) A scalar is required, independent of the coordinate systems, transforming  $U_{ii}(\mathbf{r})$  into  $U_{kk}(\mathbf{r})$ .

To have a single value to evaluate, the  $\mathbf{r}$ -dependence of  $U_{kk}(\mathbf{r})$  may be resolved in two ways:  $U_{kk}(\mathbf{0})$  (proportional to turbulent energy per unit volume) and  $\int_{\mathbb{R}^3} U_{kk}(\mathbf{r}) d\mathbf{r}$  (overall). They are related to each other through

$$U_{kk}(\mathbf{0}) = \int_{\mathbb{R}^3} d\mathbf{r} U_{kk}(\mathbf{r}) \delta(\mathbf{r}),$$

where  $\delta(\mathbf{r})$  is the Dirac delta. The relation illustrates the local character of  $U_{kk}(\mathbf{0})$  (localized by  $\delta(\mathbf{r})$ ) against the overall global character of  $\int_{\mathbb{R}^3} d\mathbf{r} U_{kk}(\mathbf{r})$ : The maximization of the latter produces a more uniform distribution of  $U_{kk}(\mathbf{r})$  throughout the space  $\mathbf{r}$ , in contrast to the former (whose  $U_{kk}(\mathbf{r})$  has much larger values in a neighborhood of  $\mathbf{r} = \mathbf{0}$ , because of  $\max U_{kk}(\mathbf{0})$ ). This greater uniformity reflects the essence of the optimal  $f$  being the broadest, without unduly larger  $U_{kk}(\mathbf{r})$  in a subregion. Further, as presented in Appendix L, simulation of the second-order model in the asymptotic steady state under  $\max U_{kk}(\mathbf{0})$  produces the numerical order pattern,  $U_{11}^{(\infty)}(\mathbf{0}) > U_{22}^{(\infty)}(\mathbf{0}) > U_{33}^{(\infty)}(\mathbf{0})$ , which is inconsistent with the experimentally obtained  $U_{11}^{(\infty)}(\mathbf{0}) > U_{33}^{(\infty)}(\mathbf{0}) > U_{22}^{(\infty)}(\mathbf{0})$  [8]. Thus, we take

$$\int_{\mathbb{R}^3} d\mathbf{r} U_{kk}(\mathbf{r}) = \int_{\mathbb{R}^3} d\mathbf{r} \int_{\mathbb{R}^3} d\mathbf{k} \tilde{U}_{kk}(\mathbf{k}) \cos(\mathbf{r} \cdot \mathbf{k}) \quad (\text{to be maximized}) \quad (33)$$

as the objective functional in the framework, which can be expressed in terms of the primary control variables in the second-order model (through the solution of Eqs. (14)) and in the third-order model (through the solutions of Eqs. (14) and (21)).

The above argument for Eq. (33) is essentially a mathematical application of Shannon entropy maximization. We now interpret and substantiate the content of Eq. (33) from a physical perspective, especially relate the integral structure to the nonlocal nature of turbulent flows. A turbulent flow may be viewed physically as containing transient eddies of various sizes. These eddies occur irregularly in space and time and consist of irregular regions of fluctuating velocity and vorticity, they are responsible for the outstanding characteristic of turbulence – its much greater ability to transport and mix momentum, kinetic energy, and contaminants than a corresponding laminar state and molecular diffusion [28, 29]. Next, we apply this qualitative description to homogeneous shear turbulence quantitatively, with the help of the two-point correlation  $\overline{w_k(\mathbf{x})w_k(\mathbf{x} + \mathbf{r})}$  which may be used to define integral length scale in turbulence study. (i) Statistically,  $\overline{w_k(\mathbf{x})w_k(\mathbf{x} + \mathbf{r})}$  is supposed to characterize the turbulent eddies centered at  $\mathbf{x}$ . The range of size of the eddies may be estimated by the range of  $\mathbf{r}$  where  $\overline{w_k(\mathbf{x})w_k(\mathbf{x} + \mathbf{r})}$  is nontrivial. (ii) These  $\mathbf{x}$ -centered eddies are directly responsible for the large-scale turbulent transport, the collective spatial intensity of these eddies may be roughly described by  $\overline{w_k(\mathbf{x})w_k(\mathbf{x} + \mathbf{r})}$  as a function of  $\mathbf{r}$ , reflecting that the larger the correlation value at  $\mathbf{r}$ , the stronger the spreading and mixing. The contribution of these  $\mathbf{x}$ -centered eddies to the mixing in  $\mathbb{R}^3$  may be approximately quantified via  $\int_{\mathbb{R}^3} d\mathbf{r} \overline{w_k(\mathbf{x})w_k(\mathbf{x} + \mathbf{r})}$ . (iii) The collective contribution of all the eddies in  $\mathbb{R}^3$  to the turbulent mixing may be approximated formally through the unbounded  $\int_{\mathbb{R}^3} d\mathbf{x} \int_{\mathbb{R}^3} d\mathbf{r} \overline{w_k(\mathbf{x})w_k(\mathbf{x} + \mathbf{r})}$  or effectively through the finite  $\int_{\mathbb{R}^3} d\mathbf{r} \overline{w_k(\mathbf{0})w_k(\mathbf{r})}$ , because of homogeneity. (iv) Strong turbulent mixing corresponds to large value of  $\int_{\mathbb{R}^3} d\mathbf{r} \overline{w_k(\mathbf{0})w_k(\mathbf{r})}$ , compatible with and favoring the maximization operation in Eq. (33). Since  $U_{kk}(\mathbf{0}) \geq |U_{kk}(\mathbf{r})|$  and  $U_{kk}(\mathbf{r})$  may be negative for some  $\mathbf{r} \neq \mathbf{0}$ , Eq. (33) promotes the positiveness of  $U_{kk}(\mathbf{r})$  as a whole. This property is further examined in Subsec. IV B, in the specific simulation of the second-order model, with regard to Figs. 1 through 3.

## F. Basic features and SOCP

Because this is an attempt to model turbulence via the interdisciplinary approach of optimal correlations, we recap what has been presented so far to help better explain the idea. It is a hierarchical formulation of statistical turbulence modeling, composed of multi-point spatial correlations. The issue of closure is resolved through maximization of the objective functional (33), subject to the constraints of equality and inequality outlined previously. Two models are constructed: The second-order model takes the second order correlations as the state variables and the contracted and degenerate third order correlations  $\tilde{\Gamma}_{ij}$  as the control variables; The third-order model contains the correlations

up to the degenerate fourth order, the degenerate correlations  $\tilde{U}_{(ij)kl}$  act as the control variables and all the others as the state variables. Therefore, statistical turbulence modeling is explored hierarchically via optimal control and convex optimization.

All the constraints of equality for the correlations are intrinsic, either derived from the fundamental equations (3) or from the self-consistency of correlation definitions or from the symmetries of inversion and mirror. The constraints of inequality are generated systematically from the Cauchy-Schwarz inequality and the non-negativity of variance of products, they hold generally and the vast majority of them do not have simple physical interpretations. The mathematical nature of these constraints raises the question of why they are required within the framework. We address this issue from several angles: Firstly, they are built on the basis that the fluctuating velocity and pressure fields are continuous and smooth, as assumed for the solutions of the Navier-Stokes equations, and the averaging is meaningful. These are feasible and reasonable conditions. Secondly, the generality of the constraints implies that the inequalities are compatible with the dynamical equations (14) and (21), as demanded by the the framework's feasibility. Thirdly, each inequality is loose individually owing to its generality, the very many such inequalities may provide collectively a rather tight restriction to the structures of the correlations, together with the dynamical equations and other constraints. Fourthly, the inequalities are not built from specific experimental data, this indicates the potential to extend and apply the framework to other turbulent flows.

The adoption of an objective functional is to satisfy all the dynamical equations and constraints, which resolves the issue of non-realizability in the analytical theories of turbulence. The adequate objective functional to adopt is a major issue addressed in the work. Inspired by the many successful applications of Shannon entropy maximization in other fields, we apply it here and infer Eq. (33) as the objective functional. We then proceed to substantiate the inferred form on the basis that physically turbulent eddies strongly promote large-scale spreading and mixing of momentum and that statistically the correlation  $w_k(\mathbf{x})w_k(\mathbf{x} + \mathbf{r})$  and  $\max_{\int_{\mathbb{R}^3} d\mathbf{r}} w_k(\mathbf{0})w_k(\mathbf{r})$  may quantify this mechanism approximately.

In our modeling of homogeneous shear turbulence, the state of motion is represented by multi-point spatial correlations. The closure strategy of optimal control and the mathematical structures of Eqs. (14) and (21) suggest that the highest order correlations are taken as the control variables and the lower order ones as state variables. Further, the divergence-free condition offers grounds to introduce primary state and control variables. All the state variables, the constraints, and the objective functional can be represented in terms of the primary control variables,  $\tilde{\Gamma}_{ij}$  in the second-order model and  $\tilde{U}_{(ij)kl}$  in the third-order model. That is, the second-order model is an optimization problem in the space of primary  $\tilde{\Gamma}_{ij}$  and the third-order model an optimization problem in the space of primary  $\tilde{U}_{(ij)kl}$ . Further, since  $\tilde{\Gamma}_{ij}$  can be represented linearly in terms of  $\tilde{U}_{(ij)kl}$ , we view the third-order model as an optimization problem in the enlarged control variable space. This viewpoint may also serve to explain mathematically why the third-order model is an improvement over the second-order model. The determination of  $\tilde{\Gamma}_{ij}$  in the second-order model or  $\tilde{U}_{(ij)kl}$  in the third-order model is achieved through maximizing the objective, subject to all the constraints relevant. A specific implementation of the second-order model is presented in Sec. IV. Because of statistical averaging, all the correlations and relations in the framework are mathematically well-behaved and regular, in contrast to the irregularly fluctuating velocity and pressure fields. Consequently, a discretization scheme of the correlations and relations faces less demand than DNS regarding mesh size in space and time, among other advantages.

It is noticed that the dynamical equations (14) and (21) are linear, the constraints are either linear or quadratically convex, and the objective (33) is linear in terms of the primary control variables. Consequently, the second-order and the third-order models, in their discretized forms, are second-order cone programs (SOCP) (see Appendix F), according to the criteria set in [20, 21].

Homogeneous shear turbulence is approximated mathematically as SOCP. As a well-formulated mathematical problem, its solutions, the multi-point correlations in the wave-number and physical spaces, are amenable numerically. For example, the asymptotic distributions of the second order correlations in the second-order model are obtained via optimization (see Figs. 1 through 3 in Subsec. IV B). Since the models are truncated, containing and resolving only lower order correlations, the adequacy of the solutions needs to be evaluated against DNS data of homogeneous shear turbulence. Also, the solved correlations in the wave-number and physical spaces may be further analyzed to answer questions like the separation between the length scales of production and dissipation of turbulent energy.

### III. ASYMPTOTIC STATES

To test the framework against experimental and DNS data, it is applied to asymptotic states at large time that are characterized by the form,

$$\psi = \psi^{(\infty)} \exp(\sigma t). \quad (34)$$

Here,  $\psi$  represents any of

$$\left\{ \tilde{U}_{ij}, \tilde{\Gamma}_{ij}, \tilde{U}_{ijk}^{(I)}, \tilde{U}_{(ij)kl}, U_{ij}, U_{ijk}, U_{(ij)kl}, Q, Q_i, Q_{ij}, \dots \right\},$$

$\psi^{(\infty)}$  is the time-independent part of  $\psi$ , and  $\sigma$  a constant denoting the exponential growth rate of the correlations. The structure is allowable by the mean flow (1), the dynamical equations, and the constraints discussed.

For the third-order model, we obtain an upper bound for  $\sigma$  by applying Eqs. (32) and (34),

$$\sigma \leq \max \sigma = 0. \quad (35)$$

Therefore, the turbulent energy per unit volume, along with all the correlations, cannot grow indefinitely, it evolves toward an asymptotic steady state of  $\sigma = 0$ , if not decaying. This result is more restrictive than the growth rate values suggested by some experimental and DNS data, e.g.  $\sigma = 0.10, 0.12, 0.14, 0.20$ , as summarized in Section 4.5 of [8] and Table 1 of [23].

Since the second-order model cannot include constraints generated by the non-negativity of variance of products, it allows  $\sigma \in (0, 1)$  to occur (see Appendix G for details).

Next, substitution of Eq. (34) into Eqs. (14) and (21) yields

$$\begin{aligned} & \frac{k_1 \exp[-2H(\sigma, \mathbf{k})]}{2|\mathbf{k}|^4} \frac{\partial}{\partial k_2} \left( |\mathbf{k}|^4 \exp[2H(\sigma, \mathbf{k})] \tilde{U}_{22}^{(\infty)}(\mathbf{k}) \right) = -\frac{k_2 k_l}{|\mathbf{k}|^2} \tilde{\Gamma}_{l2}^{(\infty)}(\mathbf{k}) + \tilde{\Gamma}_{22}^{(\infty)}(\mathbf{k}), \\ & \frac{k_1 \exp[-2H(\sigma, \mathbf{k})]}{|\mathbf{k}|^2} \frac{\partial}{\partial k_2} \left( |\mathbf{k}|^2 \exp[2H(\sigma, \mathbf{k})] \tilde{U}_{12}^{(\infty)}(\mathbf{k}) \right) \\ & = \left( 1 - \frac{2(k_1)^2}{|\mathbf{k}|^2} \right) \tilde{U}_{22}^{(\infty)}(\mathbf{k}) + \tilde{\Gamma}_{12}^{(\infty)}(\mathbf{k}) + \tilde{\Gamma}_{21}^{(\infty)}(\mathbf{k}) - \frac{k_l}{|\mathbf{k}|^2} \left( k_1 \tilde{\Gamma}_{l2}^{(\infty)}(\mathbf{k}) + k_2 \tilde{\Gamma}_{l1}^{(\infty)}(\mathbf{k}) \right), \\ & \frac{k_1 \exp[-2H(\sigma, \mathbf{k})]}{2} \frac{\partial}{\partial k_2} \left( \exp[2H(\sigma, \mathbf{k})] \tilde{U}_{11}^{(\infty)}(\mathbf{k}) \right) = \left( 1 - \frac{2(k_1)^2}{|\mathbf{k}|^2} \right) \tilde{U}_{12}^{(\infty)}(\mathbf{k}) - \frac{k_1 k_l}{|\mathbf{k}|^2} \tilde{\Gamma}_{l1}^{(\infty)}(\mathbf{k}) + \tilde{\Gamma}_{11}^{(\infty)}(\mathbf{k}), \end{aligned} \quad (36)$$

and

$$\begin{aligned} & \frac{\exp[-H(\sigma, \mathbf{k}, \mathbf{l})]}{|\mathbf{k}|^2 |\mathbf{l}|^2 |\mathbf{k} + \mathbf{l}|^2} \left( k_1 \frac{\partial}{\partial k_2} + l_1 \frac{\partial}{\partial l_2} \right) \left( |\mathbf{k}|^2 |\mathbf{l}|^2 |\mathbf{k} + \mathbf{l}|^2 \exp[H(\sigma, \mathbf{k}, \mathbf{l})] \tilde{U}_{222}^{(I\infty)}(\mathbf{k}, \mathbf{l}) \right) \\ & = -(k_l + l_l) \tilde{U}_{(2l)22}^{(\infty)}(\mathbf{k}, \mathbf{l}) + (k_2 + l_2) \frac{(k_m + l_m)(k_l + l_l)}{|\mathbf{k} + \mathbf{l}|^2} \tilde{U}_{(lm)22}^{(\infty)}(\mathbf{k}, \mathbf{l}) + \left( k_l \tilde{U}_{(2l)22}^{(\infty)} - k_2 \frac{k_m k_l}{|\mathbf{k}|^2} \tilde{U}_{(lm)22}^{(\infty)} \right) (-\mathbf{k} - \mathbf{l}, \mathbf{l}) \\ & + \left( l_l \tilde{U}_{(2l)22}^{(\infty)} - l_2 \frac{l_m l_l}{|\mathbf{l}|^2} \tilde{U}_{(lm)22}^{(\infty)} \right) (-\mathbf{k} - \mathbf{l}, \mathbf{k}), \\ & \frac{\exp[-H(\sigma, \mathbf{k}, \mathbf{l})]}{|\mathbf{k}|^2 |\mathbf{l}|^2} \left( k_1 \frac{\partial}{\partial k_2} + l_1 \frac{\partial}{\partial l_2} \right) \left( |\mathbf{k}|^2 |\mathbf{l}|^2 \exp[H(\sigma, \mathbf{k}, \mathbf{l})] \tilde{U}_{122}^{(I\infty)}(\mathbf{k}, \mathbf{l}) \right) \\ & = \left( 1 - \frac{2(k_1 + l_1)^2}{|\mathbf{k} + \mathbf{l}|^2} \right) \tilde{U}_{222}^{(I\infty)}(\mathbf{k}, \mathbf{l}) - (k_l + l_l) \tilde{U}_{(1l)22}^{(\infty)}(\mathbf{k}, \mathbf{l}) + (k_1 + l_1) \frac{(k_m + l_m)(k_l + l_l)}{|\mathbf{k} + \mathbf{l}|^2} \tilde{U}_{(lm)22}^{(\infty)}(\mathbf{k}, \mathbf{l}) \\ & + \left( k_l \tilde{U}_{(2l)12}^{(\infty)} - k_2 \frac{k_m k_l}{|\mathbf{k}|^2} \tilde{U}_{(lm)12}^{(\infty)} \right) (-\mathbf{k} - \mathbf{l}, \mathbf{l}) + \left( l_l \tilde{U}_{(2l)12}^{(\infty)} - l_2 \frac{l_m l_l}{|\mathbf{l}|^2} \tilde{U}_{(lm)12}^{(\infty)} \right) (-\mathbf{k} - \mathbf{l}, \mathbf{k}), \\ & \frac{\exp[-H(\sigma, \mathbf{k}, \mathbf{l})]}{|\mathbf{l}|^2} \left( k_1 \frac{\partial}{\partial k_2} + l_1 \frac{\partial}{\partial l_2} \right) \left( |\mathbf{l}|^2 \exp[H(\sigma, \mathbf{k}, \mathbf{l})] \tilde{U}_{112}^{(I\infty)}(\mathbf{k}, \mathbf{l}) \right) \\ & = \left( 1 - \frac{2(k_1 + l_1)^2}{|\mathbf{k} + \mathbf{l}|^2} \right) \tilde{U}_{122}^{(I\infty)}(-\mathbf{k} - \mathbf{l}, \mathbf{l}) + \left( 1 - \frac{2(k_1)^2}{|\mathbf{k}|^2} \right) \tilde{U}_{122}^{(I\infty)}(\mathbf{k}, \mathbf{l}) - (k_l + l_l) \tilde{U}_{(1l)12}^{(\infty)}(\mathbf{k}, \mathbf{l}) \\ & + (k_1 + l_1) \frac{(k_m + l_m)(k_l + l_l)}{|\mathbf{k} + \mathbf{l}|^2} \tilde{U}_{(lm)12}^{(\infty)}(\mathbf{k}, \mathbf{l}) + \left( k_l \tilde{U}_{(1l)12}^{(\infty)} - k_1 \frac{k_m k_l}{|\mathbf{k}|^2} \tilde{U}_{(lm)12}^{(\infty)} \right) (-\mathbf{k} - \mathbf{l}, \mathbf{l}) \\ & + \left( l_l \tilde{U}_{(2l)11}^{(\infty)} - l_2 \frac{l_m l_l}{|\mathbf{l}|^2} \tilde{U}_{(lm)11}^{(\infty)} \right) (-\mathbf{k} - \mathbf{l}, \mathbf{k}), \\ & \exp[-H(\sigma, \mathbf{k}, \mathbf{l})] \left( k_1 \frac{\partial}{\partial k_2} + l_1 \frac{\partial}{\partial l_2} \right) \left( \exp[H(\sigma, \mathbf{k}, \mathbf{l})] \tilde{U}_{111}^{(I\infty)}(\mathbf{k}, \mathbf{l}) \right) \end{aligned} \quad (37)$$

$$\begin{aligned}
&= \left(1 - \frac{2(k_1 + l_1)^2}{|\mathbf{k} + \mathbf{l}|^2}\right) \tilde{U}_{112}^{(I\infty)}(\mathbf{l}, -\mathbf{k} - \mathbf{l}) + \left(1 - \frac{2(k_1)^2}{|\mathbf{k}|^2}\right) \tilde{U}_{112}^{(I\infty)}(\mathbf{l}, \mathbf{k}) \\
&\quad + \left(1 - \frac{2(l_1)^2}{|\mathbf{l}|^2}\right) \tilde{U}_{112}^{(I\infty)}(\mathbf{k}, \mathbf{l}) - (k_l + l_l) \tilde{U}_{(1l)11}^{(\infty)}(\mathbf{k}, \mathbf{l}) + (k_1 + l_1) \frac{(k_m + l_m)(k_l + l_l)}{|\mathbf{k} + \mathbf{l}|^2} \tilde{U}_{(lm)11}^{(\infty)}(\mathbf{k}, \mathbf{l}) \\
&\quad + \left(k_l \tilde{U}_{(1l)11}^{(\infty)} - k_1 \frac{k_m k_l}{|\mathbf{k}|^2} \tilde{U}_{(lm)11}^{(\infty)}\right) (-\mathbf{k} - \mathbf{l}, \mathbf{l}) + \left(l_l \tilde{U}_{(1l)11}^{(\infty)} - l_1 \frac{l_m l_l}{|\mathbf{l}|^2} \tilde{U}_{(lm)11}^{(\infty)}\right) (-\mathbf{k} - \mathbf{l}, \mathbf{k}).
\end{aligned}$$

Here,

$$H(\sigma, \mathbf{k}, \mathbf{l}) = H(2\sigma/3, \mathbf{k}) + H(2\sigma/3, \mathbf{l}) + H(2\sigma/3, \mathbf{k} + \mathbf{l}), \quad H(\sigma, \mathbf{k}) = -\frac{k_2}{k_1} \left( \frac{1}{2}\sigma + (k_1)^2 + (k_3)^2 + \frac{1}{3}(k_2)^2 \right).$$

These equations may be solved under the boundary conditions from Eqs. (15) and (22),

$$\lim_{k_2 \rightarrow \pm\infty} \tilde{U}_{ij}^{(\infty)}(\mathbf{k}) = 0, \quad (38a)$$

$$\lim_{k_2 \rightarrow \pm\infty} \tilde{U}_{ijk}^{(I\infty)}(\mathbf{k}, \mathbf{l}) = \lim_{l_2 \rightarrow \pm\infty} \tilde{U}_{ijk}^{(I\infty)}(\mathbf{k}, \mathbf{l}) = 0. \quad (38b)$$

The constraints corresponding to the asymptotic states can be derived from the aforementioned ones with the help of Eq. (34), the objective functional (33) is replaced with

$$\int_{\mathbb{R}^3} d\mathbf{r} U_{kk}^{(\infty)}(\mathbf{r}) = \int_{\mathbb{R}^3} d\mathbf{r} \int_{\mathbb{R}^3} d\mathbf{k} \tilde{U}_{kk}^{(\infty)}(\mathbf{k}) \cos(\mathbf{r} \cdot \mathbf{k}) \quad (\text{to be maximized}), \quad (39)$$

owing to the linear nature of the functional and fixed  $\sigma$ .

One great challenge to the third-order model is its computational size, even restricted to the asymptotic state of  $\sigma = 0$ . There are thirty primary control variables,  $\tilde{U}_{(ij)kl}^{(\infty)}(\mathbf{k}, \mathbf{l})$ , listed in Eqs. (23) and defined in 6-dimensional space; the number of corresponding discrete control variables under a moderate mesh size is of the order of  $10^9$  or higher. Next, there are  $U_{ijk}^{(\infty)}(\mathbf{r}, \mathbf{s})$ ,  $U_{(ij)kl}^{(\infty)}(\mathbf{r}, \mathbf{s})$ , and  $Q_{ij}^{(\infty)}(\mathbf{r}, \mathbf{s})$  to be computed at collocation points of similar order of magnitude, for the purpose of enforcing the constraints outlined in Subsec. IID. This computational size is of huge-scale according to the criteria listed in [24] and poses challenges to both hardware (computer memory, number of computers, etc.) and software (a solver, especially the algorithm for such a huge-scale problem). These issues need further study in the context of randomized algorithms, distributed computing, etc. There is a close connection between the third-order model and big data [25], and research on big data is expected to help explore the model. Accordingly the third-order model may be classified as a big model.

This issue of huge-scale and its computational challenge raises a serious question about the prospect and merit of the framework proposed, especially compared with DNS, which has been employed to study homogeneous shear turbulence (see the references in [10]). It is observed that, as it resolves all structure scales of a turbulent flow, DNS is a fundamental tool in turbulence research, but it faces its own challenges. The problem most relevant to the present study is discussed below.

The Navier-Stokes equations are recognized as a chaotic dynamical system [30, 31], they govern the continuous turbulent fields of velocity and pressure. As an approximation to the continuous fields, DNS produces essentially discrete distributions, its truncation and computational errors act as a disturbing source to the continuous fields. This disturbing source affects quantitatively the individual solutions or realizations under given initial and boundary conditions solved by DNS. The question is whether this disturbance qualitatively affects the average fields predicted by DNS, because of the chaotic behavior of the Navier-Stokes equations.

In the case of homogeneous shear turbulence of concern here, DNS studies suggest that  $\sigma = 0.10, 0.18, 0.20$  (see Table 1 of [23]) and ‘‘Ideal HST in unbounded domains grows indefinitely, both in intensity and length scale. During the initial stages of shearing an isotropic turbulent flow, linear effects result in algebraic growth of the turbulent kinetic energy, which is later transformed to exponential due to nonlinearity.’’ (p.2 of [10]). These results are inconsistent with the stringent upper bound requirement (35). Also, the structures of  $\tilde{U}_{ij}^{(\infty)}(\mathbf{k})$  and the oscillation of  $\cos(\mathbf{k} \cdot \mathbf{r})$  in the Fourier transforms may yield that  $U_{ij}^{(\infty)}(\mathbf{r})$  have an effectively finite support; the length scales of the support are implicitly determined by the structure of the models, unlike the explicit timescale  $S^{-1}$  in Eqs. (1). To demonstrate this spatial boundedness, a simulation and analysis is presented in Sec. IV. The above inconsistencies highlight the difficulty faced by DNS in simulating adequately asymptotic states of homogeneous shear turbulence. In comparison, the present framework has a potential advantage: its spatial correlations are regular mathematical functions without

chaotic behavior, its mathematical structure can be specialized to exploit homogeneity, and its average turbulent flow structure is controlled directly by generic constraints from the Cauchy-Schwarz inequality and the non-negativity of variance of products, the latter guarantees Eq. (35). The trade-off for this advantage is the huge-scale computational size of the third-order model.

Furthermore, as discussed in Sec. V, there is a possibility to generalize the framework to inhomogeneous turbulence, which may provide one more tool to tackle turbulent flows. Such a possibility may also serve to justify exploration of this huge-scale model.

#### IV. ASYMPTOTIC STEADY STATE OF THE SECOND-ORDER MODEL

The asymptotic steady state solution of the second-order model is studied numerically, owing to its computational feasibility at present and its ability to provide valuable information concerning the adequacy of the objective functional, the role of the non-negativity of variance of products, and the potential of the framework.

As a special case of Eq. (34), the asymptotic states of the second-order model are characterized by

$$\{\tilde{U}_{ij}, \tilde{\Gamma}_{ij}\}(\mathbf{k}, t) = \left\{ \tilde{U}_{ij}^{(\infty)}, \tilde{\Gamma}_{ij}^{(\infty)} \right\}(\mathbf{k}) \exp(\sigma t). \quad (40)$$

Further, the equations governing  $\tilde{U}_{ij}^{(\infty)}$  and  $\tilde{\Gamma}_{ij}^{(\infty)}$  can be derived from the relevant ones discussed previously and are collected below.

*a. Consequence of symmetry* Equations (10) and (16) imply that it is sufficient to solve  $\tilde{U}_{ij}^{(\infty)}$  and  $\tilde{\Gamma}_{ij}^{(\infty)}$  in the subdomain  $\{k_1 \leq 0, k_3 \geq 0, k_2 \in \mathbb{R}\}$ , which is adopted. As intended, Eqs. (10) produce the experimentally observed [5, 8],

$$U_{13}^{(\infty)}(\mathbf{0}) = U_{23}^{(\infty)}(\mathbf{0}) = 0. \quad (41)$$

*b. Primary variables* Equations (12) and (13) imply that  $\tilde{\Gamma}_{ij}^{(\infty)}$ ,  $i = 1, 2, 3$ ,  $j = 1, 2$ , are taken as the primary variables of  $\tilde{\Gamma}_{mn}^{(\infty)}$  and  $\tilde{U}_{11}^{(\infty)}$ ,  $\tilde{U}_{12}^{(\infty)}$ , and  $\tilde{U}_{22}^{(\infty)}$  as the primary components of  $\tilde{U}_{ij}^{(\infty)}$ . The boundedness of  $\tilde{U}_{ij}^{(\infty)}$  and  $\tilde{\Gamma}_{ij}^{(\infty)}$  and the structures of Eqs. (12) through (14) suggest the transformations,

$$\tilde{\Gamma}_{ij}^{(\infty)}(\mathbf{k}) = (k_3)^2 \dot{\Gamma}_{ij}^{(\infty)}(\mathbf{k}), \quad i = 1, 2, 3, \quad j = 1, 2; \quad (42a)$$

$$\tilde{U}_{ij}^{(\infty)}(\mathbf{k}) = (k_3)^2 \dot{U}_{ij}^{(\infty)}(\mathbf{k}), \quad ij = 11, 12, 22. \quad (42b)$$

That is,  $\dot{\Gamma}_{ij}^{(\infty)}$ ,  $i = 1, 2, 3$ ,  $j = 1, 2$ , act as the primary control variables, which may be observed clearly in Eqs. (43).

*c. Formal solution of dynamical equations* With the aid of Eqs. (42) and (38a), we solve Eqs. (36) to get

$$\begin{aligned} \dot{U}_{22}^{(\infty)}(\mathbf{k}) &= \frac{2}{|k_1||\mathbf{k}|^4} \int_{-\infty}^{k_2} dk'_2 E(\mathbf{k}; k'_2; \sigma) |\mathbf{k}'|^4 \left( \frac{k'_2 k'_l}{|\mathbf{k}'|^2} \dot{\Gamma}_{l2}^{(\infty)}(\mathbf{k}') - \dot{\Gamma}_{22}^{(\infty)}(\mathbf{k}') \right), \\ \dot{U}_{12}^{(\infty)}(\mathbf{k}) &= - \frac{2}{|k_1|^2 [|k_1|^2 + (k_3)^2] |\mathbf{k}|^2} \int_{-\infty}^{k_2} dk'_2 E(\mathbf{k}; k'_2; \sigma) [F(\mathbf{k}) - F(\mathbf{k}')] |\mathbf{k}'|^4 \left( \frac{k'_2 k'_l}{|\mathbf{k}'|^2} \dot{\Gamma}_{l2}^{(\infty)}(\mathbf{k}') - \dot{\Gamma}_{22}^{(\infty)}(\mathbf{k}') \right) \\ &\quad + \frac{1}{|k_1||\mathbf{k}|^2} \int_{-\infty}^{k_2} dk'_2 E(\mathbf{k}; k'_2; \sigma) \left[ k'_l \left( k_1 \dot{\Gamma}_{l2}^{(\infty)}(\mathbf{k}') + k'_2 \dot{\Gamma}_{l1}^{(\infty)}(\mathbf{k}') \right) - |\mathbf{k}'|^2 \left( \dot{\Gamma}_{12}^{(\infty)}(\mathbf{k}') + \dot{\Gamma}_{21}^{(\infty)}(\mathbf{k}') \right) \right], \\ \dot{U}_{11}^{(\infty)}(\mathbf{k}) &= \frac{2}{|k_1|^3 [|k_1|^2 + (k_3)^2]^2} \int_{-\infty}^{k_2} dk'_2 E(\mathbf{k}; k'_2; \sigma) [F(\mathbf{k}) - F(\mathbf{k}')]^2 |\mathbf{k}'|^4 \left( \frac{k'_2 k'_l}{|\mathbf{k}'|^2} \dot{\Gamma}_{l2}^{(\infty)}(\mathbf{k}') - \dot{\Gamma}_{22}^{(\infty)}(\mathbf{k}') \right) \\ &\quad - \frac{2}{|k_1|^2 [|k_1|^2 + (k_3)^2]} \int_{-\infty}^{k_2} dk'_2 E(\mathbf{k}; k'_2; \sigma) [F(\mathbf{k}) - F(\mathbf{k}')] \\ &\quad \times \left[ k'_l \left( k_1 \dot{\Gamma}_{l2}^{(\infty)}(\mathbf{k}') + k'_2 \dot{\Gamma}_{l1}^{(\infty)}(\mathbf{k}') \right) - |\mathbf{k}'|^2 \left( \dot{\Gamma}_{12}^{(\infty)}(\mathbf{k}') + \dot{\Gamma}_{21}^{(\infty)}(\mathbf{k}') \right) \right] \\ &\quad + \frac{2}{|k_1|} \int_{-\infty}^{k_2} dk'_2 E(\mathbf{k}; k'_2; \sigma) \left( \frac{k_1 k'_l}{|\mathbf{k}'|^2} \dot{\Gamma}_{l1}^{(\infty)}(\mathbf{k}') - \dot{\Gamma}_{11}^{(\infty)}(\mathbf{k}') \right). \end{aligned} \quad (43)$$

Here,  $\mathbf{k}' = (k_1, k_2', k_3)$ ,  $k_1 < 0$ , and

$$E(\mathbf{k}; k_2'; \sigma) = \exp \left[ \frac{2(k_2 - k_2')}{k_1} \left( \frac{\sigma}{2} + (k_1)^2 + (k_3)^2 + \frac{(k_2)^2 + (k_2')^2 + k_2 k_2'}{3} \right) \right], \quad (44a)$$

$$F(\mathbf{k}) = \frac{(k_3)^2}{[|k_1|^2 + (k_3)^2]^{1/2}} \arctan \frac{k_2}{[|k_1|^2 + (k_3)^2]^{1/2}} - \frac{|k_1|^2 k_2}{|\mathbf{k}|^2}. \quad (44b)$$

*d. Constraints* Equations (25) become

$$0 \leq \tilde{U}_{\underline{ij}}^{(\infty)}(\mathbf{k}), \quad \left| \tilde{U}_{ij}^{(\infty)}(\mathbf{k}) \right|^2 \leq \tilde{U}_{\underline{ii}}^{(\infty)}(\mathbf{k}) \tilde{U}_{\underline{jj}}^{(\infty)}(\mathbf{k}), \quad (45)$$

they constrain  $\dot{\Gamma}_{ij}^{(\infty)}$  via Eqs. (13), (42b), and (43). Symmetries (16) require that

$$\left. \frac{\partial \dot{\Gamma}_{ij}^{(\infty)}(k_1, k_2, k_3)}{\partial k_3} \right|_{k_3=0} = 0, \quad ij = 11, 21, 12, 22; \quad \dot{\Gamma}_{ij}^{(\infty)}(k_1, k_2, 0) = 0, \quad ij = 31, 32. \quad (46)$$

The relevant ones in Eqs. (10) are satisfied automatically. The global constraints (17) reduce to

$$\begin{aligned} \int_{-\infty}^0 dk_1 \int_0^{+\infty} dk_3 \int_{\mathbb{R}} dk_2 (k_3)^2 \dot{\Gamma}_{11}^{(\infty)}(\mathbf{k}) &= 0, \quad \int_{-\infty}^0 dk_1 \int_0^{+\infty} dk_3 \int_{\mathbb{R}} dk_2 (k_3)^2 \dot{\Gamma}_{22}^{(\infty)}(\mathbf{k}) = 0, \\ \int_{-\infty}^0 dk_1 \int_0^{+\infty} dk_3 \int_{\mathbb{R}} dk_2 (k_3)^2 \left( \dot{\Gamma}_{12}^{(\infty)}(\mathbf{k}) + \dot{\Gamma}_{21}^{(\infty)}(\mathbf{k}) \right) &= 0, \\ \int_{-\infty}^0 dk_1 \int_0^{+\infty} dk_3 \int_{\mathbb{R}} dk_2 k_3 \left( k_1 \dot{\Gamma}_{31}^{(\infty)}(\mathbf{k}) + k_2 \dot{\Gamma}_{32}^{(\infty)}(\mathbf{k}) \right) &= 0. \end{aligned} \quad (47)$$

The model possesses scaling invariance under

$$\{ \tilde{U}_{ij}^{(\infty)}, \tilde{\Gamma}_{ij}^{(\infty)} \} \rightarrow \lambda \{ \tilde{U}_{ij}^{(\infty)}, \tilde{\Gamma}_{ij}^{(\infty)} \}, \quad \forall \lambda > 0. \quad (48)$$

It implies that, to obtain definite solutions, bounds need to be imposed on the control variables explicitly like

$$|\dot{\Gamma}_{ij}^{(\infty)}(\mathbf{k})| \leq C = 1, \quad i = 1, 2, 3, \quad j = 1, 2. \quad (49)$$

Though the resulting solutions do not yield absolute distributions of  $\tilde{U}_{ij}^{(\infty)}(\mathbf{k})$ , they provide definite normalized quantities represented by the anisotropy tensor,

$$b_{ij}^{(\infty)} = \frac{U_{ij}^{(\infty)}(\mathbf{0})}{U_{kk}^{(\infty)}(\mathbf{0})} - \frac{1}{3} \delta_{ij}, \quad (50)$$

which is used to compare against experimental data.

Equality constraint (20) reduces to

$$\frac{\sigma}{2} U_{jj}^{(\infty)}(\mathbf{0}) + U_{12}^{(\infty)}(\mathbf{0}) + \overline{w_{j,k}(\mathbf{x}) w_{j,k}(\mathbf{x})}^{(\infty)} = 0. \quad (51)$$

Its satisfaction is used to check partially the adequacy of numerical solutions.

*e. Removal of singularity* Under the supposedly bounded and continuous distributions of  $\dot{\Gamma}_{ij}^{(\infty)}$  and  $\dot{U}_{ij}^{(\infty)}$ , the singularity of Eqs. (43) at  $k_1 = 0$  is apparent. It may be shown that  $\dot{\Gamma}_{ij}^{(\infty)}(\mathbf{k}) = \dot{U}_{ij}^{(\infty)}(\mathbf{k}) = 0$  at  $k_1 = 0$  (see Appendix H for details). Considering computational feasibility, we restrict the supports of  $\dot{\Gamma}_{ij}^{(\infty)}$  and  $\dot{U}_{ij}^{(\infty)}$  to  $k_1 \leq \max k_1 < 0$  with  $|\max k_1|$  being small. This simple treatment is adequate for the state  $\sigma = 0$ .

*f. Support estimates* It is essential to the simulation that the domains of the control variables  $\dot{\Gamma}_{ij}^{(\infty)}$  and the state variables  $\dot{U}_{ij}^{(\infty)}$  be approximated by bounded supports. The existence of such supports may be inferred from the physical requirement that  $U_{kk}^{(\infty)}(\mathbf{0})$  be finite as follows. With the use of

$$\left| U_{12}^{(\infty)}(\mathbf{0}) \right| \leq \frac{1}{2} \left( U_{11}^{(\infty)}(\mathbf{0}) + U_{22}^{(\infty)}(\mathbf{0}) \right),$$

Eq. (51) is cast in the form

$$\int_{-\infty}^0 dk_1 \int_{\mathbb{R}} dk_2 \int_0^{+\infty} dk_3 (1 - \sigma - 2|\mathbf{k}|^2) \tilde{U}_{kk}^{(\infty)}(\mathbf{k}) \geq U_{33}^{(\infty)}(\mathbf{0})/4, \quad (52)$$

which, along with  $U_{33}^{(\infty)}(\mathbf{0}) > 0$  and  $\tilde{U}_{kk}^{(\infty)}(\mathbf{k}) \geq 0$ , suggests that

$$\tilde{U}_{kk}^{(\infty)}(\mathbf{k}) \text{ is large predominantly inside a neighborhood of } |\mathbf{k}|^2 \leq (1 - \sigma)/2. \quad (53)$$

It is then inferred from

$$\tilde{U}_{kk}^{(\infty)}(\mathbf{k}) = [(k_1)^2 + (k_3)^2] \dot{U}_{11}^{(\infty)}(\mathbf{k}) + 2k_1 k_2 \dot{U}_{12}^{(\infty)}(\mathbf{k}) + [(k_2)^2 + (k_3)^2] \dot{U}_{22}^{(\infty)}(\mathbf{k}) \quad (54)$$

and Eqs. (45) and (53) that

$$|\dot{U}_{ij}^{(\infty)}(\mathbf{k})| \text{ are large predominantly inside a neighborhood of } |\mathbf{k}|^2 \leq (1 - \sigma)/2. \quad (55)$$

The above relation may be further justified as follows. (i) The presence of  $|\mathbf{k}|^2$  results from the viscous dissipation term of Eq. (51), its upper bound may reflect the effect of the viscous dissipation. (ii) The more negative the value of  $\sigma$ , the greater the support of  $\dot{U}_{ij}^{(\infty)}(\mathbf{k})$ . This dependence is physically sound, since larger wave-numbers tend to carry less fluctuation turbulent energy but produce more viscous dissipation and lead to greater exponential rate of decay.

The integral structures of solutions (43) and the requirement (55) suggest  $|\mathbf{k}| \leq [(1 - \sigma)/2]^{1/2}$  as a preliminary estimate for the support of  $\dot{\Gamma}_{ij}^{(\infty)}$ . Considering the rough nature of this estimate, the restriction on computational size from the aspect of computational feasibility, and the convenience of a structured mesh for coding, we take the hexahedral estimate for the effective support of  $\dot{\Gamma}_{ij}^{(\infty)}$ ,

$$|k_1| \leq \lambda_1 [(1 - \sigma)/2]^{1/2}, \quad |k_3| \leq \lambda_3 [(1 - \sigma)/2]^{1/2}, \quad k_2 \in [K_{2L}^\Gamma(\sigma), K_{2U}^\Gamma(\sigma)]; \quad K_{2L}^\Gamma(\sigma) \equiv -\lambda_{2L} [(1 - \sigma)/2]^{1/2}, \\ K_{2U}^\Gamma(\sigma) \equiv \lambda_{2U} [(1 - \sigma)/2]^{1/2}, \quad \lambda_i \in [1, 3].$$

The incorporation of  $k_1 \leq \max k_1$  and the restriction to  $\sigma = 0$  lead to the finite support estimate of  $\dot{\Gamma}_{ij}^{(\infty)}$ ,

$$\mathcal{D}_\Gamma(0) = \left\{ \mathbf{k} : k_1 \in \left[ -\frac{\lambda_1}{2^{1/2}}, \max k_1 \right], k_3 \in \left[ 0, \frac{\lambda_3}{2^{1/2}} \right], k_2 \in \left[ K_{2L}^\Gamma(0), K_{2U}^\Gamma(0) \right] \right\}, \quad \lambda_i \in [1, 3]. \quad (56)$$

The specific values of  $\lambda_i$  are fixed from consideration of adequacy of numerical solutions via trial-and-error.

For an estimate of the support of  $\dot{U}_{ij}^{(\infty)}$ , denoted as  $\mathcal{D}_U(0)$ , solutions (43) indicate that the two supports coincide with each other in the directions of  $k_1$  and  $k_3$ , and  $K_{2L}^\Gamma(0)$  is the lower bound to  $\mathcal{D}_U(0)$  along  $k_2$ . Regarding the upper bound of  $\mathcal{D}_U(0)$  along  $k_2$ , denoted as  $\max k_2^U$ , the integral nature of the solutions implies that  $\max k_2^U > K_{2U}^\Gamma(0)$ . In simulation,  $\max k_2^U$  is treated as a constant whose value is fixed via numerical trials. Thus,

$$\mathcal{D}_U(0) = \left\{ \mathbf{k} : k_1 \in \left[ -\frac{\lambda_1}{2^{1/2}}, \max k_1 \right], k_3 \in \left[ 0, \frac{\lambda_3}{2^{1/2}} \right], k_2 \in \left[ K_{2L}^\Gamma(0), \max k_2^U \right] \right\}. \quad (57)$$

*g. Objective* The distributions of  $\tilde{U}_{ij}^{(\infty)}(\mathbf{k})$  and the oscillation of  $\cos(\mathbf{k} \cdot \mathbf{r})$  in the Fourier transforms may result in  $U_{ij}^{(\infty)}(\mathbf{r})$  being negligibly small at large  $|\mathbf{r}|$ . Thus, Eq. (39) becomes

$$\int_{\mathbb{R}^3} d\mathbf{r} U_{kk}^{(\infty)}(\mathbf{r}) = 32 \int_{-\infty}^0 dk_1 \int_{-\infty}^{+\infty} dk_2 \int_0^{+\infty} dk_3 \tilde{U}_{kk}^{(\infty)}(\mathbf{k}) \frac{\sin(L_1 k_1) \sin(L_2 k_2) \sin(L_3 k_3)}{k_1 k_2 k_3}. \quad (58)$$

Here,  $\prod_{k=1}^3 [-L_k, L_k]$  denotes the effective support for  $U_{kk}^{(\infty)}(\mathbf{r})$ . The values of  $L_k$  indicate the macro length scales beyond which the spatial correlations are negligible, which is tested and fixed below numerically.

*h. SOCP* Constrained by Eqs. (43), (45) through (47), (49), (56), and (57), the maximization problem (58) is a SOCP in its discretized form.

### A. Discretization and computation

The basic ideas involved in the numerical simulation are outlined here, the lengthy but straight-forward details are presented in Appendices I through K.

*a. Discretization and integrations* The bounded supports for  $\dot{\Gamma}_{ij}^{(\infty)}$  and  $\dot{U}_{ij}^{(\infty)}$  are specified, respectively, as

$$\mathcal{D}_\Gamma(0) = [-0.71, -0.01] \times [-1.35, 1.25] \times [0.0, 0.9], \quad \mathcal{D}_U(0) = [-0.71, -0.01] \times [-1.35, 1.65] \times [0.0, 0.9], \quad (59)$$

with the help of support estimates (56) and (57). In physical space,  $L_1 = 250$ ,  $L_2 = 60$ , and  $L_3 = 150$  are selected for Eq. (58). We need to specify these values through numerical trial tests because complicated nonlinear relations are involved in the optimization problem. The supports are discretized, respectively, with structured hexahedral meshes,

$$\begin{aligned} \mathcal{D}_\Gamma(0) &= \bigcup_{n_1=1}^{N_1-1} \bigcup_{n_2=1}^{N_2-1} \bigcup_{n_3=1}^{N_3-1} \mathcal{H}(n_1, n_2, n_3), & \mathcal{D}_U(0) &= \bigcup_{n_1=1}^{N_1-1} \bigcup_{n_2=1}^{M_2-1} \bigcup_{n_3=1}^{N_3-1} \mathcal{H}(n_1, n_2, n_3), \\ \mathcal{H}(n_1, n_2, n_3) &= [k_{1,n_1}, k_{1,n_1+1}] \times [k_{2,n_2}, k_{2,n_2+1}] \times [k_{3,n_3}, k_{3,n_3+1}]. \end{aligned}$$

In each hexahedral element  $\mathcal{H}(n_1, n_2, n_3)$  of  $\mathcal{D}_\Gamma(0)$ , the distribution of  $\dot{\Gamma}_{ij}^{(\infty)}(\mathbf{k})$  is approximated trilinearly in  $\mathbf{k}$ , together with the nodal values of  $\dot{\Gamma}_{ij}^{(\infty)}$ ,

$$\begin{aligned} \dot{\Gamma}_{ij}^{(\infty)}(\mathbf{k}) &= \frac{\dot{\Gamma}_{ij}^{(0)}(n_1, n_2, n_3)(k_{2,n_2+1} - k_2) + \dot{\Gamma}_{ij}^{(0)}(n_1, n_2 + 1, n_3)(k_2 - k_{2,n_2})}{k_{2,n_2+1} - k_{2,n_2}} \frac{k_{1,n_1+1} - k_1}{k_{1,n_1+1} - k_{1,n_1}} \frac{k_{3,n_3+1} - k_3}{k_{3,n_3+1} - k_{3,n_3}} + \dots, \\ Z &= \left\{ \dot{\Gamma}_{ij}^{(0)}(n_1, n_2, n_3) : n_1 = 1, \dots, N_1, n_2 = 1, \dots, N_2, n_3 = 1, \dots, N_3; i, j \right\} \subset \mathbb{R}^{6N_{CV}}, \quad N_{CV} = N_1 N_2 N_3. \end{aligned}$$

The piecewise linear approximation in  $\mathcal{D}_\Gamma(0)$  is adequate at small mesh element sizes, since integration operations are mainly involved for  $\dot{\Gamma}_{ij}^{(\infty)}$ . Accordingly, Eqs. (43), (47), and (58) are discretized and represented in terms of nodal values  $Z$ .

Function ‘NIntegrate’ of MATHEMATICA is used to compute the 1-dimensional integrals in Eqs. (43) over the mesh elements. Algorithms ‘Cuhre’ and ‘Divonne’ of the open source software CUBA library [32–34] are used to compute 4-dimensional integrals like Eq. (58).

*b. Constraints and optimization* Constraints (46) and (49) are enforced at the mesh nodes. Constraints (45) are imposed at collocation points defined below: (i) the points located in the middle of the mesh element edges parallel to the  $k_2$ -axis, denoted as 1C; (ii) the points located at the center of the mesh element facets parallel to the  $k_2$ -axis, denoted as 2C; (iii) the points located at the center of the mesh elements, denoted as 4C. We enforce Eqs. (45) at 1C or the combination of 1C and 4C, etc. to evaluate the impact of the collocation points.

The discretized second-order model is then cast in the form of

$$\begin{aligned} &\text{minimize} \quad a^T Z \\ &\text{subject to} \quad Z \in \mathcal{C}. \end{aligned} \quad (60)$$

Here,  $-a$  is fixed from the discretized objective (58), and  $\mathcal{C}$  is composed of the discretized constraints (45) through (47) and (49). Problem (60) is a SOCP.

*c. Parallel computing* Since the discretized model is a large-scale SOCP, the widely used and tested splitting conic solver SCS [35, 36] is employed, which is a first-order method. With regard to Eqs. (45), their imposition at {1C, 2C, 4C} under a coarser mesh or the imposition only at 1C under a finer mesh demands large RAM (well above 64GB available in a workstation), specifically in the step of generating the standard form of a SOCP necessary for the solver. Hence, it is essential to formulate and solve the discretized model (60) as a parallel computing problem, with the help of the global consensus algorithm of the alternating direction method of multipliers (ADMM) [37, 38]. The ADMM consensus algorithm consists of the following iterations  $k$ ,

$$Z^k = \bar{X}^k := \frac{1}{N} \sum_{i=1}^N X_i^k, \quad (61a)$$

$$X_i^{k+1} := \operatorname{argmin}_{X_i \in \mathcal{C}_i} \|X_i - \Lambda_i^k\|_2^2 = \Pi_{\mathcal{C}_i}(\Lambda_i^k), \quad (61b)$$

$$\tilde{Y}_i^{k+1} := \tilde{Y}_i^k + X_i^{k+1} - \bar{X}^{k+1}, \quad \frac{1}{N} \sum_{i=1}^N \tilde{Y}_i^0 = 0. \quad (61c)$$

Here, there are  $N$  computing processing elements used in parallel,  $\{\mathcal{C}_i : i = 1, \dots, N\}$  is a partition of  $\mathcal{C}$ . In the  $i$ -th element,  $X_i \in \mathbb{R}^{6N_{\text{cv}}}$  is the local variable,  $Y_i = \rho \tilde{Y}_i$  the dual variable associated with the consensus constraint  $X_i - Z = 0$ ,  $\rho (> 0)$  the penalty parameter in the augmented Lagrangian, and  $Z$  acts as the common global variable. Next,  $\|\cdot\|_2$  is the Euclidean norm,  $\Lambda_i^k = \bar{X}^k - (a/\rho + \tilde{Y}_i^k)$ , and  $\Pi_{\mathcal{C}_i}(\Lambda_i^k)$  denotes Euclidean projection of vector  $\Lambda_i^k$  onto  $\mathcal{C}_i$ ,  $i = 1, \dots, N$ . The  $X_i$ -update (61b) is computed by SCS. (See Appendix K for details.)

The convergence of the iterative process (61) is guaranteed analytically [37, 39]. To terminate the iterative process, the conventional stopping criteria [37] are adopted,

$$\begin{aligned} \|R^k\|_2 &= \left( \sum_{i=1}^N \|X_i^k - \bar{X}^k\|_2^2 \right)^{1/2} \leq \sqrt{N}(\epsilon^{\text{abs}} + \|\bar{X}^k\|_2 \epsilon^{\text{rel}}), \\ \|S^k\|_2 &= \left( N\rho^2 \|\bar{X}^k - \bar{X}^{k-1}\|_2^2 \right)^{1/2} \leq \rho\sqrt{N}(\epsilon^{\text{abs}} + \|\bar{X}^k\|_2 \epsilon^{\text{rel}}), \end{aligned} \quad (62)$$

where  $\|R^k\|_2$  and  $\|S^k\|_2$  are, respectively, the squared norms of the primal and dual residuals,  $R^k$  and  $S^k$ , at the  $k$ -th iteration,  $\epsilon^{\text{abs}}$  and  $\epsilon^{\text{rel}}$  denote, respectively, the absolute and relative tolerances. The implementation is based mainly on the works of [36–43]. The values of  $\rho = 1$ ,  $\epsilon^{\text{abs}} = 10^{-4}$ , and  $\epsilon^{\text{rel}} = 10^{-3}$  are employed and are adequate for the present exploration.

*d. Specifics* In the numerical simulation, a single mesh size along the directions of  $k_1$ ,  $k_2$ , and  $k_3$  is used to discretize the supports uniformly; two specific mesh sizes 0.1 and 0.05 are employed and denoted by (I) and (II), respectively. No finer meshes are employed because of the resulting large computational size.

Different versions of the discretized model result from various combinations of mesh size and constraints in order to test their effects. Regarding the constraints, we select L & 1C, L & 1C & 4C, and L & 1C & 2C & 4C, where L & 1C & 4C, say, stands for the imposition of all the linear constraints and Eqs. (45) at  $\{1C, 4C\}$ . The numbers of parallel computing processing elements are  $N = 3, 6, 12$ , respectively, for L & 1C (I), L & 1C & 4C (I), and L & 1C & 2C & 4C (I), and  $N = 12$  for L & 1C (II). The adequacy of the mathematical formulation and numerical solutions is indicated partially by the fact that separate calculations of  $U_{12}^{(\infty)}(\mathbf{0})$  and  $\overline{w_{j,k} w_{j,k}}^{(\infty)}(\mathbf{0})$  yield the ratio

$$U_{12}^{(\infty)}(\mathbf{0}) / \overline{w_{j,k} w_{j,k}}^{(\infty)}(\mathbf{0}) = -1.000,$$

consistent with the exact value of  $-1$  dictated by the global balance equation (51) under  $\sigma = 0$ . Also, the choice of  $L_k$  is adequate, as indicated by the distribution trends of the correlation functions  $R_{ii}^{(\infty)}(r_1, 0, 0)$ ,  $R_{ii}^{(\infty)}(0, r_2, 0)$ , and  $R_{ii}^{(\infty)}(0, 0, r_3)$  and their negligible values at  $r_k = L_k$  displayed in Figs. 1 through 3, that are required by the self-consistency of being a support. Here, the correlation functions are defined via

$$R_{ii}^{(\infty)}(\mathbf{r}) = U_{ii}^{(\infty)}(\mathbf{r}) / U_{ii}^{(\infty)}(\mathbf{0}).$$

## B. Numerical results and discussion

To evaluate the proposed framework, experimental data summarized in p.81 of [8] and DNS data from [9, 10] are taken as the basis of comparison. To this end, the optimal solutions are used to compute the following dimensionless quantities: (a) the nontrivial components of the anisotropy tensor  $b_{ij}^{(\infty)}$  of Eq. (50); (b) the ratio of turbulent energy  $K$  to viscous dissipation  $\varepsilon$  [8],

$$(SK/\varepsilon)^{(\infty)} = U_{kk}^{(\infty)}(\mathbf{0}) / \overline{w_{j,k} w_{j,k}}^{(\infty)}(\mathbf{0}),$$

where  $S$  is from Eq. (1); (c) the ratio of  $G = -\overline{w_i w_j} V_{i,j}$  (a dimensional quantity defined in [8] without the use of Eqs. (2)) to dissipation,

$$(G/\varepsilon)^{(\infty)} = -2 U_{12}^{(\infty)}(\mathbf{0}) / \overline{w_{j,k} w_{j,k}}^{(\infty)}(\mathbf{0}),$$

TABLE I. Data from optimal solutions and experiments.

Constraints	$(b_{11}^{(\infty)}, b_{22}^{(\infty)}, b_{33}^{(\infty)}, b_{12}^{(\infty)}, (SK/\varepsilon)^{(\infty)}, (G/\varepsilon)^{(\infty)})$
L & 1C (I)	(0.3908, -0.2674, -0.1234, -0.1329, 7.521, 2.000)
L & 1C & 4C (I)	(0.3944, -0.2642, -0.1302, -0.1388, 7.205, 2.000)
L & 1C & 2C & 4C (I)	(0.4153, -0.2676, -0.1478, -0.1351, 7.400, 2.000)
L & 1C (II)	(0.5031, -0.2951, -0.2080, -0.1161, 8.613, 2.000)
Experimental [8]	(0.203, -0.143, -0.06, -0.156, 5.54, 1.73)

which characterizes the extent of turbulent mean shear [8]. It is noted that the experimental values quoted in Table I are “plausible target of asymptotic data” because of “the strong discrepancy between data” [8], but they are taken as the basis for comparison, since they are representative.

Table I lists the predicted values of

$$(b_{11}^{(\infty)}, b_{22}^{(\infty)}, b_{33}^{(\infty)}, b_{12}^{(\infty)}, (SK/\varepsilon)^{(\infty)}, (G/\varepsilon)^{(\infty)})$$

for various versions of the discretized model under  $\sigma = 0$ . A few observations may be made about the pattern of the predicted and the comparison with experimental values.

*a.* Under mesh (I), the three combinations of constraints produce nearly the same quantitative results, though the corresponding distributions of  $\tilde{U}_{ij}^{(\infty)}$  in the wave-number space differ in details. The same relative numerical order as that of the experimental data is produced as follows,

$$b_{11}^{(\infty)} > 0 > b_{33}^{(\infty)} > b_{22}^{(\infty)}. \quad (63)$$

Under mesh (II), L & 1C produces the results quantitatively similar to those of (I), the order pattern (63) holds, though the values of  $b_{11}^{(\infty)}$ ,  $b_{11}^{(\infty)} - b_{33}^{(\infty)}$ , and  $b_{11}^{(\infty)} - b_{22}^{(\infty)}$  are higher. No imposition of 2C or 4C is carried out under (II), because of the following considerations: First, as displayed in Table I, the same relative order pattern (63) is obtained, independent of the constraints imposed under (I) and independent of mesh size reduction from (I) to (II) under L & 1C. We infer from this independence that such a relative order pattern may not change under L & 1C & 4C (II) and L & 1C & 2C & 4C (II) within the model. Second, the required parallel processing elements are about 50 and 100, not available to this study.

*b.* For the numerical solutions, separate calculations of  $\overline{w_{j,k}w_{j,k}}^{(\infty)}(\mathbf{0})$  and  $U_{12}^{(\infty)}(\mathbf{0})$  give  $(G/\varepsilon)^{(\infty)} = 2.000$ , consistent with the value of 2 dictated by (51) under  $\sigma = 0$ . Unequal to 2, the experimental value of  $(G/\varepsilon)^{(\infty)} = 1.73$  may result from the deviation from the asymptotic state of  $\sigma = 0$  in experiments and experimental errors.

Regarding the values of  $b_{11}^{(\infty)}$ ,  $b_{22}^{(\infty)}$ , and  $b_{33}^{(\infty)}$ , the predictions differ significantly from the experiments. This discrepancy may be attributed to the non-enforceability of the non-negativity of variance of products (31) within the second-order model, as explained below. The results of L & 1C (II) are taken as the basis for comparison.

As mentioned in Subsec. II A, the global equality constraints (17)/(47) provide a distributive mechanism of distributing  $\tilde{U}_{kk}^{(\infty)}(\mathbf{k})$  among its components  $\tilde{U}_{ii}^{(\infty)}(\mathbf{k})$  and  $U_{kk}^{(\infty)}(\mathbf{0})$  among its components  $U_{ii}^{(\infty)}(\mathbf{0})$ : a larger  $U_{11}^{(\infty)}(\mathbf{0})$  is accompanied by a smaller  $U_{22}^{(\infty)}(\mathbf{0})$  and/or  $U_{33}^{(\infty)}(\mathbf{0})$ . Equivalently, a positive larger  $b_{11}^{(\infty)}$  is accompanied by a negative larger  $b_{22}^{(\infty)}$  and/or  $b_{33}^{(\infty)}$ , as required by  $b_{kk}^{(\infty)} = 0$ . This is the pattern displayed by the prediction data of L & 1C (II): the predicted  $b_{ii}^{(\infty)}(\mathbf{0})$  are about twice to thrice of the experimental values.

The predicted values show that maximization of the objective (58) makes  $U_{11}^{(\infty)}(\mathbf{0})$  unduly large relative to  $U_{22}^{(\infty)}(\mathbf{0})$  and  $U_{33}^{(\infty)}(\mathbf{0})$  within the second-order model. As indicated by Eqs. (48) and (49), the model does not have a natural mechanism to bound from above  $U_{11}^{(\infty)}(\mathbf{0})$ ,  $U_{11}^{(\infty)}(\mathbf{0}) - U_{22}^{(\infty)}(\mathbf{0})$ , and  $U_{11}^{(\infty)}(\mathbf{0}) - U_{33}^{(\infty)}(\mathbf{0})$ . Hence, a combination of the distributive mechanism and the maximization causes such a large difference between the predicted and the experimental values.

To remedy this problem, we need a mechanism to bound from above  $U_{11}^{(\infty)}(\mathbf{0})$ ,  $U_{11}^{(\infty)}(\mathbf{0}) - U_{22}^{(\infty)}(\mathbf{0})$ , and  $U_{11}^{(\infty)}(\mathbf{0}) - U_{33}^{(\infty)}(\mathbf{0})$ . The non-negativity requirement (31) may play such a role, as evidenced by the specific examples (32),

$$\left( U_{ij}^{(\infty)}(\mathbf{r}) \right)^2 \leq U_{\underline{ii}\underline{jj}}^{(\infty)}(\mathbf{r}, \mathbf{r}), \quad \left| U_{\underline{ii}}^{(\infty)}(\mathbf{r}) - U_{\underline{jj}}^{(\infty)}(\mathbf{r}) \right|^2 \leq U_{\underline{ii}\underline{ii}}^{(\infty)}(\mathbf{r}, \mathbf{r}) + U_{\underline{jj}\underline{jj}}^{(\infty)}(\mathbf{r}, \mathbf{r}) + 2U_{\underline{ii}\underline{jj}}^{(\infty)}(\mathbf{r}, \mathbf{r}) - 4U_{\underline{ij}\underline{ij}}^{(\infty)}(\mathbf{r}, \mathbf{r}). \quad (64)$$

These inequalities, together with others from Eq. (31), expectedly produce certain upper bounds on  $|U_{ij}^{(\infty)}(\mathbf{0})|$  and  $|U_{ii}^{(\infty)}(\mathbf{0}) - U_{jj}^{(\infty)}(\mathbf{0})|$  with  $\tilde{U}_{(ij)kl}^{(\infty)}$  as the control variables, because the left-hand sides of these inequalities depend on

$\tilde{U}_{(ij)kl}^{(\infty)}$  quadratically while the right-hand sides depend on  $\tilde{U}_{(ij)kl}^{(\infty)}$  linearly. This observation provides a ground for the need of the third-order model. Within the third-order model, the coupling interaction among the two mechanisms of distribution and bounding and the maximization of the objective (58) is expected to make  $b_{ii}^{(\infty)}$  closer to the experimental values than those produced by the second-order model.

c. Both the distributive and the bounding mechanisms seem related to the issue of isotropization [1, 44], which needs to be explored within the third-order model.

We evaluate below the correlation function predictions of the second-order model under L & 1C (II) against the DNS studies of [9, 10]. Figures 1(a), 2(a), and 3(a) show the predicted distributions of the correlation functions  $R_{ii}^{(\infty)}$  along  $r_1$ ,  $r_2$ , and  $r_3$ , respectively. Also, for the convenience of comparison, we have extracted DNS data from Figs. 5 of [10] and present them in Figs. 1(b), 2(b), and 3(b).

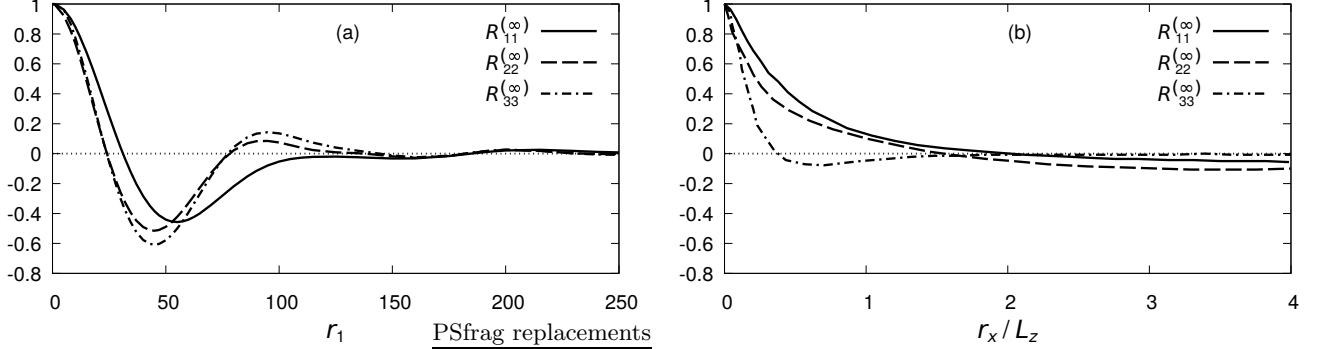


FIG. 1. Two-point correlation functions  $R_{ii}^{(\infty)}(\cdot, 0, 0)$ . (a) Simulation of the second-order model. The streamwise length scale  $L_{\text{strm}} \sim 250$ . (b) DNS data.  $R_{11}^{(\infty)}$ ,  $R_{22}^{(\infty)}$ , and  $R_{33}^{(\infty)}$  are extracted, respectively, from Figs. 5(a), 5(b), and 5(c) with  $A_{xz} = 8$  of [10].

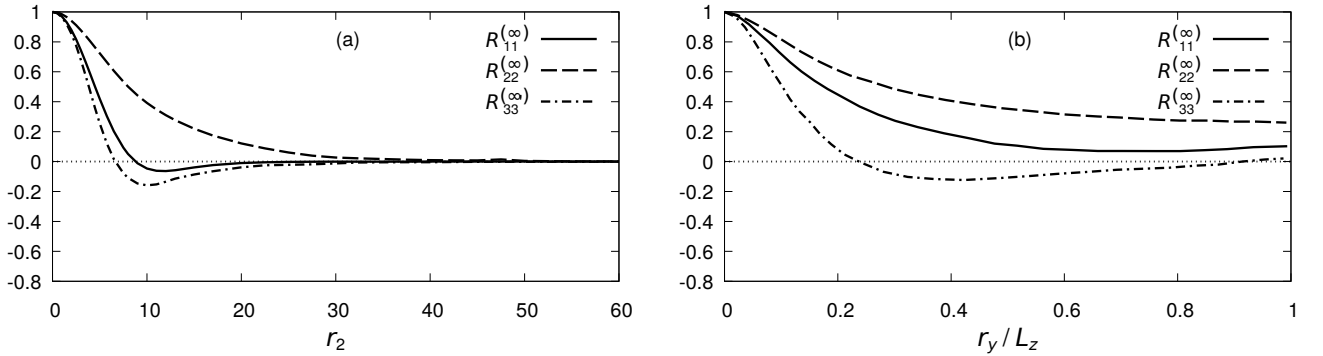


FIG. 2. Two-point correlation functions  $R_{ii}^{(\infty)}(0, \cdot, 0)$ . (a) Simulation of the second-order model. The vertical length scale  $L_{\text{vert}} \sim 50$ . (b) DNS data.  $R_{11}^{(\infty)}$ ,  $R_{22}^{(\infty)}$ , and  $R_{33}^{(\infty)}$  are extracted, respectively, from Figs. 5(d), 5(e), and 5(f) with  $A_{xz} = 8$  of [10].

Considering the fundamental defect of the second-order model — its lack of a bounding mechanism discussed above, we analyze and compare these predictions with DNS data in a qualitative fashion. Clearly the ranges of  $r_k$  in Figs. 1(a), 2(a), and 3(a) indicate the existence of three distinct characteristic macro length scales beyond which the two-point correlations are effectively negligible:  $L_{\text{strm}} \sim 250$  (streamwise along the  $r_1$ -direction),  $L_{\text{vert}} \sim 50$  (vertical along the  $r_2$ -direction),  $L_{\text{span}} \sim 120$  (spanwise along the  $r_3$ -direction), and they are in the numerical order of  $L_{\text{strm}} > L_{\text{span}} > L_{\text{vert}}$ . This order may reflect underlying physics: (i) The only nontrivial mean velocity component in the sheared flow is the streamwise velocity  $V_1' = x_2'$  (dimensionless from Eqs. (1) and (2)), it produces streaks [10], and thus, the corresponding correlations have the longest range and  $L_{\text{strm}}$  is the largest (Fig. 1(a)). This appears to be supported partially by Fig. 6 of [9] (which is obtained in transient state and not reproduced here). (ii) In the

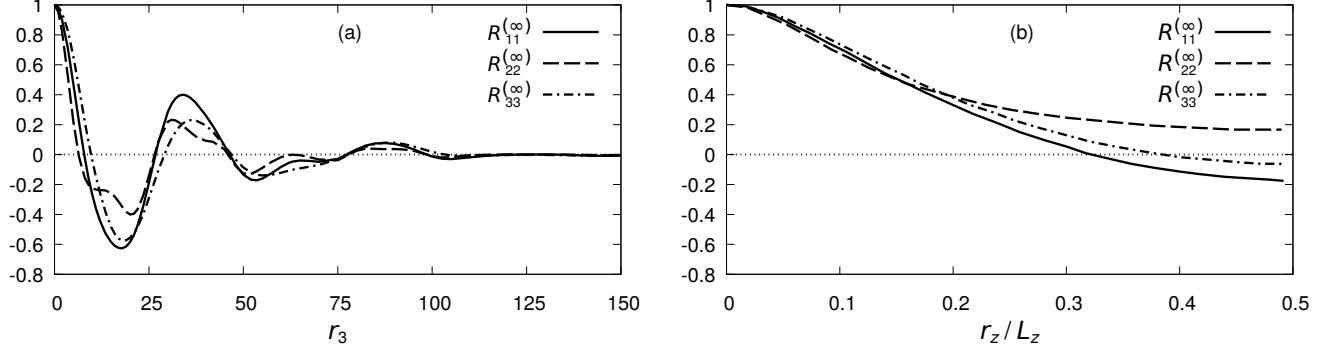


FIG. 3. Two-point correlation functions  $R_{ii}^{(\infty)}(0,0,\cdot)$ . (a) Simulation of the second-order model. The spanwise length scale  $L_{\text{span}} \sim 120$ . (b) DNS data.  $R_{11}^{(\infty)}$ ,  $R_{22}^{(\infty)}$ , and  $R_{33}^{(\infty)}$  are extracted, respectively, from Figs. 5(g), 5(h), and 5(i) with  $A_{xz} = 8$  of [10].

vertical  $r_2$ -direction, the mean shearing  $\partial V_1'/\partial x_2' = 1$  tends to suppress the velocity fluctuations, which results in the smallest  $b_{22}^{(\infty)}$  ( $U_{22}^{(\infty)}(\mathbf{0})$ ) among  $b_{ii}^{(\infty)}$  ( $U_{ii}^{(\infty)}(\mathbf{0})$ ) [8, 45]. This suppression may also make the range of the vertical correlations the shortest and  $L_{\text{vert}}$  the smallest (Fig. 2(a)). (iii) Along the spanwise  $r_3$ -direction,  $V_3' = 0$  and no suppression is present, their combined effect may make  $L_{\text{span}}$  the middle scale between  $L_{\text{strm}}$  and  $L_{\text{vert}}$  (Fig. 3(a)). We cannot check this numerical order of the characteristic length scales by using the DNS data in Figs. 1(b), 2(b), and 3(b) because the latter do not have a sufficiently large computational box/flow domain to yield negligible values of  $R_{ii}^{(\infty)}$  at the respective boundaries. The boundedness of these length scales is incompatible with that length scales in (ideal) homogeneous shear turbulence are accepted as growing indefinitely large in DNS [10].

It is interesting to notice that the presence of such bounded macro length scales may be essential for the experimental measurement of the flow properties of homogeneous shear turbulence. Otherwise, unbounded macro correlation scales imply that measurement of  $U_{ij}(\mathbf{r})$  would be affected significantly by a laboratory setup of finite size and even measurement of Reynolds stress  $U_{ij}(\mathbf{0})$  would become unreliable, considering the close interaction among  $U_{ij}(\mathbf{0})$  and  $U_{ij}(\mathbf{r})$ . This result of three bounded macro length scales may be viewed as a merit contributed by the second-order model.

Regarding the distribution patterns of  $R_{ii}^{(\infty)}(\mathbf{r})$ , the predictions are quite different from those of DNS reproduced in Figs. 1(b), 2(b), and 3(b). (i) Compared with Fig. 1(b), the negative values of the streamwise distributions in Fig. 1(a) are much larger in magnitude. The predicted local maxima of  $R_{ii}^{(\infty)}$  and minima of  $R_{11}^{(\infty)}$  and  $R_{22}^{(\infty)}$  do not exist in the DNS data either. (ii) About the vertical distributions, the trends of  $R_{22}^{(\infty)}$  and  $R_{33}^{(\infty)}$  in Fig. 2(a) are compatible with those in Fig. 2(b), but the predicted  $R_{11}^{(\infty)}$  has a locally negative minimum which is absent in Fig. 2(b). (iii) Figure 3(a) shows the complex wave-like spanwise distributions with local minima and maxima, incompatible with the monotonically decreasing pattern displayed in Fig. 3(b).

The above comparisons reveal a major flawed feature of the prediction — the local negative minima of  $R_{ii}^{(\infty)}(\mathbf{r})$  are either too large in magnitude or present spuriously. The cause can be attributed to the mathematical structure of the second-order model in the space of control variables  $\dot{\Gamma}_{ij}^{(\infty)}$ , especially the structures of  $U_{ij}^{(\infty)}$  and the constraints in terms of  $\dot{\Gamma}_{ij}^{(\infty)}$ : the maximization of objective (58) still produces this feature, even though it has the tendency to promote overall large and positive  $U_{ii}^{(\infty)}(\mathbf{r})$ . It is expected that the third-order model has the potential to modify this feature and improve the prediction of  $R_{ii}^{(\infty)}(\mathbf{r})$ , based on the following considerations: (a) Physically, the third-order model is an improved model which includes the third order correlations (their evolution and associated constraints), the nonnegativity of variance of products, etc. (b) Mathematically,  $\tilde{U}_{(ij)kl}^{(\infty)}$  act as the control variables, the optimization problem is formulated in the enlarged control variable space of  $\tilde{U}_{(ij)kl}^{(\infty)}$ , the mathematical structures of  $U_{ij}^{(\infty)}$  and the constraints in term of  $\tilde{U}_{(ij)kl}^{(\infty)}$  are different from those of the second-order model. These new structures may correct the flawed feature, together with the maximization of objective (58) which tends to promote overall large and positive  $U_{ii}^{(\infty)}(\mathbf{r})$ . With this improvement, the correlation patterns may be closer to those produced by DNS.

## V. CONCLUSION

The ideas from theories of optimal control and convex optimization are used to model homogeneous shear turbulence of an incompressible Newtonian fluid. The intent is to explore an approach of optimal correlations to help resolve the issues of non-realizability and restriction to homogeneity encountered by analytical theories of turbulence. The multi-point spatial correlations of velocity and pressure fluctuations up to the degenerate fourth order are included in the framework. Two models are formulated: The second-order model takes the second order correlations as state variables and the contracted and degenerate third order correlations as the control variables; The third-order model takes both the second and the third order correlations as state variables and the degenerate fourth order correlations as the control variables.

For both models, the primary dynamical equations of evolution are presented. The sources of constraints are discussed, namely the correlation definitions, the inversion and mirror symmetries, the Cauchy-Schwarz inequality, and the non-negativity of variance of products. The constraints of the non-negativity of variance of products provide a mechanism to bound all the correlations and to dictate that the maximum exponential growth rate of the correlations in the asymptotic state be zero, contradicting DNS data. Shannon entropy is used to argue for  $\max \int_{\mathbb{R}^3} d\mathbf{r} U_{kk}(\mathbf{r})$  as the alternative objective functional, the latter is then substantiated from the perspective of strong mixing in physical turbulence. The models are second-order cone programs in their discretized forms.

Restricted by computational feasibility at present, only the asymptotic steady state of the second-order model is solved numerically. As part of the basis for evaluation, the non-trivial values of the anisotropy tensor  $b_{ij}^{(\infty)}$  are compared between the prediction and the experiments [8], and they are given here: (a)  $b_{11}^{(\infty)} = 0.5031 > b_{33}^{(\infty)} = -0.2080 > b_{22}^{(\infty)} = -0.2951$  (Prediction) versus  $b_{11}^{(\infty)} = 0.203 > b_{33}^{(\infty)} = -0.06 > b_{22}^{(\infty)} = -0.143$  (Experiment); (b)  $b_{12}^{(\infty)} = -0.1161$  (Prediction) versus  $b_{12}^{(\infty)} = -0.156$  (Experiment). The qualitative agreement with regard to the relative numerical order pattern among  $b_{11}^{(\infty)}$ ,  $b_{22}^{(\infty)}$ , and  $b_{33}^{(\infty)}$  is encouraging, indicating the potential of the framework. However, there are significant quantitative differences between the predicated and the experimental values. The non-enforceability of the non-negativity of variance of products within the second-order model is identified as the cause. Regarding the prediction of the second order correlation functions  $R_{ii}^{(\infty)}(\mathbf{r})$ , the results are mixed too: (a) The streamwise, vertical, and spanwise characteristic macro length scales are estimated as finite for the two-point correlations, in contrast to DNS where they are accepted to be indefinitely large. The relative numerical order of the scales appear consistent with the physical flow. (b) The  $\mathbf{r}$ -dependent distribution patterns display a major flawed feature that local negative minima are either too large in magnitude or present spuriously. The mathematical structures of  $U_{ij}^{(\infty)}$  and the constraints in the space of control variables  $\dot{\Gamma}_{ij}^{(\infty)}$  are recognized as the cause for this erroneous prediction. It is then inferred that the third-order model is necessary and has potential to improve predictions, on the basis of the following considerations: (i) It is an improvement over the second-order model. It contains the third order and degenerate fourth order correlations, the non-negativity of variance of products, etc. The resulting mathematical structure of the optimization problem exists in the enlarged space of control variables  $\tilde{U}_{(ij)kl}^{(\infty)}$  and may predict better. (ii) The model contains both the distributive mechanism of distributing turbulent energy among its three components and the bounding mechanism to bound from above these components and their differences. However, implementation of the model needs further study as it is a huge-scale problem. Also, algorithms specific to multi-dimensional integrals (up to 10-dimensions) that arise in the model need to be developed in order to improve convergence rates and compute efficiently the huge number of integrals necessary for the implementation of the constraints. Alternatively, to avoid this issue of integration, we may explore how to solve the third-order model in physical space.

It is noted that the dynamical equations of evolution for the mean flow fields and for the spatial correlations may be easily derived for inhomogeneous turbulent flows of an incompressible Newtonian fluid. The above listed sources of constraints, such as the correlation definitions, the Cauchy-Schwarz inequality, and the non-negativity of variance of products, are also the sources of constraints for such flows and may be formulated accordingly. Further, the issue of Shannon entropy, its substitute, and the physical interpretation may be discussed similarly. Therefore, the present exploration of homogeneous shear turbulence as a second-order cone program may shed light on modeling inhomogeneous turbulent flows. A similar comment may be made regarding some other motion systems too. Further, it will be interesting to explore the possibility of a second-order model suitable for LES.

## ACKNOWLEDGMENTS

I thank Professor M. Ramakrishna, Aerospace Engineering, IIT Madras, for meaningful discussions, and I thank Dr. Parag Ravindran, Mechanical Engineering, IIT Madras, for help rewording the manuscript. I thank the developers

of the open-source packages CUBA Library, CVXPY, SCS, and MPICH whose codes made the simulation easier, and I thank CVX Research, Inc. for granting me a free academic license for CVX Professional to use MOSEK.

The computational codes and their output data files may be accessed via

[https://drive.google.com/drive/folders/1s4e6\\_\\_AkdQQTmCCXKvmoCr3iPyrh0b6T?usp=sharing](https://drive.google.com/drive/folders/1s4e6__AkdQQTmCCXKvmoCr3iPyrh0b6T?usp=sharing)

### Appendix A: Symmetries of inversion and mirror

The derivation of the inversion and mirror symmetries (7) is outlined in this appendix.

The geometric and kinematic symmetries underlying the mean flow field (1) suggest that, under the spatial inversion  $\{\mathbf{x}, \mathbf{y}, \mathbf{z}\} \rightarrow \{-\mathbf{x}, -\mathbf{y}, -\mathbf{z}\}$ , the statistical correlations transform according to

$$\begin{aligned} \overline{w_i(\mathbf{x})w_j(\mathbf{y})} &= \overline{(-w_i(-\mathbf{x}))(-w_j(-\mathbf{y}))}, & \overline{w_i(\mathbf{x})w_j(\mathbf{y})w_k(\mathbf{z})} &= \overline{(-w_i(-\mathbf{x}))(-w_j(-\mathbf{y}))(-w_k(-\mathbf{z}))}, \\ \overline{q(\mathbf{x})w_j(\mathbf{y})} &= \overline{q(-\mathbf{x})(-w_j(-\mathbf{y}))}, \dots \end{aligned} \quad (\text{A1})$$

which results in the inversion symmetry equalities of Eqs. (7) under homogeneity.

Next, the geometric and kinematic symmetries of the mean flow field suggest the plane inversion symmetry under the plane transformation  $\{\mathbf{x}, \mathbf{y}, \mathbf{z}\} \rightarrow \{(-x_1, -x_2, x_3), (-y_1, -y_2, y_3), (-z_1, -z_2, z_3)\}$ :  $w_1$  and  $w_2$  change their signs and  $w_3$  and  $q$  do not change signs in the correlations, such as

$$\begin{aligned} \overline{w_1(\mathbf{x})w_1(\mathbf{y})} &= \overline{(-w_1(-x_1, -x_2, x_3))(-w_1(-y_1, -y_2, y_3))}, & \overline{w_1(\mathbf{x})w_3(\mathbf{y})} &= \overline{(-w_1(-x_1, -x_2, x_3))w_3(-y_1, -y_2, y_3)}, \\ \overline{q(\mathbf{x})w_2(\mathbf{y})} &= \overline{q(-x_1, -x_2, x_3)(-w_2(-y_1, -y_2, y_3))}, \dots \end{aligned} \quad (\text{A2})$$

Combining this plane inversion symmetry with the spatial inversion symmetry (A1) leads to the statistical symmetry of mirror under  $\{\mathbf{x}, \mathbf{y}, \mathbf{z}\} \rightarrow \{\mathbf{x}' = (x_1, x_2, -x_3), \mathbf{y}' = (y_1, y_2, -y_3), \mathbf{z}' = (z_1, z_2, -z_3)\}$ ,

$$\overline{w_i(\mathbf{x})w_j(\mathbf{y})} = (-1)^{\delta_{i3} + \delta_{j3}} \overline{w_{\underline{i}}(\mathbf{x}')w_{\underline{j}}(\mathbf{y}')}, \quad \overline{q(\mathbf{x})w_i(\mathbf{y})} = (-1)^{\delta_{i3}} \overline{q(\mathbf{x}')w_{\underline{i}}(\mathbf{y}')}, \dots \quad (\text{A3})$$

Further, imposition of homogeneity produces the mirror symmetry constraints of Eqs. (7).

### Appendix B: Detail for the second-order model

The derivation of constraints (17) is outlined here. Integration of  $(k_k + l_k)\tilde{U}_{kij}^{(I)}(\mathbf{k}, \mathbf{l}) = 0$  of Eqs. (9a) gives

$$\int_{\mathbb{R}^3} \int_{\mathbb{R}^3} d\mathbf{k} dl k_k \left( \tilde{U}_{kji}^{(I)}(\mathbf{l}, \mathbf{k}) + \tilde{U}_{kij}^{(I)}(\mathbf{l}, \mathbf{k}) \right) = 0.$$

This equality is operated upon as follows,

$$\int_{-\infty}^{+\infty} dk_1 = \int_{-\infty}^0 dk_1 + \int_0^{+\infty} dk_1, \quad (\mathbf{k}, \mathbf{l}) \rightarrow -(\mathbf{k}, \mathbf{l}), \quad \tilde{U}_{kij}^{(I)}(-\mathbf{k}, -\mathbf{l}) = -\tilde{U}_{kij}^{(I)}(\mathbf{k}, \mathbf{l}).$$

The second part and the third part are applied to the term  $\int_0^{+\infty} dk_1$  of the first part; together with the use of Eqs. (11), the operation results in the mentioned constraints.

### Appendix C: Detail for the third-order model

The third order correlations  $\tilde{U}_{ijk}$  are state variables. Along with Eqs. (10), the divergence-free constraints for  $\tilde{U}_{ijk}$  in Eqs. (9a) are solved to yield

$$\begin{aligned} \tilde{U}_{113}^{(I)}(\mathbf{k}, \mathbf{l}) &= -\frac{l_1}{l_3}\tilde{U}_{111}^{(I)}(\mathbf{k}, \mathbf{l}) - \frac{l_2}{l_3}\tilde{U}_{112}^{(I)}(\mathbf{k}, \mathbf{l}), & \tilde{U}_{123}^{(I)}(\mathbf{k}, \mathbf{l}) &= -\frac{l_1}{l_3}\tilde{U}_{112}^{(I)}(\mathbf{l}, \mathbf{k}) - \frac{l_2}{l_3}\tilde{U}_{122}^{(I)}(\mathbf{k}, \mathbf{l}), \\ \tilde{U}_{223}^{(I)}(\mathbf{k}, \mathbf{l}) &= -\frac{l_1}{l_3}\tilde{U}_{122}^{(I)}(-\mathbf{l} - \mathbf{k}, \mathbf{k}) - \frac{l_2}{l_3}\tilde{U}_{222}^{(I)}(\mathbf{k}, \mathbf{l}), \\ \tilde{U}_{133}^{(I)}(\mathbf{k}, \mathbf{l}) &= \frac{k_1 l_1}{k_3 l_3}\tilde{U}_{111}^{(I)}(\mathbf{k}, \mathbf{l}) + \frac{l_1 k_2}{k_3 l_3}\tilde{U}_{112}^{(I)}(\mathbf{l}, \mathbf{k}) + \frac{k_1 l_2}{k_3 l_3}\tilde{U}_{112}^{(I)}(\mathbf{k}, \mathbf{l}) + \frac{k_2 l_2}{k_3 l_3}\tilde{U}_{122}^{(I)}(\mathbf{k}, \mathbf{l}), \end{aligned}$$

$$\begin{aligned}
\tilde{U}_{233}^{(I)}(\mathbf{k}, \mathbf{l}) &= \frac{k_1 l_1}{k_3 l_3} \tilde{U}_{112}^{(I)}(\mathbf{k}, -\mathbf{l} - \mathbf{k}) + \frac{k_2 l_1}{k_3 l_3} \tilde{U}_{122}^{(I)}(-\mathbf{l} - \mathbf{k}, \mathbf{k}) + \frac{k_1 l_2}{k_3 l_3} \tilde{U}_{122}^{(I)}(-\mathbf{l} - \mathbf{k}, \mathbf{l}) + \frac{k_2 l_2}{k_3 l_3} \tilde{U}_{222}^{(I)}(\mathbf{k}, \mathbf{l}), \\
\tilde{U}_{333}^{(I)}(\mathbf{k}, \mathbf{l}) &= -\frac{l_1 k_1 (k_1 + l_1)}{k_3 l_3 (k_3 + l_3)} \tilde{U}_{111}^{(I)}(\mathbf{k}, \mathbf{l}) - \frac{l_1 (k_1 + l_1) k_2}{k_3 l_3 (k_3 + l_3)} \tilde{U}_{112}^{(I)}(\mathbf{l}, \mathbf{k}) - \frac{k_1 (k_1 + l_1) l_2}{k_3 l_3 (k_3 + l_3)} \tilde{U}_{112}^{(I)}(\mathbf{k}, \mathbf{l}) \\
&\quad - \frac{k_1 l_1 (k_2 + l_2)}{k_3 l_3 (k_3 + l_3)} \tilde{U}_{112}^{(I)}(\mathbf{k}, -\mathbf{l} - \mathbf{k}) - \frac{l_1 k_2 (k_2 + l_2)}{k_3 l_3 (k_3 + l_3)} \tilde{U}_{122}^{(I)}(\mathbf{k}, -\mathbf{l} - \mathbf{k}) - \frac{k_1 l_2 (k_2 + l_2)}{k_3 l_3 (k_3 + l_3)} \tilde{U}_{122}^{(I)}(\mathbf{l}, -\mathbf{l} - \mathbf{k}) \\
&\quad - \frac{(k_1 + l_1) k_2 l_2}{k_3 l_3 (k_3 + l_3)} \tilde{U}_{122}^{(I)}(\mathbf{k}, \mathbf{l}) - \frac{k_2 l_2 (k_2 + l_2)}{k_3 l_3 (k_3 + l_3)} \tilde{U}_{222}^{(I)}(\mathbf{k}, \mathbf{l}).
\end{aligned} \tag{C1}$$

The components not present above can be obtained with the aid of Eqs. (10).

#### Appendix D: Examples of inequalities involving only the second order correlations

With the help of Eqs. (27), Eqs. (26) can be verified directly,

$$\begin{aligned}
\overline{\tilde{\omega}_1 \tilde{\omega}_1}(\mathbf{k}) &\geq \left( |k_3| \sqrt{\tilde{U}_{22}(\mathbf{k})} - |k_2| \sqrt{\tilde{U}_{33}(\mathbf{k})} \right)^2 + 2|k_2 k_3| \left( \sqrt{\tilde{U}_{22}(\mathbf{k}) \tilde{U}_{33}(\mathbf{k})} - |\tilde{U}_{23}(\mathbf{k})| \right), \\
\overline{\tilde{\omega}_1 \tilde{\omega}_1}(\mathbf{k}) \overline{\tilde{\omega}_3 \tilde{\omega}_3}(\mathbf{k}) - \left( \overline{\tilde{\omega}_1 \tilde{\omega}_3}(\mathbf{k}) \right)^2 &= (k_2)^2 [(k_3)^2 + 2(k_1)^2] \left( \tilde{U}_{11}(\mathbf{k}) \tilde{U}_{22}(\mathbf{k}) - (\tilde{U}_{12}(\mathbf{k}))^2 \right) \\
&\quad + (k_1 k_2)^2 \left( \tilde{U}_{22}(\mathbf{k}) \tilde{U}_{33}(\mathbf{k}) - (\tilde{U}_{23}(\mathbf{k}))^2 \right) + (k_2)^2 [(k_2)^2 + 2(k_1)^2 + 2(k_3)^2] \left( \tilde{U}_{11}(\mathbf{k}) \tilde{U}_{33}(\mathbf{k}) - (\tilde{U}_{13}(\mathbf{k}))^2 \right), \\
\tilde{U}_{11}(\mathbf{k}) \overline{\tilde{\omega}_1 \tilde{\omega}_1}(\mathbf{k}) - \left| \overline{\tilde{\omega}_1 \tilde{\omega}_1}(\mathbf{k}) \right|^2 &= [(k_3)^2 + 2(k_2)^2] \left( \tilde{U}_{11}(\mathbf{k}) \tilde{U}_{22}(\mathbf{k}) - (\tilde{U}_{12}(\mathbf{k}))^2 \right) + (k_2)^2 \left( \tilde{U}_{11}(\mathbf{k}) \tilde{U}_{33}(\mathbf{k}) - (\tilde{U}_{13}(\mathbf{k}))^2 \right), \\
\tilde{U}_{11}(\mathbf{k}) \overline{\tilde{\omega}_2 \tilde{\omega}_2}(\mathbf{k}) - \left| \overline{\tilde{\omega}_1 \tilde{\omega}_2}(\mathbf{k}) \right|^2 &= (k_1)^2 \left( \tilde{U}_{11}(\mathbf{k}) \tilde{U}_{33}(\mathbf{k}) - (\tilde{U}_{13}(\mathbf{k}))^2 \right).
\end{aligned} \tag{D1}$$

The remaining ones are obtained by symmetry.

For the derivation of Eq. (29), inequalities (28) are combined, operated on with the help of the following inequality,

$$\left[ (\lambda \tilde{a} f_a)^{1/2} - (\tilde{b} f_b / \lambda)^{1/2} \right]^2 \geq 0, \quad \lambda = \left( \int_{\mathbb{R}^3} d\mathbf{k} \tilde{b}(\mathbf{k}) f_b / \int_{\mathbb{R}^3} d\mathbf{k} \tilde{a}(\mathbf{k}) f_a \right)^{1/2},$$

and then integrated to obtain

$$\left| \int_{\mathbb{R}^3} d\mathbf{k} \tilde{c}(\mathbf{k}) f_c \right|^2 \leq \int_{\mathbb{R}^3} d\mathbf{k} \tilde{a}(\mathbf{k}) f_a \int_{\mathbb{R}^3} d\mathbf{k} \tilde{b}(\mathbf{k}) f_b.$$

As an example, consider

$$a = w_i(\mathbf{y}) - w_i(\mathbf{x}) + \alpha [w_i(\mathbf{z}') - w_i(\mathbf{z})], \quad b = \omega_j(\mathbf{z}') - \omega_j(\mathbf{z}) - \beta [\omega_j(\mathbf{y}) - \omega_j(\mathbf{x})]. \tag{D2}$$

The Cauchy-Schwarz inequality  $|\overline{ab}|^2 \leq \overline{aa} \overline{bb}$  is applied to obtain

$$\left| \int_{\mathbb{R}^3} d\mathbf{k} \overline{\tilde{w}_i \tilde{\omega}_j}(\mathbf{k}) f_c \right|^2 \leq \int_{\mathbb{R}^3} d\mathbf{k} \tilde{U}_{ii}(\mathbf{k}) f_a \int_{\mathbb{R}^3} d\mathbf{k} \overline{\tilde{\omega}_j \tilde{\omega}_j}(\mathbf{k}) f_b, \tag{D3}$$

where

$$\begin{aligned}
f_a &= 4 \left( \left| \sin \frac{\mathbf{r} \cdot \mathbf{k}}{2} \right|^2 + \left| \alpha \sin \frac{(\mathbf{s}' - \mathbf{s}) \cdot \mathbf{k}}{2} \right|^2 + 2 \sin \frac{\mathbf{r} \cdot \mathbf{k}}{2} \alpha \sin \frac{(\mathbf{s}' - \mathbf{s}) \cdot \mathbf{k}}{2} \cos \frac{(\mathbf{s}' + \mathbf{s} - \mathbf{r}) \cdot \mathbf{k}}{2} \right) \\
&\geq 4 \left( \left| \sin \frac{\mathbf{r} \cdot \mathbf{k}}{2} \right| - \left| \alpha \sin \frac{(\mathbf{s}' - \mathbf{s}) \cdot \mathbf{k}}{2} \right| \right)^2, \\
f_b &= 4 \left( \left| \sin \frac{(\mathbf{s}' - \mathbf{s}) \cdot \mathbf{k}}{2} \right|^2 + \left| \beta \sin \frac{\mathbf{r} \cdot \mathbf{k}}{2} \right|^2 - 2 \sin \frac{(\mathbf{s}' - \mathbf{s}) \cdot \mathbf{k}}{2} \beta \sin \frac{\mathbf{r} \cdot \mathbf{k}}{2} \cos \frac{(\mathbf{s}' + \mathbf{s} - \mathbf{r}) \cdot \mathbf{k}}{2} \right) \\
&\geq 4 \left( \left| \sin \frac{(\mathbf{s}' - \mathbf{s}) \cdot \mathbf{k}}{2} \right| - \left| \beta \sin \frac{\mathbf{r} \cdot \mathbf{k}}{2} \right| \right)^2,
\end{aligned} \tag{D4}$$

$$f_c = \iota(1 + \alpha\beta) \left[ \sin[\mathbf{k} \cdot (\mathbf{s}' - \mathbf{r})] - \sin[\mathbf{k} \cdot (\mathbf{s} - \mathbf{r})] - \sin(\mathbf{k} \cdot \mathbf{s}') + \sin(\mathbf{k} \cdot \mathbf{s}) \right],$$

$$f_a f_b - |f_c|^2 = 16 \left( \alpha \left| \sin \frac{(\mathbf{s}' - \mathbf{s}) \cdot \mathbf{k}}{2} \right|^2 - \beta \left| \sin \frac{\mathbf{r} \cdot \mathbf{k}}{2} \right|^2 + (1 - \alpha\beta) \sin \frac{\mathbf{r} \cdot \mathbf{k}}{2} \sin \frac{(\mathbf{s}' - \mathbf{s}) \cdot \mathbf{k}}{2} \cos \frac{(\mathbf{s}' + \mathbf{s} - \mathbf{r}) \cdot \mathbf{k}}{2} \right)^2.$$

Inequalities (D4) imply automatic satisfaction of Eq. (D3), by the use of Eqs. (25), (26), (28), and (29).

Next,  $|\overline{ab}|^2 \leq \overline{aa} \overline{bb}$  is applied to two more examples,

$$a = w_i(\mathbf{y}) - w_i(\mathbf{x}) + \alpha[w_i(\mathbf{z}') - w_i(\mathbf{z})], \quad b = w_j(\mathbf{z}') - w_j(\mathbf{z}) - \beta[w_j(\mathbf{y}) - w_j(\mathbf{x})]; \quad (\text{D5a})$$

$$a = w_i(\mathbf{y}) - w_i(\mathbf{x}) + \alpha[\omega_i(\mathbf{z}') - \omega_i(\mathbf{z})], \quad b = \omega_j(\mathbf{z}') - \omega_j(\mathbf{z}) - \beta[\omega_j(\mathbf{y}) - \omega_j(\mathbf{x})]. \quad (\text{D5b})$$

A straight-forward operation results in the following constraints of inequality,

$$\left| \int_{\mathbb{R}^3} d\mathbf{k} \tilde{U}_{ij}(\mathbf{k}) f_c \right|^2 \leq \int_{\mathbb{R}^3} d\mathbf{k} \tilde{U}_{ii}(\mathbf{k}) f_a \int_{\mathbb{R}^3} d\mathbf{k} \tilde{U}_{jj}(\mathbf{k}) f_b, \quad (\text{D6a})$$

$$\left| \int_{\mathbb{R}^3} d\mathbf{k} \overline{\tilde{\omega}_i \tilde{\omega}_j}(\mathbf{k}) f_c \right|^2 \leq \int_{\mathbb{R}^3} d\mathbf{k} \overline{\tilde{\omega}_i \tilde{\omega}_i}(\mathbf{k}) f_a \int_{\mathbb{R}^3} d\mathbf{k} \overline{\tilde{\omega}_j \tilde{\omega}_j}(\mathbf{k}) f_b. \quad (\text{D6b})$$

Here,  $f_a$  and  $f_b$  are given by Eqs. (D4), and

$$f_c = \cos[\mathbf{k} \cdot (\mathbf{s}' - \mathbf{r})] - \cos[\mathbf{k} \cdot (\mathbf{s} - \mathbf{r})] - \cos(\mathbf{k} \cdot \mathbf{s}') + \cos(\mathbf{k} \cdot \mathbf{s}) + 2\alpha(1 - \cos[\mathbf{k} \cdot (\mathbf{s}' - \mathbf{s})])$$

$$- \alpha\beta(\cos[\mathbf{k} \cdot (\mathbf{s}' - \mathbf{r})] - \cos[\mathbf{k} \cdot (\mathbf{s} - \mathbf{r})] - \cos(\mathbf{k} \cdot \mathbf{s}') + \cos(\mathbf{k} \cdot \mathbf{s})) - 2\beta(1 - \cos(\mathbf{k} \cdot \mathbf{r})), \quad (\text{D7})$$

$$f_a f_b - |f_c|^2 = 16(1 + \alpha\beta)^2 \left| \sin \frac{\mathbf{r} \cdot \mathbf{k}}{2} \sin \frac{(\mathbf{s}' - \mathbf{s}) \cdot \mathbf{k}}{2} \right|^2 \left( 1 - \left| \cos \frac{(\mathbf{s}' + \mathbf{s} - \mathbf{r}) \cdot \mathbf{k}}{2} \right|^2 \right).$$

Therefore, inequalities (D6) are satisfied automatically because of elementary constraints (25).

### Appendix E: Application of Shannon entropy

This appendix discusses the application of Shannon entropy to the framework. The argument intends to be conceptual and illustrative. It serves the purpose of obtaining an objective functional.

*a. Discretized representation* Consider the equations of motion (3) for  $w_i$  and  $q$ . In numerical simulation, the domain of motion  $\mathbb{R}^3$  is replaced with a cube  $\mathcal{D} = [-L, L]^3$  with  $L$  chosen appropriately.

The fluctuation fields  $w_i$  and  $q$  are represented in terms of a truncated function basis  $\{\psi_m(\mathbf{x}) : m = 1, \dots, M\}$ ,

$$w_i(\mathbf{x}, t) = c_{i,m}(t) \psi_m(\mathbf{x}), \quad q = c_{0,m}(t) \psi_m(\mathbf{x}), \quad (\text{E1})$$

where  $\mathbf{c} = \{c_{i,j}\}$  characterize the turbulent fluctuations and contain  $M_c = 4M$  elements. The dynamical equations of  $\mathbf{c}(t)$  may be derived from Eqs. (3) and (E1), that are not required in a formal argument below.

On the basis of Eqs. (E1), we introduce a probability density function  $f(\mathbf{c})$  to describe  $w_i$  and  $q$  statistically, instead of a complicated probability density functional  $\hat{f}(w_i(\mathbf{x}, t), q(\mathbf{x}, t))$ . Though  $\mathbf{c}$  depends on  $t$ ,  $f(\mathbf{c})$  may be viewed effectively as a function, since  $\mathbf{c}$  is to be discretized.  $|w_i(\mathbf{x}, t)|$  are supposedly bounded. Hence,  $f$  has a support  $[-c_0, c_0]^{M_c}$  for some positive constant  $c_0$  which is yet to be fixed as part of the treatment. Further, the structure of  $f$  is constrained by the definition of  $f$  ( $f(\mathbf{c}) \geq 0$ ,  $\int f(\mathbf{c}) d\mathbf{c} = 1$ ),  $\int \mathbf{c} f(\mathbf{c}) d\mathbf{c} = \mathbf{0}$ , the dynamical equations (to be discretized in time), and the constraints for the spatial correlations developed (without the imposition of homogeneity throughout  $\mathcal{D}$ , especially in the boundary subregion). All these constraints may be expressed in terms of  $\mathbf{c}$  via intermediate representations, such as

$$\overline{w_k(\mathbf{x}, t)} = \psi_m(\mathbf{x}) \int_{\{|c_{i,j}| \leq c_0\}} c_{k,m} f(\mathbf{c}) d\mathbf{c}, \quad \overline{w_k(\mathbf{x}, t) w_l(\mathbf{y}, t)} = \psi_m(\mathbf{x}) \psi_n(\mathbf{y}) \int_{\{|c_{i,j}| \leq c_0\}} c_{k,m} c_{l,n} f(\mathbf{c}) d\mathbf{c}, \dots$$

*b. Differential and Shannon entropies* We define the differential entropy [15, 17, 18],

$$H(f) = - \int_{\{|c_{i,j}| \leq c_0\}} f(\mathbf{c}) \log f(\mathbf{c}) d\mathbf{c}. \quad (\text{E2})$$

For convenience, we do not adopt the concept of relative entropy [17, 18], since it does not affect the alternative objective obtained (see Eq. (33)). If necessary, a relative entropy may be defined by the use of the uniform probability density function over the support of  $f$ .

To evaluate  $H(f)$  numerically, a uniform mesh (of size  $\Delta$  in each direction) is adopted to discretize the support of  $f$ . The centers of mesh elements are

$$\mathcal{M} = \prod_{k,l} \{c_{k,l} = -c_0 + (m_{k,l} - 1/2)\Delta : m_{k,l} = 1, \dots, 2c_0/\Delta\}. \quad (\text{E3})$$

We approximate  $f$  simply via the nodal values  $\{f(\theta)\} = \{f(\theta) : \theta \in \mathcal{M}\}$  (piecewise constant). We then resort to the basic composite midpoint rule for equal mesh elements to discretize and approximate  $H(f)$ ,

$$H(f) \approx -\Delta^{M_c} \sum_{\theta \in \mathcal{M}} f(\theta) \log f(\theta) = H_\Delta(f) + \log(\Delta^{M_c}) \sum_{\theta \in \mathcal{M}} [f(\theta)\Delta^{M_c}]. \quad (\text{E4})$$

$H_\Delta(f)$  is the Shannon entropy associated with the discretized  $f$  [18],

$$H_\Delta(f) = - \sum_{\theta \in \mathcal{M}} [f(\theta)\Delta^{M_c}] \log [f(\theta)\Delta^{M_c}], \quad (\text{E5})$$

with  $f(\theta)\Delta^{M_c}$  representing the  $\theta$ -element probability.

Similarly, the correlations and all the aforementioned constraints may be represented in terms of the nodal values  $\{f(\theta)\}$ , these resulting constraints are to be enforced at adequately selected collocation points in  $\mathcal{D}$  at time instant  $t$ . The unknown  $\{f(\theta)\}$  are constrained by all these discretized constraints. According to information theory [15–18],  $H_\Delta(f)$  is a measure of uncertainty of the discretized fluctuations (for  $\{c_{i,j}\}$  to take the discrete values in  $\mathcal{M}$ ),  $\{f(\theta)\}$  may be found through maximization of  $H_\Delta(f)$  subject to the discretized constraints. This idea is adopted here.

In numerical simulation, an adequately small and finite value of  $\Delta$  is fixed to carry out the above procedure of maximization. In this procedure, by the definition of  $f$ ,

$$\sum_{\theta \in \mathcal{M}} [f(\theta)\Delta^{M_c}] = 1 \quad (\text{E6})$$

is enforced. Combination of Eqs. (E4) and (E6) yields

$$\max H_\Delta(f) \Leftrightarrow \max H(f), \quad (\text{E7})$$

in the sense that the optimal discrete values  $\{f(\theta)\}$  from  $\max H_\Delta(f)$  approximate the optimal continuous density function  $f$  from  $\max H(f)$ . Therefore, from a numerical simulation point of view, the maximization of Shannon entropy effectively implies the maximization of the differential entropy  $\max H(f)$ . Considering the debate regarding  $\max H(f)$  as a principle, we take  $\max H_\Delta(f)$  as the starting point and  $\max H(f)$  as the approximate and effective consequence, because  $f$  needs to be solved numerically, if ever possible.

*c. Alternative objective* There are tremendous difficulties to solve  $\max H(f)$ , such as the computationally formidable size of a discretized  $f$ , numerical integration in very high  $M_c$ -dimensions, etc. An alternative objective needs to be sought which is computationally feasible or explorable and is closely related to  $\max H(f)$ .

The solution of  $\max H(f)$  is the broadest distribution  $f$  with a large spread-out, characterized partially by large values of the second order moments, according to probability theory,

$$\int_{\{|c_{i,j}| \leq c_0\}} c_{\underline{k},m} c_{\underline{k},n} f(\mathbf{c}) d\mathbf{c},$$

which affects the second order correlations through

$$U_{\underline{k}\underline{k}}(\mathbf{r}) = \psi_m(\mathbf{0})\psi_n(\mathbf{r}) \int_{\{|c_{i,j}| \leq c_0\}} c_{\underline{k},m} c_{\underline{k},n} f(\mathbf{c}) d\mathbf{c}, \quad (\text{E8})$$

which holds expectedly for  $\mathbf{r} = \mathbf{y} - \mathbf{x}$  with  $\mathbf{x}$  and  $\mathbf{y}$  away from the boundary subregion. This selection of the second order moments and the second order correlations is needed, because an objective should reflect the direct and collective effect of all the dynamical equations and the constraints for the correlations. To construct a single objective from Eq. (E8), a scalar quantity is required which is independent of the Cartesian coordinate systems chosen to describe the turbulent motion, in order to satisfy objectivity. The natural choice is the trace of the second order correlations,  $U_{kk}(\mathbf{r})$ .

## Appendix F: Second-order cone programming

Both models, in their discretized forms, are SOCP, according to the criteria set in [20, 21].

Within the third-order model,  $\tilde{U}_{(ij)kl}$  act as the control variables,  $\tilde{U}_{ij}$ ,  $\tilde{U}_{ijk}^{(I)}$ ,  $\tilde{Q}_j$ ,  $\tilde{Q}_j^{(I)}$ ,  $\tilde{Q}_{ij}$ , and their corresponding quantities in physical space are state variables. With the help of the method of characteristics, Eqs. (14) and (21) may be formally solved, the state variables are related to the control variables linearly, and thus, all the state variables, the constraints, and the dynamical equations of evolution are expressed explicitly in terms of  $\tilde{U}_{(ij)kl}$ , as is the objective functional (33).

Computationally,  $\tilde{U}_{(ij)kl}(\mathbf{k}, \mathbf{l}, t)$  need to be discretized inside an adequate bounded support in the  $(\mathbf{k}, \mathbf{l})$ -space and in  $t$ . To establish the discretized third-order model as a SOCP, it is sufficient to consider the following: (a) The support is discretized into a finite element mesh. (b) At instant  $t = t^m$ , inside each element the spatial distributions of  $\tilde{U}_{(ij)kl}(\mathbf{k}, \mathbf{l}, t^m)$  are approximated linearly in terms of the  $\tilde{U}_{(ij)kl}$  at the nodes of the element; the collection of all these nodal control variables is denoted by  $\{\delta_i^m\}$ . (c) At fixed  $\mathbf{k}$  and  $\mathbf{l}$ , the temporal distributions of  $\tilde{U}_{(ij)kl}(\mathbf{k}, \mathbf{l}, t)$  in  $t \in [t^{m-1}, t^m]$  are approximated linearly in terms of  $\tilde{U}_{(ij)kl}(\mathbf{k}, \mathbf{l}, t^{m-1})$  and  $\tilde{U}_{(ij)kl}(\mathbf{k}, \mathbf{l}, t^m)$ . (d) At  $t^m$ , all the state variables depend linearly on  $\{\delta_i^m\}$  (and on  $\{\delta_i^{m-1}\}$  too, which is known). (e) All the linear constraints and the objective have linear forms in terms of  $\{\delta_i^m\}$ . (f) The quadratic constraints from the Cauchy-Schwarz inequality take the form,

$$\left\| \begin{bmatrix} 2(c_i \delta_i^m + c_0) \\ (a_i - b_i) \delta_i^m + a_0 - b_0 \end{bmatrix} \right\|_2 \leq (a_i + b_i) \delta_i^m + a_0 + b_0, \quad (\text{F1})$$

where  $a_k$ ,  $b_k$ , and  $c_k$  are independent of  $\{\delta_i^m\}$ ,  $a_0$ ,  $b_0$ , and  $c_0$  depend on  $\{\delta_i^{m-1}\}$ . (g) The quadratic constraints from Eq. (31) are of the form,

$$\left\| \begin{bmatrix} \frac{1}{2}(1 - a'_i \delta_i^m - a'_0) \\ c'_i \delta_i^m + c'_0 \end{bmatrix} \right\|_2 \leq \frac{1}{2}(1 + a'_i \delta_i^m + a'_0), \quad 0 \leq a'_i \delta_i^m + a'_0, \quad (\text{F2})$$

where  $a'_k$  and  $c'_k$  are independent of  $\{\delta_i^m\}$ ,  $a'_0$  and  $c'_0$  depend on  $\{\delta_i^{m-1}\}$ . It then follows that the discretized third-order model is a SOCP, according to the criteria in [20, 21]. Similarly, in a discretized form, the second-order model is shown to be a SOCP with  $\tilde{\Gamma}_{ij}$  as the control variables; The relevant details of discretization in the asymptotic states are given in Appendix I.

## Appendix G: Other upper bound for growth rate

Combination of Eqs. (20), (25), and (34) results in

$$\frac{\sigma}{2} U_{jj}^{(\infty)}(\mathbf{0}) = -U_{12}^{(\infty)}(\mathbf{0}) - \overline{w_{j,k}(\mathbf{x})w_{j,k}(\mathbf{x})}^{(\infty)}, \quad (\text{G1a})$$

$$\left| U_{12}^{(\infty)}(\mathbf{0}) \right| \leq \sqrt{U_{11}^{(\infty)}(\mathbf{0})U_{22}^{(\infty)}(\mathbf{0})} \leq \frac{1}{2} \left( U_{11}^{(\infty)}(\mathbf{0}) + U_{22}^{(\infty)}(\mathbf{0}) \right) = \frac{1}{2} \left( U_{jj}^{(\infty)}(\mathbf{0}) - U_{33}^{(\infty)}(\mathbf{0}) \right), \quad (\text{G1b})$$

which, along with  $U_{kk}^{(\infty)}(\mathbf{0}) > 0$  and the positive viscous dissipation, leads to

$$\sigma \leq 1 - \frac{\overline{2w_{j,k}(\mathbf{x})w_{j,k}(\mathbf{x})}^{(\infty)} + U_{33}^{(\infty)}(\mathbf{0})}{U_{jj}^{(\infty)}(\mathbf{0})} < 1. \quad (\text{G2})$$

This inequality implies that the second-order model may allow the asymptotic solution with  $\sigma \in (0, 1)$  to emerge out of a transient state, violating  $\max \sigma = 0$  of Eq. (35). To obtain an affirmative answer to this possibility, we resort to the mathematical structure that the second-order model and specifically  $\tilde{U}_{ij}^{(\infty)}$  depend on  $\sigma$  only via  $E(\mathbf{k}; k'_2; \sigma)$  defined by Eq. (44a). Function  $E(\mathbf{k}; k'_2; \sigma)$  indicates that, only in certain subregions,  $\sigma$  affects  $\tilde{U}_{ij}^{(\infty)}$  significantly, as explained next.

Suppose that in the case of  $\sigma = 0$  there exists a feasible solution  $\{\tilde{U}_{ij}^{(\infty)}, \dot{\Gamma}_{ij}^{(\infty)}\}_{\sigma=0}$  which takes the value of zero in the subregion,

$$\mathcal{R}_0 = \{\mathbf{k} : k_1 \in [-(K_0)^{1/2}, 0]\}, \quad (\text{G3})$$

where  $K_0$  is a positive constant. We argue that this feasible solution is also a feasible solution for certain positive values of  $\sigma$ . Under the condition of

$$|\sigma| < K_0/50, \quad \text{say,} \quad (\text{G4})$$

there is,

$$(k_1)^2 + (k_3)^2 + \frac{(k_2)^2 + (k'_2)^2 + k_2 k'_2}{3} \geq K_0 \gg \frac{|\sigma|}{2}, \quad \forall k_1 \leq -(K_0)^{1/2}. \quad (\text{G5})$$

That is, within the range (G4),  $\sigma$  has a negligible effect on  $E(\mathbf{k}; k'_2; \sigma)$  and  $\tilde{U}_{ij}^{(\infty)}(\mathbf{k})$ ,  $\forall \mathbf{k} \notin \mathcal{R}_0$ . For  $\mathbf{k} \in \mathcal{R}_0$ ,  $\sigma$  has no effect on  $\tilde{U}_{ij}^{(\infty)}$ , owing to the condition underlying  $\mathcal{R}_0$ . Hence, this  $\{\tilde{U}_{ij}^{(\infty)}, \dot{\Gamma}_{ij}^{(\infty)}\}_{\sigma=0}$  is also a feasible solution for the values of  $\sigma$  satisfying the restriction (G4). This feasible solution guarantees the existence of optimal solutions to the second-order model for the values of  $\sigma$  satisfying (G4). Such a feasible solution of  $\sigma = 0$  may be obtained numerically (say, with an appropriate choice of a rather small support for  $\dot{\Gamma}_{ij}^{(\infty)}$  to reduce the computational size, allowable by the boundary conditions and constraints of the model). As an example, we consider the asymptotic steady state simulation of the second-order model, specifically the supports in Eqs. (59) and the associated solutions. Equations (59) and (G3) yield  $(K_0)^{1/2} = 0.01$ , the corresponding values of  $|\sigma|$  in (G4) can be obtained, though they are quite small.

### Appendix H: Limiting behavior under $k_1 \rightarrow 0^-$

Since the primary component solutions (43) appear to be singular at  $k_1 = 0$ , this issue and the associated limiting behavior under  $k_1 \rightarrow 0^-$  are discussed in this appendix. Both  $\dot{U}_{ij}^{(\infty)}$  and  $\dot{\Gamma}_{ij}^{(\infty)}$  are supposedly bounded and smooth in the wave-number space on the basis of  $U_{ij}^{(\infty)}(\mathbf{r})$  and  $U_{(ij)k}^{(\infty)}(\mathbf{r})$  being bounded and smooth. For simplicity, the discussion is restricted to  $\sigma = 0$  and the original formal solutions (H1) (leading to Eqs. (43)) are analyzed,

$$\dot{U}_{22}^{(\infty)}(\mathbf{k}) = \int_{-\infty}^{k_2} dk'_2 \frac{2|\mathbf{k}'|^4 E(\mathbf{k}; k'_2; \sigma)}{|k_1||\mathbf{k}|^4} \left( \frac{k'_2 k'_l}{|\mathbf{k}'|^2} \dot{\Gamma}_{l2}^{(\infty)}(\mathbf{k}') - \dot{\Gamma}_{22}^{(\infty)}(\mathbf{k}') \right), \quad (\text{H1a})$$

$$\begin{aligned} \dot{U}_{12}^{(\infty)}(\mathbf{k}) = \int_{-\infty}^{k_2} dk'_2 \frac{|\mathbf{k}'|^2 E(\mathbf{k}; k'_2; \sigma)}{|k_1||\mathbf{k}|^2} \left[ - \left( 1 - \frac{2(k_1)^2}{|\mathbf{k}'|^2} \right) \dot{U}_{22}^{(\infty)}(\mathbf{k}') + \frac{k'_l}{|\mathbf{k}'|^2} \left( k_1 \dot{\Gamma}_{l2}^{(\infty)}(\mathbf{k}') + k'_2 \dot{\Gamma}_{l1}^{(\infty)}(\mathbf{k}') \right) \right. \\ \left. - \left( \dot{\Gamma}_{12}^{(\infty)}(\mathbf{k}') + \dot{\Gamma}_{21}^{(\infty)}(\mathbf{k}') \right) \right], \end{aligned} \quad (\text{H1b})$$

$$\dot{U}_{11}^{(\infty)}(\mathbf{k}) = \int_{-\infty}^{k_2} dk'_2 \frac{2E(\mathbf{k}; k'_2; \sigma)}{|k_1|} \left[ - \left( 1 - \frac{2(k_1)^2}{|\mathbf{k}'|^2} \right) \dot{U}_{12}^{(\infty)}(\mathbf{k}') + \frac{k_1 k'_l}{|\mathbf{k}'|^2} \dot{\Gamma}_{l1}^{(\infty)}(\mathbf{k}') - \dot{\Gamma}_{11}^{(\infty)}(\mathbf{k}') \right], \quad (\text{H1c})$$

where  $\mathbf{k}' = (k_1, k'_2, k_3)$ ,  $k_1 < 0$ . They are obtained with the use of Eqs. (36), (38a), and (42).

First, consider Eq. (H1c) in the form of

$$\dot{U}_{11}^{(\infty)}(\mathbf{k}) = \int_{-\infty}^{k_2} dk'_2 \rho_{11}^{(\infty)}(\mathbf{k}; k'_2), \quad (\text{H2a})$$

$$\rho_{11}^{(\infty)}(\mathbf{k}; k'_2) = \frac{2E(\mathbf{k}; k'_2; \sigma)}{|k_1|} \left[ - \left( 1 - \frac{2(k_1)^2}{|\mathbf{k}'|^2} \right) \dot{U}_{12}^{(\infty)}(\mathbf{k}') + \frac{k_1 k'_l \dot{\Gamma}_{l1}^{(\infty)}(\mathbf{k}')}{|\mathbf{k}'|^2} - \dot{\Gamma}_{11}^{(\infty)}(\mathbf{k}') \right]. \quad (\text{H2b})$$

To make  $\dot{U}_{11}^{(\infty)}$  bounded and smooth, the control variables  $\dot{\Gamma}_{ij}^{(\infty)}$  need to behave such that the density function  $\rho_{11}^{(\infty)}(\mathbf{k}; k'_2)$  with  $k_2 k_3 \neq 0$  has a definite limit under  $k_1 \rightarrow 0^-$  and  $k'_2 \rightarrow k_2^-$ ,

$$\lim_{k_1 \rightarrow 0^-} \lim_{k'_2 \rightarrow k_2^-} \rho_{11}^{(\infty)}(\mathbf{k}; k'_2) = \lim_{k'_2 \rightarrow k_2^-} \lim_{k_1 \rightarrow 0^-} \rho_{11}^{(\infty)}(\mathbf{k}; k'_2), \quad (\text{H3})$$

which results in

$$\lim_{k_1 \rightarrow 0^-} \left( \frac{|\mathbf{k}|^2 \dot{U}_{12}^{(\infty)}(\mathbf{k}) + |\mathbf{k}|^2 \dot{\Gamma}_{11}^{(\infty)}(\mathbf{k})}{k_1} - k_2 \dot{\Gamma}_{21}^{(\infty)}(\mathbf{k}) - k_3 \dot{\Gamma}_{31}^{(\infty)}(\mathbf{k}) \right) = 0, \quad \forall k_2 k_3 \neq 0, \quad (\text{H4a})$$

$$\lim_{k_1 \rightarrow 0^-} \rho_{11}^{(\infty)}(\mathbf{k}; k'_2) = 0. \quad (\text{H4b})$$

Second, Eq. (H4a) implies that  $\dot{U}_{12}^{(\infty)}(\mathbf{k})/k_1$  needs to be well-defined, providing the ground to analyze Eq. (H1b) in the form,

$$\frac{\dot{U}_{12}^{(\infty)}(\mathbf{k})}{k_1} = \int_{-\infty}^{k_2} dk'_2 \rho_{12}^{(\infty)}(\mathbf{k}; k'_2), \quad (\text{H5a})$$

$$\rho_{12}^{(\infty)}(\mathbf{k}; k'_2) = \frac{|\mathbf{k}'|^2 E(\mathbf{k}; k'_2; \sigma)}{|k_1|^2 |\mathbf{k}'|^2} \left[ \left( 1 - \frac{2(k_1)^2}{|\mathbf{k}'|^2} \right) \dot{U}_{22}^{(\infty)}(\mathbf{k}') - \frac{k'_l (k_1 \dot{\Gamma}_{12}^{(\infty)}(\mathbf{k}') + k'_2 \dot{\Gamma}_{l1}^{(\infty)}(\mathbf{k}'))}{|\mathbf{k}'|^2} + \dot{\Gamma}_{12}^{(\infty)}(\mathbf{k}') + \dot{\Gamma}_{21}^{(\infty)}(\mathbf{k}') \right]. \quad (\text{H5b})$$

Applying a similar argument for the existence of limit under  $k_1 \rightarrow 0^-$  and  $k'_2 \rightarrow k_2^-$  to  $\rho_{12}^{(\infty)}(\mathbf{k}; k'_2)$  leads to

$$\lim_{k_1 \rightarrow 0^-} \left( \frac{|\mathbf{k}'|^2 \dot{U}_{22}^{(\infty)}(\mathbf{k})}{(k_1)^2} - \frac{k_2 [\dot{\Gamma}_{11}^{(\infty)}(\mathbf{k}) + \dot{\Gamma}_{22}^{(\infty)}(\mathbf{k})]}{k_1} + \frac{[(k_2)^2 + (k_3)^2] \dot{\Gamma}_{12}^{(\infty)}(\mathbf{k}) + (k_3)^2 \dot{\Gamma}_{21}^{(\infty)}(\mathbf{k})}{(k_1)^2} - \frac{k_3 [k_2 \dot{\Gamma}_{31}^{(\infty)}(\mathbf{k}) + k_1 \dot{\Gamma}_{32}^{(\infty)}(\mathbf{k})]}{(k_1)^2} \right) = 0, \quad \forall k_2 k_3 \neq 0. \quad (\text{H6})$$

Third, the structure of Eq. (H6) motivates the consideration of  $\dot{U}_{22}^{(\infty)}(\mathbf{k})/(k_1)^2$ , and Eq. (H1a) is written as

$$\frac{\dot{U}_{22}^{(\infty)}(\mathbf{k})}{(k_1)^2} = \int_{-\infty}^{k_2} dk'_2 \rho_{22}^{(\infty)}(\mathbf{k}; k'_2), \quad (\text{H7a})$$

$$\rho_{22}^{(\infty)}(\mathbf{k}; k'_2) = \frac{2|\mathbf{k}'|^4 E(\mathbf{k}; k'_2; \sigma)}{|k_1|^3 |\mathbf{k}'|^4} \left( \frac{k'_2 k'_l \dot{\Gamma}_{l2}^{(\infty)}(\mathbf{k}')}{|\mathbf{k}'|^2} - \dot{\Gamma}_{22}^{(\infty)}(\mathbf{k}') \right). \quad (\text{H7b})$$

Applying a similar argument for the existence of limit under  $k_1 \rightarrow 0^-$  and  $k'_2 \rightarrow k_2^-$  to  $\rho_{22}^{(\infty)}(\mathbf{k}; k'_2)$ , we obtain

$$\lim_{k_1 \rightarrow 0^-} \frac{k_2 k_1 \dot{\Gamma}_{12}^{(\infty)}(\mathbf{k}) - (k_3)^2 \dot{\Gamma}_{22}^{(\infty)}(\mathbf{k}) + k_2 k_3 \dot{\Gamma}_{32}^{(\infty)}(\mathbf{k})}{|k_1|^3} = 0, \quad \forall k_2 k_3 \neq 0. \quad (\text{H8})$$

Since  $\dot{\Gamma}_{ij}^{(\infty)}$ ,  $ij = 11, 21, 31, 12, 22, 32$ , are the primary control variables, we may infer from Eqs. (H4a), (H6), and (H8) that

$$\dot{\Gamma}_{11}^{(\infty)}(\mathbf{k}) \propto k_1, \quad \dot{\Gamma}_{21}^{(\infty)}(\mathbf{k}) \propto (k_1)^2, \quad \dot{\Gamma}_{31}^{(\infty)}(\mathbf{k}) \propto (k_1)^2, \quad \dot{\Gamma}_{12}^{(\infty)}(\mathbf{k}) \propto (k_1)^2, \quad \dot{\Gamma}_{22}^{(\infty)}(\mathbf{k}) \propto (k_1)^3, \quad \dot{\Gamma}_{32}^{(\infty)}(\mathbf{k}) \propto (k_1)^3, \\ \forall k_2 k_3 \neq 0 \text{ and small } |k_1|. \quad (\text{H9})$$

Then, under the supposed continuity of  $\dot{\Gamma}_{ij}^{(\infty)}$  in the wave-number space, Eqs. (H9) imply that

$$\dot{\Gamma}_{ij}^{(\infty)}(0, k_2, k_3) = 0. \quad (\text{H10})$$

Regarding the values of  $\dot{U}_{ij}^{(\infty)}(0, k_2, k_3)$ , Eqs. (H4a) and (H6) imply

$$\dot{U}_{12}^{(\infty)}(0, k_2, k_3) = \dot{U}_{22}^{(\infty)}(0, k_2, k_3) = 0. \quad (\text{H11})$$

A combination of Eqs. (H4b) and (H2a) implies

$$\dot{U}_{11}^{(\infty)}(0, k_2, k_3) = 0. \quad (\text{H12})$$

A rigorous but lengthy proof for the above result may also be offered with the help of bounded  $\dot{U}_{11}^{(\infty)}$ , Eq. (H4a), and the property of  $E(\mathbf{k}; k'_2; 0)$ .

### Appendix I: Discretization

The supports  $\mathcal{D}_\Gamma(0)$  and  $\mathcal{D}_U(0)$  are estimated in Eqs. (56) and (57). They are discretized, respectively, with structured hexahedral meshes,

$$\begin{aligned} \mathcal{D}_\Gamma(0) &= \bigcup_{n_1=1}^{N_1-1} \bigcup_{n_2=1}^{N_2-1} \bigcup_{n_3=1}^{N_3-1} \mathcal{H}(n_1, n_2, n_3), & \mathcal{D}_U(0) &= \bigcup_{n_1=1}^{N_1-1} \bigcup_{n_2=1}^{M_2-1} \bigcup_{n_3=1}^{N_3-1} \mathcal{H}(n_1, n_2, n_3), \\ \mathcal{H}(n_1, n_2, n_3) &= [k_{1,n_1}, k_{1,n_1+1}] \times [k_{2,n_2}, k_{2,n_2+1}] \times [k_{3,n_3}, k_{3,n_3+1}]. \end{aligned} \quad (I1)$$

The distribution of  $\dot{\Gamma}_{ij}^{(\infty)}$  in each element  $\mathcal{H}(n_1, n_2, n_3)$  of  $\mathcal{D}_\Gamma(0)$  is approximated by the trilinear distribution,

$$\begin{aligned} \dot{\Gamma}_{ij}^{(\infty)}(\mathbf{k}') &= \chi_{[k_{1,n_1}, k_{1,n_1+1}]}(k_1) \chi_{[k_{2,n_2}, k_{2,n_2+1}]}(k_2') \chi_{[k_{3,n_3}, k_{3,n_3+1}]}(k_3) \dot{\Gamma}_{ij}^{(\infty)'}(\mathbf{k}', n_1, n_2, n_3), \\ \dot{\Gamma}_{ij}^{(\infty)'}(\mathbf{k}', n_1, n_2, n_3) &= \frac{\dot{\Gamma}_{ij}^{(0)}(n_1, n_2, n_3)(k_{2,n_2+1} - k_2') + \dot{\Gamma}_{ij}^{(0)}(n_1, n_2 + 1, n_3)(k_2' - k_{2,n_2})}{k_{2,n_2+1} - k_{2,n_2}} \frac{k_{1,n_1+1} - k_1}{k_{1,n_1+1} - k_{1,n_1}} \frac{k_{3,n_3+1} - k_3}{k_{3,n_3+1} - k_{3,n_3}} \\ &+ \frac{\dot{\Gamma}_{ij}^{(0)}(n_1 + 1, n_2, n_3)(k_{2,n_2+1} - k_2') + \dot{\Gamma}_{ij}^{(0)}(n_1 + 1, n_2 + 1, n_3)(k_2' - k_{2,n_2})}{k_{2,n_2+1} - k_{2,n_2}} \frac{k_1 - k_{1,n_1}}{k_{1,n_1+1} - k_{1,n_1}} \frac{k_{3,n_3+1} - k_3}{k_{3,n_3+1} - k_{3,n_3}} \\ &+ \frac{\dot{\Gamma}_{ij}^{(0)}(n_1, n_2, n_3 + 1)(k_{2,n_2+1} - k_2') + \dot{\Gamma}_{ij}^{(0)}(n_1, n_2 + 1, n_3 + 1)(k_2' - k_{2,n_2})}{k_{2,n_2+1} - k_{2,n_2}} \frac{k_{1,n_1+1} - k_1}{k_{1,n_1+1} - k_{1,n_1}} \frac{k_3 - k_{3,n_3}}{k_{3,n_3+1} - k_{3,n_3}} \\ &+ \frac{\dot{\Gamma}_{ij}^{(0)}(n_1 + 1, n_2, n_3 + 1)(k_{2,n_2+1} - k_2') + \dot{\Gamma}_{ij}^{(0)}(n_1 + 1, n_2 + 1, n_3 + 1)(k_2' - k_{2,n_2})}{k_{2,n_2+1} - k_{2,n_2}} \frac{k_1 - k_{1,n_1}}{k_{1,n_1+1} - k_{1,n_1}} \frac{k_3 - k_{3,n_3}}{k_{3,n_3+1} - k_{3,n_3}}. \end{aligned} \quad (I2)$$

Here,  $\chi_{[k_{1,n_1}, k_{1,n_1+1}]}$  and the like denote the characteristic functions and  $\dot{\Gamma}_{ij}^{(0)}(n_1, n_2, n_3)$  denote the nodal values. The piecewise trilinear approximations (I2) may be adequate at small mesh element sizes since integration operations are mainly involved in the distribution of the control variables.

Substitution of Eqs. (I2) into Eqs. (43) gives

$$\begin{aligned} \dot{U}_{22}^{(\infty)}(\mathbf{k}) &= \frac{2\chi_{[k_{1,n_1}, k_{1,n_1+1}]}(k_1)\chi_{[k_{3,n_3}, k_{3,n_3+1}]}(k_3)}{|k_1||\mathbf{k}|^4} \\ &\times \sum_{n_2=1}^{N_2-1} \int_{k_{2,1}}^{k_2} dk_2' E(\mathbf{k}; k_2'; 0) |\mathbf{k}'|^4 \chi_{[k_{2,n_2}, k_{2,n_2+1}]}(k_2') \left( \frac{k_2' k_1}{|\mathbf{k}'|^2} \dot{\Gamma}_{i2}^{(\infty)'}(\mathbf{k}', n_1, n_2, n_3) - \dot{\Gamma}_{22}^{(\infty)'}(\mathbf{k}', n_1, n_2, n_3) \right), \end{aligned} \quad (I3a)$$

$$\begin{aligned} \dot{U}_{12}^{(\infty)}(\mathbf{k}) &= -\frac{2\chi_{[k_{1,n_1}, k_{1,n_1+1}]}(k_1)\chi_{[k_{3,n_3}, k_{3,n_3+1}]}(k_3)}{|k_1|^2[|k_1|^2 + (k_3)^2]|\mathbf{k}|^2} \\ &\times \sum_{n_2=1}^{N_2-1} \int_{k_{2,1}}^{k_2} dk_2' E(\mathbf{k}; k_2'; 0) (F(\mathbf{k}) - F(\mathbf{k}')) |\mathbf{k}'|^4 \chi_{[k_{2,n_2}, k_{2,n_2+1}]}(k_2') \\ &\times \left( \frac{k_2' k_1}{|\mathbf{k}'|^2} \dot{\Gamma}_{i2}^{(\infty)'}(\mathbf{k}', n_1, n_2, n_3) - \dot{\Gamma}_{22}^{(\infty)'}(\mathbf{k}', n_1, n_2, n_3) \right) \\ &+ \frac{1}{|k_1||\mathbf{k}|^2} \chi_{[k_{1,n_1}, k_{1,n_1+1}]}(k_1) \chi_{[k_{3,n_3}, k_{3,n_3+1}]}(k_3) \\ &\times \sum_{n_2=1}^{N_2-1} \int_{k_{2,1}}^{k_2} dk_2' E(\mathbf{k}; k_2'; 0) \chi_{[k_{2,n_2}, k_{2,n_2+1}]}(k_2') \\ &\times \left[ k_1' \left( k_1 \dot{\Gamma}_{i2}^{(\infty)'}(\mathbf{k}', n_1, n_2, n_3) + k_2' \dot{\Gamma}_{i1}^{(\infty)'}(\mathbf{k}', n_1, n_2, n_3) \right) \right. \\ &\quad \left. - |\mathbf{k}'|^2 \left( \dot{\Gamma}_{12}^{(\infty)'}(\mathbf{k}', n_1, n_2, n_3) + \dot{\Gamma}_{21}^{(\infty)'}(\mathbf{k}', n_1, n_2, n_3) \right) \right], \end{aligned} \quad (I3b)$$

$$\begin{aligned}
\tilde{U}_{11}^{(\infty)}(\mathbf{k}) &= \frac{2\chi_{[k_1, n_1, k_1, n_1+1]}(k_1)\chi_{[k_3, n_3, k_3, n_3+1]}(k_3)}{|k_1|^3[|k_1|^2 + (k_3)^2]^2} \\
&\times \sum_{n_2=1}^{N_2-1} \int_{k_{2,1}}^{k_2} dk'_2 E(\mathbf{k}; k'_2; 0) (F(\mathbf{k}) - F(\mathbf{k}'))^2 |\mathbf{k}'|^4 \chi_{[k_2, n_2, k_2, n_2+1]}(k'_2) \\
&\quad \times \left( \frac{k'_2 k'_l}{|\mathbf{k}'|^2} \dot{\Gamma}_{l2}^{(\infty)'}(\mathbf{k}', n_1, n_2, n_3) - \dot{\Gamma}_{22}^{(\infty)'}(\mathbf{k}', n_1, n_2, n_3) \right) \\
&- \frac{2\chi_{[k_1, n_1, k_1, n_1+1]}(k_1)\chi_{[k_3, n_3, k_3, n_3+1]}(k_3)}{|k_1|^2[|k_1|^2 + (k_3)^2]} \\
&\times \sum_{n_2=1}^{N_2-1} \int_{k_{2,1}}^{k_2} dk'_2 E(\mathbf{k}; k'_2; 0) (F(\mathbf{k}) - F(\mathbf{k}')) \chi_{[k_2, n_2, k_2, n_2+1]}(k'_2) \\
&\quad \times \left[ k'_l \left( k_1 \dot{\Gamma}_{l2}^{(\infty)'}(\mathbf{k}', n_1, n_2, n_3) + k'_2 \dot{\Gamma}_{l1}^{(\infty)'}(\mathbf{k}', n_1, n_2, n_3) \right) \right. \\
&\quad \left. - |\mathbf{k}'|^2 \left( \dot{\Gamma}_{12}^{(\infty)'}(\mathbf{k}', n_1, n_2, n_3) + \dot{\Gamma}_{21}^{(\infty)'}(\mathbf{k}', n_1, n_2, n_3) \right) \right] \\
&+ \frac{2\chi_{[k_1, n_1, k_1, n_1+1]}(k_1)\chi_{[k_3, n_3, k_3, n_3+1]}(k_3)}{|k_1|} \\
&\times \sum_{n_2=1}^{N_2-1} \int_{k_{2,1}}^{k_2} dk'_2 E(\mathbf{k}; k'_2; 0) \chi_{[k_2, n_2, k_2, n_2+1]}(k'_2) \left( \frac{k_1 k'_l}{|\mathbf{k}'|^2} \dot{\Gamma}_{l1}^{(\infty)'}(\mathbf{k}', n_1, n_2, n_3) - \dot{\Gamma}_{11}^{(\infty)'}(\mathbf{k}', n_1, n_2, n_3) \right). \quad (13c)
\end{aligned}$$

The expressions may be recast further with the help of

$$E(\mathbf{k}; k'_2; \sigma) = E(\mathbf{k}; k_2, n_2; \sigma) E((k_1, k_2, n_2, k_3); k'_2; \sigma), \quad (14)$$

which is used in coding for the calculation of  $\tilde{U}_{11}^{(\infty)}$ ,  $\tilde{U}_{12}^{(\infty)}$ , and  $\tilde{U}_{22}^{(\infty)}$  at the collocation points specified in Appendix J.

In the evaluation of the objective and the second order correlations in the physical space, three types of integrals are computed, owing to the primary components  $\tilde{U}_{11}^{(\infty)}$ ,  $\tilde{U}_{12}^{(\infty)}$ , and  $\tilde{U}_{22}^{(\infty)}$ . They are

$$\begin{aligned}
&\int_{-\infty}^0 dk_1 \int_0^{+\infty} dk_3 \int_{\mathbb{R}} dk_2 \Psi_{22}(\mathbf{k}, \mathbf{r}) \dot{U}_{22}^{(\infty)}(\mathbf{k}) \\
&= \sum \iiint \frac{2\Psi_{22}(\mathbf{k}, \mathbf{r}) E(\mathbf{k}; k'_2; 0) |\mathbf{k}'|^4}{|k_1| |\mathbf{k}|^4} \left( \frac{k'_2 k'_l}{|\mathbf{k}'|^2} \dot{\Gamma}_{l2}^{(\infty)'}(\mathbf{k}', n_1, n_2, n_3) - \dot{\Gamma}_{22}^{(\infty)'}(\mathbf{k}', n_1, n_2, n_3) \right), \quad (15a)
\end{aligned}$$

$$\begin{aligned}
&\int_{-\infty}^0 dk_1 \int_0^{+\infty} dk_3 \int_{\mathbb{R}} dk_2 \Psi_{12}(\mathbf{k}, \mathbf{r}) \dot{U}_{12}^{(\infty)}(\mathbf{k}) \\
&= \sum \iiint \frac{-2\Psi_{12}(\mathbf{k}, \mathbf{r}) E(\mathbf{k}; k'_2; 0) (F(\mathbf{k}) - F(\mathbf{k}')) |\mathbf{k}'|^4}{|k_1|^2 [ |k_1|^2 + (k_3)^2 ] |\mathbf{k}|^2} \left( \frac{k'_2 k'_l}{|\mathbf{k}'|^2} \dot{\Gamma}_{l2}^{(\infty)'}(\mathbf{k}', n_1, n_2, n_3) - \dot{\Gamma}_{22}^{(\infty)'}(\mathbf{k}', n_1, n_2, n_3) \right) \\
&\quad + \sum \iiint \frac{\Psi_{12}(\mathbf{k}, \mathbf{r}) E(\mathbf{k}; k'_2; 0) |\mathbf{k}'|^2}{|k_1| |\mathbf{k}|^2} \left[ \frac{k'_l}{|\mathbf{k}'|^2} \left( k_1 \dot{\Gamma}_{l2}^{(\infty)'}(\mathbf{k}', n_1, n_2, n_3) + k'_2 \dot{\Gamma}_{l1}^{(\infty)'}(\mathbf{k}', n_1, n_2, n_3) \right) \right. \\
&\quad \left. - \dot{\Gamma}_{12}^{(\infty)'}(\mathbf{k}', n_1, n_2, n_3) - \dot{\Gamma}_{21}^{(\infty)'}(\mathbf{k}', n_1, n_2, n_3) \right], \quad (15b)
\end{aligned}$$

$$\begin{aligned}
&\int_{-\infty}^0 dk_1 \int_0^{+\infty} dk_3 \int_{\mathbb{R}} dk_2 \Psi_{11}(\mathbf{k}, \mathbf{r}) \dot{U}_{11}^{(\infty)}(\mathbf{k}) \\
&= \sum \iiint \frac{2\Psi_{11}(\mathbf{k}, \mathbf{r}) E(\mathbf{k}; k'_2; 0) (F(\mathbf{k}) - F(\mathbf{k}'))^2 |\mathbf{k}'|^4}{|k_1|^3 [ |k_1|^2 + (k_3)^2 ]^2} \left( \frac{k'_2 k'_l}{|\mathbf{k}'|^2} \dot{\Gamma}_{l2}^{(\infty)'}(\mathbf{k}', n_1, n_2, n_3) - \dot{\Gamma}_{22}^{(\infty)'}(\mathbf{k}', n_1, n_2, n_3) \right) \\
&\quad + \sum \iiint \frac{-2\Psi_{11}(\mathbf{k}, \mathbf{r}) E(\mathbf{k}; k'_2; 0) (F(\mathbf{k}) - F(\mathbf{k}'))}{|k_1|^2 [ |k_1|^2 + (k_3)^2 ]} \left[ k'_l \left( k_1 \dot{\Gamma}_{l2}^{(\infty)'}(\mathbf{k}', n_1, n_2, n_3) + k'_2 \dot{\Gamma}_{l1}^{(\infty)'}(\mathbf{k}', n_1, n_2, n_3) \right) \right. \\
&\quad \left. - |\mathbf{k}'|^2 \left( \dot{\Gamma}_{12}^{(\infty)'}(\mathbf{k}', n_1, n_2, n_3) + \dot{\Gamma}_{21}^{(\infty)'}(\mathbf{k}', n_1, n_2, n_3) \right) \right]
\end{aligned}$$

$$+ \sum \iiint \frac{2\Psi_{11}(\mathbf{k}, \mathbf{r})E(\mathbf{k}; k'_2; 0)}{|k_1|} \left( \frac{k_1 k'_1}{|\mathbf{k}'|^2} \dot{\Gamma}_{11}^{(\infty)'}(\mathbf{k}', n_1, n_2, n_3) - \dot{\Gamma}_{11}^{(\infty)'}(\mathbf{k}', n_1, n_2, n_3) \right). \quad (\text{I5c})$$

Here,

$$\sum \iiint = \sum_{n_1=1}^{N_1-1} \sum_{n_3=1}^{N_3-1} \sum_{n_2=1}^{N_2-1} \int_{k_{1,n_1}}^{k_{1,n_1+1}} dk_1 \int_{k_{3,n_3}}^{k_{3,n_3+1}} dk_3 \left[ \int_{k_{2,n_2}}^{k_{2,n_2+1}} dk_2 \int_{k_{2,n_2}}^{k_2} dk'_2 + \int_{k_{2,n_2}}^{k_{2,n_2+1}} dk'_2 \int_{k_{2,n_2+1}}^{k_{2,M_2}} dk_2 \right],$$

and  $\Psi_{ij}$  denote the relevant functions. The proof of (I5) is outlined below.

In the derivations of Eqs. (I5), the following operations are carried out, together with Eqs. (I3). We start with the set of equalities,

$$\int_{-\infty}^0 dk_1 \int_0^\infty dk_3 = \sum_{n_1=1}^{N_1-1} \sum_{n_3=1}^{N_3-1} \int_{k_{1,n_1}}^{k_{1,n_1+1}} dk_1 \int_{k_{3,n_3}}^{k_{3,n_3+1}} dk_3, \quad \int_{\mathbb{R}} dk_2 = \int_{k_{2,1}}^{k_{2,N_2}} dk_2 + \int_{k_{2,N_2}}^{k_{2,M_2}} dk_2, \quad (\text{I6a})$$

$$\int_{k_{2,1}}^{k_{2,N_2}} dk_2 = \sum_{m_2=1}^{N_2-1} \int_{k_{2,m_2}}^{k_{2,m_2+1}} dk_2, \quad \int_{k_{2,N_2}}^{k_{2,M_2}} dk_2 \int_{k_{2,1}}^{k_2} dk'_2 = \int_{k_{2,N_2}}^{k_{2,M_2}} dk_2 \int_{k_{2,1}}^{k_{2,N_2}} dk'_2, \quad (\text{I6b})$$

$$\int_{k_{2,1}}^{k_{2,N_2}} dk'_2 \chi_{(k_{2,n_2}, k_{2,n_2+1})}(k'_2) = \int_{k_{2,n_2}}^{k_{2,n_2+1}} dk'_2 \chi_{(k_{2,n_2}, k_{2,n_2+1})}(k'_2),$$

$$\begin{aligned} & \sum_{m_2=1}^{N_2-1} \int_{k_{2,m_2}}^{k_{2,m_2+1}} dk_2 \int_{k_{2,1}}^{k_2} dk'_2 \sum_{n_2=1}^{N_2-1} \chi_{(k_{2,n_2}, k_{2,n_2+1})}(k'_2) \Phi(n_2 \dots) \\ &= \sum_{m_2=1}^{N_2-1} \int_{k_{2,m_2}}^{k_{2,m_2+1}} dk_2 \sum_{n_2=1}^{m_2} \int_{k_{2,n_2}}^{k_2} dk'_2 \chi_{(k_{2,n_2}, k_{2,n_2+1})}(k'_2) \Phi(n_2 \dots) \\ &= \sum_{m_2=1}^{N_2-1} \int_{k_{2,m_2}}^{k_{2,m_2+1}} dk_2 \int_{k_{2,m_2}}^{k_2} dk'_2 \chi_{(k_{2,m_2}, k_{2,m_2+1})}(k'_2) \Phi(m_2 \dots) \\ &+ \sum_{m_2=2}^{N_2-1} \int_{k_{2,m_2}}^{k_{2,m_2+1}} dk_2 \sum_{n_2=1}^{m_2-1} \left( \int_{k_{2,n_2}}^{k_{2,m_2}} dk'_2 + \int_{k_{2,m_2}}^{k_2} dk'_2 \right) \chi_{(k_{2,n_2}, k_{2,n_2+1})}(k'_2) \Phi(n_2 \dots) \\ &= \sum_{m_2=1}^{N_2-1} \int_{k_{2,m_2}}^{k_{2,m_2+1}} dk_2 \int_{k_{2,m_2}}^{k_2} dk'_2 \chi_{(k_{2,m_2}, k_{2,m_2+1})}(k'_2) \Phi(m_2 \dots) \\ &+ \sum_{m_2=2}^{N_2-1} \int_{k_{2,m_2}}^{k_{2,m_2+1}} dk_2 \sum_{n_2=1}^{m_2-1} \int_{k_{2,n_2}}^{k_{2,n_2+1}} dk'_2 \chi_{(k_{2,n_2}, k_{2,n_2+1})}(k'_2) \Phi(n_2 \dots). \end{aligned} \quad (\text{I6c})$$

Equalities (I6a) and (I6b) are self-explanatory, Eqs. (I6c) may be verified directly with the use of properties of characteristic functions. Applying Eqs. (I6) to Eq. (I3a) step-by-step results in

$$\begin{aligned} & \int_{k_{1,n_1}}^{k_{1,n_1+1}} dk_1 \int_{k_{3,n_3}}^{k_{3,n_3+1}} dk_3 \int_{\mathbb{R}} dk_2 \Psi_{22}(\mathbf{k}, \mathbf{r}) \dot{U}_{22}^{(\infty)}(\mathbf{k}) \\ &= \sum_{m_2=2}^{N_2-1} \sum_{n_2=1}^{m_2-1} \int_{k_{1,n_1}}^{k_{1,n_1+1}} dk_1 \int_{k_{3,n_3}}^{k_{3,n_3+1}} dk_3 \int_{k_{2,m_2}}^{k_{2,m_2+1}} dk_2 \int_{k_{2,n_2}}^{k_{2,n_2+1}} dk'_2 \chi_{(k_{2,n_2}, k_{2,n_2+1})}(k'_2) \frac{2\Psi_{22}(\mathbf{k}, \mathbf{r})E(\mathbf{k}; k'_2; \sigma)|\mathbf{k}'|^4 [n_2 \dots]}{|k_1||\mathbf{k}|^4} \\ &+ \sum_{m_2=1}^{N_2-1} \int_{k_{1,n_1}}^{k_{1,n_1+1}} dk_1 \int_{k_{3,n_3}}^{k_{3,n_3+1}} dk_3 \int_{k_{2,m_2}}^{k_{2,m_2+1}} dk_2 \int_{k_{2,m_2}}^{k_2} dk'_2 \chi_{(k_{2,m_2}, k_{2,m_2+1})}(k'_2) \frac{2\Psi_{22}(\mathbf{k}, \mathbf{r})E(\mathbf{k}; k'_2; \sigma)|\mathbf{k}'|^4 [m_2 \dots]}{|k_1||\mathbf{k}|^4} \\ &+ \sum_{n_2=1}^{N_2-1} \int_{k_{1,n_1}}^{k_{1,n_1+1}} dk_1 \int_{k_{3,n_3}}^{k_{3,n_3+1}} dk_3 \int_{k_{2,N_2}}^{k_{2,M_2}} dk_2 \int_{k_{2,n_2}}^{k_{2,n_2+1}} dk'_2 \chi_{(k_{2,n_2}, k_{2,n_2+1})}(k'_2) \frac{2\Psi_{22}(\mathbf{k}, \mathbf{r})E(\mathbf{k}; k'_2; \sigma)|\mathbf{k}'|^4 [n_2 \dots]}{|k_1||\mathbf{k}|^4}, \end{aligned} \quad (\text{I7})$$

where  $[n_2 \dots]$  denotes the big bracketed quantity in Eq. (I3a).

With regard to Eq. (I7), the characteristic functions are redundant and may be removed. For the first term on its right-hand side, we have

$$\begin{aligned} & \sum_{m_2=2}^{N_2-1} \sum_{n_2=1}^{m_2-1} \int_{k_{1,n_1}}^{k_{1,n_1+1}} dk_1 \int_{k_{3,n_3}}^{k_{3,n_3+1}} dk_3 \int_{k_{2,m_2}}^{k_{2,m_2+1}} dk_2 \int_{k_{2,n_2}}^{k_{2,n_2+1}} dk'_2 \Phi(n_2 \dots) \\ &= \sum_{n_2=1}^{N_2-2} \sum_{m_2=n_2+1}^{N_2-1} \int_{k_{1,n_1}}^{k_{1,n_1+1}} dk_1 \int_{k_{3,n_3}}^{k_{3,n_3+1}} dk_3 \int_{k_{2,m_2}}^{k_{2,m_2+1}} dk_2 \int_{k_{2,n_2}}^{k_{2,n_2+1}} dk'_2 \Phi(n_2 \dots). \end{aligned} \quad (\text{I8})$$

This equality is proved via mathematical induction: It is simple to verify that the relation holds for  $N_2 = 3$ ; It is straight-forward to check that if the relation holds for  $N_2 \geq 3$ , it holds for  $(N_2 + 1)$ . Further, the right-hand side of Eq. (I8) is recast in the form of

$$\sum_{n_2=1}^{N_2-2} \sum_{m_2=n_2+1}^{N_2-1} \int_{k_{2,m_2}}^{k_{2,m_2+1}} dk_2 \int_{k_{2,n_2}}^{k_{2,n_2+1}} dk'_2 = \sum_{n_2=1}^{N_2-2} \int_{k_{2,n_2+1}}^{k_{2,N_2}} dk_2 \int_{k_{2,n_2}}^{k_{2,n_2+1}} dk'_2 = \sum_{n_2=1}^{N_2-1} \int_{k_{2,n_2+1}}^{k_{2,N_2}} dk_2 \int_{k_{2,n_2}}^{k_{2,n_2+1}} dk'_2.$$

Applying the above results to Eq. (I7) yields Eq. (I5a).

The same procedure is used to prove Eqs. (I5b) and (I5c).

## Appendix J: Discretized model

The main parts of the discretized second-order model and their derivations and productions are described in this appendix.

Objective (58) is represented in terms of  $\dot{\Gamma}_{ij}^{(0)}$ , with the help of Eqs. (54) and (I5). Algorithms ‘Cuhre’ and ‘Divonne’ of the open source software package CUBA library [32–34] are used to compute the four-dimensional integrals in Eqs. (I5).

The discrete control variables at the nodes are directly constrained by Eqs. (46), (49), and the support (56),

$$\begin{aligned} & \dot{\Gamma}_{ij}^{(0)}(n_1, n_2, n_3) = 0, \quad n_1 \in \{1, N_1\} \quad \text{or} \quad n_2 \in \{1, N_2\} \quad \text{or} \quad n_3 = N_3, \quad \forall i, j; \\ & \dot{\Gamma}_{ij}^{(0)}(n_1, n_2, 2) = \dot{\Gamma}_{ij}^{(0)}(n_1, n_2, 1), \quad ij = 11, 21, 12, 22; \quad \dot{\Gamma}_{ij}^{(0)}(n_1, n_2, 1) = 0, \quad ij = 31, 32; \\ & |\dot{\Gamma}_{ij}^{(0)}(n_1, n_2, n_3)| \leq 1, \quad 2 \leq n_1 \leq N_1 - 1, \quad 2 \leq n_2 \leq N_2 - 1, \quad 1 \leq n_3 \leq N_3 - 1, \quad \forall i, j. \end{aligned} \quad (\text{J1})$$

Substituting Eqs. (I2) into Eqs. (47) and integrating analytically the integrals over the elements in  $\mathcal{D}_\Gamma(0)$  give four global linear equality constraints for  $\dot{\Gamma}_{ij}^{(0)}$ .

To implement the constraints of inequality (45), we select three types of collocation points in  $\mathcal{D}_U(0)$ , according to the integral structures of the discretized solutions (I3) with respect to  $k'_2$ .

*a. Collocation points for constraints 1C* The points are located in the middle of the element edges parallel to the  $k_2$ -axis,

$$k_1 = k_{1,n_1}, \quad k_3 = k_{3,n_3}, \quad k_2 = (k_{2,n_2} + k_{2,n_2+1})/2. \quad (\text{J2})$$

Equations (I3) indicate that  $\tilde{U}_{ij}^{(\infty)}(\mathbf{k})$  and Eqs. (45) evaluated at these collocation points involve only

$$\dot{\Gamma}_{ij}^{(0)}(n_1, n'_2, n_3), \quad n'_2 \in \{1, \dots, n_2 + 1\},$$

like 1-column parallel to the  $k_2$ -axis. Accordingly, the collocation points (J2) are denoted as 1C. This 1C is also used to identify the collection of constraints (45) evaluated at the 1C collocation points; A similar practice is adopted for the other two types, 2C ( $2Ck_1$ ,  $2Ck_3$ ) and 4C, below.

*b. Collocation points for constraints 2C* The points are located in the center of the element facets parallel to the  $k_2$ -axis,

$$k_1 = k_{1,n_1}, \quad k_3 = (k_{3,n_3} + k_{3,n_3+1})/2, \quad k_2 = (k_{2,n_2} + k_{2,n_2+1})/2; \quad (\text{J3a})$$

$$k_1 = (k_{1,n_1} + k_{1,n_1+1})/2, \quad k_3 = k_{3,n_3}, \quad k_2 = (k_{2,n_2} + k_{2,n_2+1})/2. \quad (\text{J3b})$$

Constraints (45) evaluated at the collocation points (J3) involve either

$$\dot{\Gamma}_{ij}^{(0)}(n_1, n'_2, n'_3), \quad n'_3 \in \{n_3, n_3 + 1\}, \quad n'_2 \in \{1, \dots, n_2 + 1\},$$

or

$$\dot{\Gamma}_{ij}^{(0)}(n'_1, n'_2, n_3), \quad n'_1 \in \{n_1, n_1 + 1\}, \quad n'_2 \in \{1, \dots, n_2 + 1\},$$

like 2-columns parallel to the  $k_2$ -axis, these collocation points are denoted as 2C. Specifically, the set associated with Eqs (J3a) is denoted as  $2Ck_1$  and the set associated with Eqs. (J3b) is denoted as  $2Ck_3$ .

*c. Collocation points for constraints 4C* The points are located in the center of the elements,

$$k_1 = (k_{1,n_1} + k_{1,n_1+1})/2, \quad k_3 = (k_{3,n_3} + k_{3,n_3+1})/2, \quad k_2 = (k_{2,n_2} + k_{2,n_2+1})/2. \quad (\text{J4})$$

Constraints (45) evaluated at these collocation points involve

$$\dot{\Gamma}_{ij}^{(0)}(n'_1, n'_2, n'_3), \quad n'_1 \in \{n_1, n_1 + 1\}, \quad n'_3 \in \{n_3, n_3 + 1\}, \quad n'_2 \in \{1, \dots, n_2 + 1\},$$

like 4-columns parallel to the  $k_2$ -axis. Accordingly the collocation points (J4) are referred to as 4C.

The evaluation of Eqs. (I3) at collocation points 1C, 2C, and 4C results in the need to compute a collection of 1-dimensional integrals with respect to  $k'_2$  over the mesh elements. Function ‘NIntegrate’ of the commercial software MATHEMATICA is used to compute these integrals (with the default “Global Adaptive Strategy” and global error tolerance).

### Appendix K: Algorithm for parallel computing

This appendix outlines the major procedural steps in the solution of the discretized second-order model, including details essential for the development of the ADMM consensus algorithm and the use of the open-source SCS solver.

In Appendix J, the discretized model is presented in its natural form in terms of  $\dot{\Gamma}_{ij}^{(0)}$ . For convenience to employ the ideas developed and the notations commonly adopted in ADMM algorithm [37, 38], the above discretized model is recast in the ADMM form,

$$\begin{aligned} & \text{minimize} && a^T Z \\ & \text{subject to} && Z \in \mathcal{C}. \end{aligned} \quad (\text{K1})$$

Here,  $Z$  denotes the vector associated with

$$\left\{ \dot{\Gamma}_{ij}^{(0)}(n_1, n_2, n_3) : n_1 = 1, \dots, N_1, \quad n_2 = 1, \dots, N_2, \quad n_3 = 1, \dots, N_3; \quad i, j \right\} \subset \mathbb{R}^{6N_{CV}}, \quad N_{CV} = N_1 N_2 N_3,$$

through the one-to-one linear mapping specified by the pseudocode,

```

n = 0
FOR n1 = 1 to N1
  FOR n2 = 1 to N2
    FOR n3 = 1 to N3
      n = n + 1
      Z[n] =  $\dot{\Gamma}_{11}^{(0)}(n_1, n_2, n_3)$ 
    END FOR
  END FOR
END FOR

: {21,31,12,22}
FOR n1 = 1 to N1
  FOR n2 = 1 to N2
    FOR n3 = 1 to N3

```

$$\begin{aligned}
n &= n + 1 \\
Z[n] &= \dot{\Gamma}_{32}^{(0)}(n_1, n_2, n_3) \\
&\text{END FOR} \\
&\text{END FOR} \\
&\text{END FOR}
\end{aligned} \tag{K2}$$

The quantity,  $-a^T Z$ , represents the discretized objective functional (58) to be tested,

$$-a^T Z = 32 \int_{-\infty}^0 dk_1 \int_0^{+\infty} dk_3 \int_{-\infty}^{+\infty} dk_2 \tilde{U}_{kk}^{(\infty)}(\mathbf{k}) \frac{\sin(L_1 k_1) \sin(L_2 k_2) \sin(L_3 k_3)}{k_1 k_2 k_3}, \tag{K3}$$

whose right-hand side is evaluated with the help of Eqs. (54) and (I5). Equality (K3) is used to determine the coefficient vector  $a$  with the aid of Eq. (K2). The set of constraints  $\mathcal{C}$  in Eqs. (K1) consists of the local linear constraints (J1), the four global linear constraints of equality, and the constraints of 1C or {1C, 2C, 4C} or some other choices, as discussed in Appendix J.

Next, for parallelization, the global consensus problem formulation [37, 38] is employed to write Eqs. (K1) in an equivalent form,

$$\begin{aligned}
&\text{minimize} \quad \sum_{i=1}^N f_i(X_i) \\
&\text{subject to} \quad X_i - Z = 0, \quad i = 1, \dots, N.
\end{aligned} \tag{K4}$$

$X_i \in \mathbb{R}^{6N_{\text{cv}}}$ ,  $i = 1, \dots, N$ , denote the local variables associated, respectively, with the  $N$  computing processing elements (or processes), and  $Z$  is the common global variable. The function  $f_i$  is defined as

$$f_i(X_i) = a^T X_i + I_{\mathcal{C}_i}(X_i). \tag{K5}$$

$I_{\mathcal{C}_i}$  is the indicator function of the convex set  $\mathcal{C}_i$ ; the collection  $\{\mathcal{C}_i : i = 1, \dots, N\}$  is a partition of  $\mathcal{C}$ . The size of each  $\mathcal{C}_i$  is controlled by the computer memory available for the generation of standard conic form.

To apply ADMM to solve Eqs. (K4) iteratively, the augmented Lagrangian [37, 38] is employed,

$$L_\rho(X, Z, Y) = \sum_{i=1}^N [f_i(X_i) + (Y_i)^T (X_i - Z) + (\rho/2) \|X_i - Z\|_2^2], \tag{K6}$$

where

$$X = (X_1, \dots, X_N) \in (\mathbb{R}^{6N_{\text{cv}}})^N, \quad Y = (Y_1, \dots, Y_N) \in (\mathbb{R}^{6N_{\text{cv}}})^N,$$

$Y_i$  is the dual variable associate with the consensus equality constraint  $X_i - Z = 0$  in Eqs. (K4), and  $\rho (> 0)$  is the penalty parameter. The ADMM algorithm consists of the following iterations [37, 38],

$$\begin{aligned}
X^{k+1} &:= \underset{X}{\operatorname{argmin}} L_\rho(X, Z^k, Y^k), \quad Z^{k+1} := \underset{Z}{\operatorname{argmin}} L_\rho(X^{k+1}, Z, Y^k), \\
Y^{k+1} &:= Y^k + \rho [X^{k+1} - (Z^{k+1}, \dots, Z^{k+1})], \quad k = 0, 1, \dots,
\end{aligned} \tag{K7}$$

which may be manipulated in a straight-forward fashion [37] to obtain the ADMM consensus algorithm in the numerical simulation,

$$Z^k = \bar{X}^k := \frac{1}{N} \sum_{i=1}^N X_i^k, \tag{K8a}$$

$$X_i^{k+1} := \underset{X_i \in \mathcal{C}_i}{\operatorname{argmin}} \|X_i - \Lambda_i^k\|_2^2 = \Pi_{\mathcal{C}_i}(\Lambda_i^k), \tag{K8b}$$

$$\tilde{Y}_i^{k+1} := \tilde{Y}_i^k + X_i^{k+1} - \bar{X}^{k+1}, \quad \frac{1}{N} \sum_{i=1}^N \tilde{Y}_i^0 = 0. \tag{K8c}$$

Here,

$$\Lambda_i^k = \bar{X}^k - (\tilde{a} + \tilde{Y}_i^k), \quad (\text{K9})$$

and  $\Pi_{\mathcal{C}_i}(\Lambda_i^k)$  denotes Euclidean projection of vector  $\Lambda_i^k$  onto  $\mathcal{C}_i$ ,  $i = 1, \dots, N$ . In the above derivation, we have used Eq. (K5) and the scaled,

$$Y_i^k = \rho \tilde{Y}_i^k, \quad a = \rho \tilde{a}.$$

The key part of the consensus algorithm is the  $X_i$ -update (K8b) whose computation is discussed below.

The convergence of the iterative process (K8) is guaranteed analytically [37, 39]. To terminate the iterative process, the conventional stopping criteria [37] are adopted. First, the primal and dual residuals,  $R^k$  and  $S^k$ , and their squared norms at the  $k$ -th iteration are calculated through

$$\begin{aligned} R^k &= (X_1^k - \bar{X}^k, \dots, X_N^k - \bar{X}^k), \quad S^k = -\rho(\bar{X}^k - \bar{X}^{k-1}, \dots, \bar{X}^k - \bar{X}^{k-1}); \\ \|R^k\|_2^2 &= \sum_{i=1}^N \|X_i^k - \bar{X}^k\|_2^2, \quad \|S^k\|_2^2 = N\rho^2 \|\bar{X}^k - \bar{X}^{k-1}\|_2^2. \end{aligned} \quad (\text{K10})$$

These residuals converge to zero as the iterative process proceeds, according to the convergence theory [37]. The stopping criteria are

$$\|R^k\|_2 \leq \epsilon^{\text{pri}}, \quad \|S^k\|_2 \leq \epsilon^{\text{dual}}, \quad (\text{K11})$$

where  $\epsilon^{\text{pri}}$  and  $\epsilon^{\text{dual}}$  denote, respectively, the feasibility tolerances for the primal and dual feasibility conditions [37]. Further, the tolerances are expressed in terms of the absolute and relative criteria,  $\epsilon^{\text{abs}}$  and  $\epsilon^{\text{rel}}$  [37],

$$\epsilon^{\text{pri}} = \sqrt{N}(\epsilon^{\text{abs}} + \|\bar{X}^k\|_2 \epsilon^{\text{rel}}), \quad \epsilon^{\text{dual}} = \rho \sqrt{N}(\epsilon^{\text{abs}} + \|\bar{X}^k\|_2 \epsilon^{\text{rel}}). \quad (\text{K12})$$

The values of  $\rho = 1$ ,  $\epsilon^{\text{abs}} = 10^{-4}$ , and  $\epsilon^{\text{rel}} = 10^{-3}$  are employed and are adequate for the present exploration of the second-order model.

The open source conic solver, SCS in C [35], is used to compute the  $X_i$ -update (K8b) in the  $i$ -th processing element. The solver employs a first-order method to solve large convex cone programs, suitable to the large-scale nature of the present problem. Because the solver accepts only standard forms, we resort to the open source package CVXPY [40] with its default solver SCS (denoted as CVXPY/SCS hereafter) to generate such forms. To this end, the  $X_i$ -update (K8b) is first cast in the equivalent ADMM form,

$$\begin{aligned} &\text{minimize} \quad \|X_i - \Lambda_i^k\|_2^2 \\ &\text{subject to} \quad X_i \in \mathcal{C}_i. \end{aligned} \quad (\text{K13})$$

This subproblem has an equivalent representation in the natural form in terms of  $\dot{\Gamma}_{ij}^{(0)}$  as presented in Appendix J. Since this natural form is much easier to code and acceptable to CVXPY, CVXPY/SCS is applied to this natural form, while  $\mathcal{C}_i$  is coded according to the disciplined convex programming (DCP) ruleset [41] as required. The standard form associated with Eqs. (K13) is then obtained,

$$\begin{aligned} &\text{minimize} \quad c_i^T x_i \\ &\text{subject to} \quad A_i x_i + s_i = b_i^k, \quad s_i \in \mathcal{K}_i. \end{aligned} \quad (\text{K14})$$

Here,  $\mathcal{K}_i$  denotes the convex cone composed of  $\mathcal{C}_i$ , described by a group of dimension parameters and dimension array (defined in [35] and README.md of SCS package [36]). Independent of  $\Lambda_i^k$ , vector  $c_i$ , matrix  $A_i$ , and cone  $\mathcal{K}_i$  are fixed completely by  $\mathcal{C}_i$ , i.e., they remain constant for all the iterations  $k$ . The value of vector  $b_i^k$  depends on both  $\mathcal{C}_i$  and  $\Lambda_i^k$ , the dependence on the latter is characterized by the (underneath stacked) pattern of

$$\begin{aligned} b_i^k &= \left( \dots, \underbrace{1, 1, -2\Lambda_i^k[1], \dots, 1, 1, -2\Lambda_i^k[N_{\text{CV}}]}_{3N_{\text{CV}} \text{ components}}, \underbrace{1, 1, -2\Lambda_i^k[N_{\text{CV}} + 1], \dots, 1, 1, -2\Lambda_i^k[2N_{\text{CV}}]}_{3N_{\text{CV}} \text{ components}}, \right. \\ &\quad \left. \underbrace{\dots}_{3 \times 3N_{\text{CV}} \text{ components}}, \underbrace{1, 1, -2\Lambda_i^k[5N_{\text{CV}} + 1], \dots, 1, 1, -2\Lambda_i^k[6N_{\text{CV}}], \dots}_{3N_{\text{CV}} \text{ components}} \right), \end{aligned} \quad (\text{K15})$$

while the components outside the (underneath stacked) pattern are fixed by  $\mathcal{C}_i$  itself. It then follows from Eqs. (K9) and (K15) that  $b_i^k$  evolves as iteration  $k$  proceeds and its update is straight-forward.

The above scheme of standard form generations leads to a mapping between  $x_i$  of the standard form and  $\dot{\Gamma}_{ij}^{(0)}$  of the natural form specified by the pseudocode,

```

n = 0
FOR n1 = 1 to N1
  FOR n3 = 1 to N3
    FOR n2 = 1 to N2
      n = n + 1
       $\dot{\Gamma}_{11}^{(0)}(n_1, n_2, n_3) = x_i[n]$ 
    END FOR
  END FOR
END FOR

: {21,31,12,22}
FOR n3 = 1 to N3
  FOR n2 = 1 to N2
    n = n + 1
     $\dot{\Gamma}_{32}^{(0)}(n_1, n_2, n_3) = x_i[n]$ 
  END FOR
END FOR
END FOR

```

(K16)

The relationship between  $x_i$  of the standard form (K14) and  $X_i$  of the ADMM form (K13) is determined through the composition of mappings (K2) and (K16),

$$x_i \xrightarrow{\text{Eq. (K16)}} \left\{ \dot{\Gamma}_{ij}^{(0)}(n_1, n_2, n_3) \right\} \xrightarrow{\text{Eq. (K2)}} Z = X_i. \quad (\text{K17})$$

To implement the ADMM consensus scheme (K8), the constraint set  $\mathcal{C}$  of Eqs. (K1) in its natural form is first partitioned into  $N$  subsets  $\mathcal{C}_i$ ,  $i = 1, \dots, N$ ; the value of  $N$  is fixed on the basis that the computer memory required to generate the standard form (K14) be less than the 64GB available. Then, CVXPY/SCS is applied to the natural form associated with Eqs. (K13) to determine both  $\{c_i, A_i, \mathcal{K}_i\}$  and the pattern of  $b_i^k$  that specify the standard form.

The solver, SCS, solves Eqs. (K14) and returns the optimal solution  $(x_i^*, y_i^*, s_i^*)$  where  $x_i^*$  is the solution of the primal problem (K14) and  $y_i^*$  is the solution of its dual problem. The parameters controlling the computational procedure are taken from the examples of [36].

Suppose that all the quantities,

$$\{X_i^k, \tilde{Y}_i^k : i = 1, \dots, N\},$$

contained in Eqs. (K8) are known at the  $k$ -th iteration, then

$$\{X_i^{k+1}, \tilde{Y}_i^{k+1} : i = 1, \dots, N\}$$

are determined in parallel as follows:

- 1: Compute  $\Lambda_i^k$  from Eq. (K9) and  $b_i^k$  from Eq. (K15) for all  $i$ ;
- 2: Solve Eqs. (K14) with SCS to obtain optimal solutions  $(x_i^{*(k+1)}, y_i^{*(k+1)}, s_i^{*(k+1)})$  for all  $i$ , with the previously obtained  $(x_i^{*(k)}, y_i^{*(k)}, s_i^{*(k)})$  to warm start the solver.
- 3: Compute  $\{X_i^{k+1}, \bar{X}^{k+1}, \tilde{Y}_i^{k+1}\}$  with the help of the optimal solutions obtained in Step 2 and Eqs. (K17), (K8a), and (K8c).
- 4: Check the stopping criteria (K11); If not satisfied, go to Step 1.

TABLE II. The predicted nontrivial components of Reynolds stress tensor and viscous dissipation under  $\max U_{kk}^{(\infty)}(\mathbf{0})$ .

Constraints	$(\tau_{11}^{(\infty)}, \tau_{22}^{(\infty)}, \tau_{33}^{(\infty)}, \tau_{12}^{(\infty)}, \epsilon^{(\infty)})$
L & 1C (I)	(3.519, 1.091, 1.015, -1.559, 1.560)
L & 1C & 4C (I)	(3.476, 1.070, 1.014, -1.539, 1.539)
L & 1C & 2C & 4C (I)	(3.469, 1.069, 1.014, -1.536, 1.537)
L & 1C (II)	(4.625, 1.160, 1.155, -1.768, 1.769)

Following conventional practice, we usually start with the initial iteration condition,

$$X_i^0 = Y_i^0 = 0, \quad x_i^{*(0)} = 0, \quad y_i^{*(0)} = s_i^{*(0)} = 0, \quad i = 1, \dots, N.$$

In case it is required to improve a solution obtained,

$$\{X_i, Y_i, x_i, y_i, s_i : i = 1, \dots, N\},$$

or to test whether such a solution may be further improved or to study how it varies under the modification of some parameter values, the available solution is taken as the initial iteration condition to warm start the iteration process.

We code the idea and procedure outlined above in C by modifying the MPI code of [42] and the examples of [36] and we implement the parallel computing with MPICH [43].

### Appendix L: Turbulent energy as an objective

In the case of the second-order model in the asymptotic state with  $\sigma = 0$ , we have tested the possibility of  $U_{kk}^{(\infty)}(\mathbf{0})$  as an objective functional which is maximized. Its numerical and computational implementation is the same as that of  $\int_{\mathbb{R}^3} d\mathbf{r} U_{kk}^{(\infty)}(\mathbf{r})$ , the only modification is the replacement of  $\int_{\mathbb{R}^3} d\mathbf{r} U_{kk}^{(\infty)}(\mathbf{r})$  with  $U_{kk}^{(\infty)}(\mathbf{0})$ .

Table II lists the predicted nontrivial components of the Reynolds stress tensor  $\tau_{ij}^{(\infty)} = U_{ij}^{(\infty)}(\mathbf{0})$  and the predicted viscous dissipation  $\epsilon^{(\infty)} = \overline{w_{j,k} w_{j,k}}^{(\infty)}(\mathbf{0})$  under various combinations of constraints and mesh sizes. The meanings of the elements in the column ‘Constraints’ are the same as those of Table I. The adequacy of the solutions is partially indicated by separate computations of  $\tau_{12}^{(\infty)}$  and  $\epsilon^{(\infty)}$  and the ratio,

$$-\tau_{12}^{(\infty)}/\epsilon^{(\infty)} \in [0.9994, 0.9996],$$

consistent with the exact value of 1 dictated by Eq. (51) under  $\sigma = 0$ .

Though the predicted values of  $U_{11}^{(\infty)}(\mathbf{0})$  change significantly when the mesh size is reduced from 0.1 of (I) to 0.05 of (II), all these discretized model versions produce the same numerical order pattern,  $U_{11}^{(\infty)}(\mathbf{0}) > U_{22}^{(\infty)}(\mathbf{0}) > U_{33}^{(\infty)}(\mathbf{0})$  (with  $U_{33}^{(\infty)}(\mathbf{0})$  very close to  $U_{22}^{(\infty)}(\mathbf{0})$ ); this pattern is incompatible with the experimental result that  $U_{33}^{(\infty)}(\mathbf{0})$  is significantly higher than  $U_{22}^{(\infty)}(\mathbf{0})$ , (see Section 4.5 of [8] or infer the relative values from the experimental values presented in Table I).

- 
- [1] P. A. Davidson, *Turbulence, an Introduction for Scientists and Engineers* (Cambridge University Press, 2004).
  - [2] M. Lesieur, *Turbulence in Fluids*, 4th ed. (Springer, 2008).
  - [3] S. A. Orszag, *J. Fluid Mech.* **41**, 363 (1970).
  - [4] T. Tatsumi, *Adv. Appl. Mech.* **20**, 39 (1980).
  - [5] P. Sagaut and C. Cambon, *Homogeneous Turbulence Dynamics* (Cambridge University Press, 2008).
  - [6] E. E. O’Brien and G. C. Francis, *J. Fluid Mech.* **13**, 369 (1962).
  - [7] Y. Ogura, *J. Fluid Mech.* **16**, 33 (1963).
  - [8] J. Piquet, *Turbulent Flows. Models and Physics* (Springer, 1999).
  - [9] M. M. Rogers and P. Moin, *J. Fluid Mech.* **176**, 33 (1987).
  - [10] A. Sekimoto, S. Dong, and J. Jimenez, *Phys. Fluids* **28**, 035101 (2016).
  - [11] L. Tao and M. Ramakrishna, *Int. J. Adv. Eng. Sci. Appl. Math.* **3**, 37 (2011).
  - [12] E. Hopf, *J. Ratl. Mech. Anal.* **1**, 87 (1952).

- [13] W. D. McComb, *The Physics of Fluid Turbulence* (Oxford University Press, 1990).
- [14] U. Schumann, *Phys. Fluids* **20**, 721 (1977).
- [15] C. E. Shannon, *Bell Syst. Tech. J.* **27**, 379 (1948); **27**, 623 (1948).
- [16] E. T. Jaynes, *Phys. Rev.* **106**, 620 (1957); **108**, 171 (1957).
- [17] E. T. Jaynes, *Papers on Probability, Statistics, and Statistical Physics*, edited by R. D. Rosenkrantz (D. Reidel [Kluwer], 1983).
- [18] T. M. Cover and J. A. Thomas, *Elements of Information Theory*, 2nd ed. (Wiley-Interscience, 2006).
- [19] S. F. Edwards and W. D. McComb, *J. Phys. A* **2**, 157 (1969).
- [20] M. S. Lobo, L. Vandenderghe, S. Boyd, and H. Le Bret, *Linear Algebra and its Applications* **284**, 193 (1998).
- [21] F. Alizadeh and D. Goldfarb, *Linear Algebra and Its Applications* **284**, 193 (2003).
- [22] S. Boyd and L. Vandenberghe, *Convex Optimization* (Cambridge University Press, 2009).
- [23] J. C. Isaza and L. R. Collins, *J. Fluid Mech.* **637**, 213 (2009).
- [24] Y. Nesterov, *Math. Program. Ser. A* **146**, 275 (2014).
- [25] V. Cevher, S. Becker, and M. Schmidt, *IEEE Signal Processing Magazine*, September, 32 (September, 2014).
- [26] A. S. Monin and A. M. Yaglom, *Statistical Fluid Mechanics: Mechanics of Turbulence*, edited by J. L. Lumley, Vol. 2 (MIT Press, 1975).
- [27] H. H. Bruun, *Hot-Wire Anemometry, Principles and Signal Analysis* (Oxford University Press, 1995).
- [28] P. A. Durbin and B. A. P. Reif, *Statistical Theory and Modeling for Turbulent Flows*, 2nd ed. (Wiley, 2011).
- [29] H. Tennekes and J. L. Lumley, *A First Course in Turbulence* (MIT Press, 1972).
- [30] T. Bohr, M. H. Jensen, G. Paladin, and A. Vulpiani, *Dynamical Systems Approach to Turbulence* (Cambridge University Press, 1998).
- [31] P. Holmes, J. L. Lumley, and G. Berkooz, *Turbulence, Coherent Structures, Dynamical Systems and Symmetry* (Cambridge University Press, 1996).
- [32] T. Hahn, *Comput. Phys. Commun.* **168**, 78 (2005).
- [33] T. Hahn, *Nuclear Instruments & Methods in Physics Research* **A559**, 273 (2006).
- [34] <http://www.feynarts.de/cuba>.
- [35] B. O'Donoghue, E. Chu, N. Parikh, and S. Boyd, *J. Optim. Theory Appl.* **169**, 1042 (2016).
- [36] B. O'Donoghue, E. Chu, N. Parikh, and S. Boyd, *SCS: Splitting Conic Solver*, version 1.2.6. <https://github.com/cvxgrp/scs> (April, 2016).
- [37] S. Boyd, N. Parikh, E. Chu, B. Peleato, and J. Eckstein, *Foundations and Trends in Machine Learning* **3**, 1 (2010).
- [38] N. Parikh and S. Boyd, *Foundations and Trends in Optimization* **1**, 123 (2013).
- [39] J. Eckstein and D. P. Bertsekas, *Mathematical Programming* **55**, 293 (1992).
- [40] S. Diamond and S. Boyd, *J. Machine Learning Research* **17**, 1 (2016).
- [41] M. C. Grant and S. P. Boyd, *The CVX Users' Guide Release 2.1*, CVX Research, Inc. (October 24, 2014).
- [42] S. Boyd, N. Parikh, E. Chu, B. Peleato, and J. Eckstein, *MPI example for alternating direction method of multipliers*. [https://web.stanford.edu/~boyd/papers/admm\\_mpi/](https://web.stanford.edu/~boyd/papers/admm_mpi/) (February 24, 2011).
- [43] A. Amer, P. Balaji, W. Bland, W. Gropp, R. Latham, H. L. H, L. Oden, A. J. Pena, K. Raffanetti, S. Seo, R. Thakur, and J. Zhang, *MPICH User's Guide Version 3.2*, Mathematics and Computer Science Division, Argonne National Laboratory (November 11, 2015).
- [44] J. Rota, *Statistical Theory of Inhomogeneous Turbulence. Part 1*, Tech. Rep. NASA TT F-14, 560 (October, 1972).
- [45] S. Kida and M. Tanaka, *J. Fluid Mech.* **274**, 43 (1994).